


January 2022

## Xpo1 As A Therapeutic Target In Gastric Cancer

Rachel Sexton  
*Wayne State University*

Follow this and additional works at: [https://digitalcommons.wayne.edu/oa\\_dissertations](https://digitalcommons.wayne.edu/oa_dissertations)

 Part of the [Biology Commons](#)

---

### Recommended Citation

Sexton, Rachel, "Xpo1 As A Therapeutic Target In Gastric Cancer" (2022). *Wayne State University Dissertations*. 3606.

[https://digitalcommons.wayne.edu/oa\\_dissertations/3606](https://digitalcommons.wayne.edu/oa_dissertations/3606)

This Open Access Dissertation is brought to you for free and open access by DigitalCommons@WayneState. It has been accepted for inclusion in Wayne State University Dissertations by an authorized administrator of DigitalCommons@WayneState.

**XPO1 AS A THERAPEUTIC TARGET IN GASTRIC CANCER**

by

**RACHEL E. SEXTON**

**DISSERTATION**

Submitted to the Graduate School

of Wayne State University,

Detroit, Michigan,

in partial fulfillment of the requirements

for the degree of

**DOCTOR OF PHILOSOPHY**

2022

Major: Cancer Biology

Approved by:

_____ Advisor	_____ Date
_____	_____
_____	_____
_____	_____
_____	_____

## **DEDICATION**

I would like to dedicate this thesis to those impacted by gastric cancer and those who have bravely fought this disease. Although this disease is considered a rare cancer in the United States, there are still many families affected. My family has been personally touched as my uncle's brother was diagnosed with gastric cancer in 2017 and quickly succumbed to this disease. Gastric cancer and gastrointestinal cancer awareness and attention is urgently needed not only to identify treatments that are more effective but also ways to enhance earlier detection. Due to the prevalence in the United States, cancers such as breast and prostate get largely more attention and resources in both the basic science and translational research areas. With more attention towards identifying the mechanisms and underlying mutations that cause gastric cancer, we can move towards increasing the overall survival rates and making an impact on patient lives.

## **ACKNOWLEDGMENTS**

I would like to acknowledge my mentor, Dr. Azmi, for allowing me the guidance, freedom, and creativity to develop this project into what is presented. Dr. Azmi believed in my work and my project from the beginning and provided me with the encouragement to pursue this work. Not only Dr. Azmi but also the Azmi lab as a whole has been supportive and helpful throughout my graduate studies. I would also like to thank the Flow Cytometry core, Epidemiology core and BioBanking core for their guidance throughout graduate school as well as LC Sciences for their help with much of the sequencing data. I would also like to acknowledge Dr. Speyer for giving me the training and encouragement to pursue a career in cancer research and guidance throughout my time in graduate school as well as my committee members for their ability to guide my research and demand of me the highest standards of quality scientific work. Finally, I would like to acknowledge my friends and family who have all been supportive of me throughout my time in graduate school.

## TABLE OF CONTENTS

Dedication.....	ii
Acknowledgements.....	.iii
Table of contents.....	iv
List of Tables.....	x
List of Figures.....	.xi
List of Abbreviations .....	xii
CHAPTER 1- GASTRIC CANCER.....	1
1.1 Gastric Cancer is a Heterogeneous Disease.....	1
1.1.1 Inter-Tumor Heterogeneity.....	1
1.1.2 Intra-Tumor Heterogeneity.....	2
1.2 Gastric Cancer Treatments.....	3
1.2.1 First Generation Treatment Strategies.....	4
1.2.2 New Treatment Outlooks.....	5
CHAPTER 2- HISTORY OF THE NUCLEAR EXPORT PATHWAY.....	7
2.1 Initial Discoveries.....	7
2.1.1 Leptomycin B.....	7
2.1.2 Leptomycin B as an <i>in vitro</i> tool to study nuclear export.....	8
2.1.3 Nuclear export is upregulated in several malignancies.....	9
2.1.4 Nuclear export is a complex process.....	10
2.2 Strategies to safely inhibit nuclear export.....	10
2.2.1 Bacterial nuclear export inhibitors.....	12
2.2.2 Herbal nuclear export inhibitors.....	12

2.2.3 Synthetic nuclear export inhibitors .....	13
2.2.4 First and second-generation selective inhibitors of nuclear export (SINE) .....	15
2.3 Clinical progress of selinexor.....	16
2.3.1 Pharmacokinetic properties of selinexor.....	16
2.3.2 Pharmacodynamic properties of selinexor.....	17
2.3.3 Patient demographics and selinexor.....	17
2.4 Conclusions.....	18
<b>CHAPTER 3- XPO1 IS UPREGULATED IN GASTRIC CANCER.....</b>	<b>19</b>
3.1 Introduction.....	19
3.2 Materials and Methods.....	19
3.2.1 Cell lines, culture conditions and reagents.....	19
3.2.2 XPO1 silencing .....	21
3.2.3 XPO1 transient overexpression.....	21
3.2.4 Colony formation.....	22
3.2.5 MTT assay.....	22
3.2.6 Trypan blue cell viability assay.....	23
3.2.7 Immunohistochemistry.....	23
3.2.8 Western blotting.....	25
3.2.9 Statistics.....	26
3.3 Results.....	27
3.3.1 XPO1 overexpression occurs in gastric cancer cell lines and patient tissues.....	27
3.3.2 XPO1 expression and survival disparities.....	27

3.3.3 XPO1 upregulation is pathogenic in gastric cancer .....	32
3.3.4 XPO1 knockdown reduces gastric cancer viability .....	35
3.4 Conclusions .....	35
<b>CHAPTER 4-TARGETING XPO1 IN GASTRIC CANCER .....</b>	<b>36</b>
4.1 Introduction .....	36
4.2 Materials and Methods .....	36
4.2.1 Cell lines, culture conditions and reagents .....	36
4.2.2 Apoptotic analysis .....	37
4.2.3 Cell cycle arrest .....	38
4.2.4 Colony formation assay .....	38
4.2.5 MTT assay .....	39
4.2.6 Trypan blue cell viability assay .....	39
4.2.7 Immunofluorescence assay .....	40
4.2.8 Spheroid formation assay.....	40
4.2.9 Western blotting.....	41
4.2.10 Statistics.....	42
4.3 Results.....	42
4.3.1 SINE inhibits gastric cancer cellular proliferation .....	42
4.3.2 SINE treatment in normal gastric cells .....	44
4.3.3 Physiological role of XPO1 knockdown in gastric cancer cells .....	46
4.3.4 Cell cycle arrest induces apoptosis after SINE treatment .....	51
4.3.5 Conclusions.....	52
<b>CHAPTER 5-SELINEXOR ENHANCES THE THERAPEUTIC EFFICACY OF COMMONLY USED CHEMOTHERAPEUTICS .....</b>	<b>54</b>

<b>5.1 Introduction .....</b>	<b>54</b>
<b>5.2 Paclitaxel mechanism of action .....</b>	<b>54</b>
<b>5.3 Materials and Methods.....</b>	<b>55</b>
<b>5.3.1 Cell lines, culture conditions and reagents .....</b>	<b>55</b>
<b>5.3.2 Trypan blue cell viability assay .....</b>	<b>56</b>
<b>5.3.3 Cell Cycle analysis .....</b>	<b>56</b>
<b>5.3.4 Xenograft studies.....</b>	<b>57</b>
<b>5.3.5 Statistics.....</b>	<b>58</b>
<b>5.4 Results.....</b>	<b>58</b>
<b>5.4.1 Selinexor enhances the therapeutic efficacy of paclitaxel in <i>vitro</i>.....</b>	<b>58</b>
<b>5.4.2 Selinexor enhances the therapeutic efficacy of nab-paclitaxel in <i>vivo</i></b> <b>.....</b>	<b>64</b>
<b>5.4.3 Conclusions.....</b>	<b>64</b>
<b>CHAPTER 6- SINE ENHANCES DNA DAMAGING CHEMOTHERAPEUTICS .....</b>	<b>67</b>
<b>6.1 Introduction.....</b>	<b>67</b>
<b>6.2 Materials and Methods .....</b>	<b>69</b>
<b>6.2.1 Cell lines, culture conditions and reagents .....</b>	<b>69</b>
<b>6.2.2 Trypan blue cell viability assay.....</b>	<b>70</b>
<b>6.2.3 MTT assay.....</b>	<b>71</b>
<b>6.2.4 Apoptotic analysis.....</b>	<b>72</b>
<b>6.2.5 Cell cycle analysis.....</b>	<b>72</b>
<b>6.2.6 Database search.....</b>	<b>73</b>
<b>6.2.7 Immunofluorescence assay.....</b>	<b>73</b>
<b>6.2.8 RNA extraction.....</b>	<b>74</b>



6.2.9 Western blot.....	75
6.2.10 WBP5 silencing.....	75
6.2.11 In vivo xenograft.....	76
6.2.12 Statistics.....	77
<b>6.3 Results.....</b>	<b>77</b>
6.3.1 XPO1 sensitizes gastric cancer cells to DNA damaging agents.....	77
6.3.2 XPO1 downregulation suppresses DNA damage repair proteins.....	80
6.3.3 XPO1 downregulation suppresses one-carbon metabolism.....	87
6.3.4 Oxaliplatin, 5-fluorouracil and selinexor induces substantial cell death .....	89
<b>6.4 Conclusions.....</b>	<b>95</b>
<b>CHAPTER 7- SMALL NONCODING RNAs IN GASTRIC CANCER .....</b>	<b>100</b>
<b>7.1 Introduction .....</b>	<b>100</b>
<b>7.2 Background.....</b>	<b>100</b>
7.2.1 Overview of small noncoding RNAs.....	100
7.2.2 MicroRNAs.....	101
7.2.3 Circular RNAs.....	102
7.2.4 Long-noncoding RNAs.....	102
7.2.5 PiwiRNAs.....	103
7.2.6 Small noncoding RNAs in gastric cancer.....	103
<b>7.3 Materials and Methods.....</b>	<b>105</b>
7.3.1 Cell lines, culture conditions and reagents.....	105
7.3.2 RNA extraction.....	105
7.3.3 Noncoding RNA data analysis (miRNA) .....	106

7.3.4 Noncoding RNA data analysis (piRNA) .....	107
7.3.5 Circular RNA data analysis (circRNA) .....	109
7.3.6 Trypan blue cell viability assay.....	109
7.3.7 MTT assay.....	110
7.3.8 RASGEF1A knockdown.....	110
7.3.9 Colony formation .....	111
7.3.10 RNA extraction and RT-qPCR .....	111
7.3.11 miRNA extraction and RT-qPCR .....	112
7.3.12 Database search.....	113
7.3.13 Statistics .....	113
<b>7.4 Results .....</b>	<b>113</b>
7.4.1 XPO1 transports a variety of small noncoding RNAs to the cytoplasm .....	113
7.4.2 Modulation of microRNAs leads to gastric cancer growth .....	114
7.4.3 Ras signaling is targeted by miR-7974 and miR-129-1-3p .....	119
7.4.4 miR-7974 and miR-129-1-3p alter gastric cancer sensitivity to selinexor.....	122
7.4.5 Differential changes in small noncoding RNAs are related to chemotherapeutic resistance.....	126
<b>7.5 Conclusions.....</b>	<b>128</b>
<b>CHAPTER 8- OVERALL CONCLUSIONS .....</b>	<b>129</b>
<b>CHAPTER 9- FUTURE DIRECTIONS .....</b>	<b>132</b>
<b>REFERENCES.....</b>	<b>134</b>
<b>ABSTRACT .....</b>	<b>155</b>
<b>AUTOBIOGRAPHICAL STATEMENT.....</b>	<b>157</b>

## LIST OF TABLES

Table 1: Descriptive characteristics of gastric cancer cell lines.....	20
Table 2: Patient demographics for XPO1 IHC study.....	24
Table 3: XPO1 expression from gastric cancer patient tissues (AA vs CA) .....	31
Table 4: IC <sub>50</sub> values of SINE compounds in gastric cancer cell lines .....	43
Table 5: Synergy analysis of paclitaxel and SINE.....	59
Table 6: Ploidy status of SNU-1 and SNU-16 cell line after treatment with SINE and/or paclitaxel.....	61
Table 7: <i>In vivo</i> efficacies of nab-paclitaxel and selinexor toward the SNU-1 xenografts. Female ICR-SCID mice .....	66
Table 8: Upregulation of genes involved in nuclear transport in multi-cancer cohort.....	78
Table 9: IC <sub>50</sub> values and synergy calculations for SNU-1 and SNU-16 cell lines with oxaliplatin, 5-fluorouracil and selinexor.....	82
Table 10: <i>In vivo</i> efficacies of oxaliplatin, 5-FU and selinexor in SNU-16 xenografts.....	97
Table 11: Top differentially expressed small noncoding RNAs after selinexor treatment .....	115
Table 12: RASGEFs are targeted by miR-7974 and miR-129-1-3p .....	121

## LIST OF FIGURES

Figure 1.1: Overview of the nuclear export process via XPO1/CRM1.....	11
Figure 1.2: Inhibitors of XPO1 activity.....	14
Figure 2.1: XPO1 expression is upregulated in gastric cancer cell lines.....	28
Figure 2.2: XPO1 is overexpressed in gastric cancer patients.....	29
Figure 2.3: XPO1 overexpression induces gastric cancer proliferation.....	33
Figure 2.4: Knockdown of XPO1 causes reduction in gastric cancer cell viability.....	35
Figure 3.1: SINEs reduce colony formation and 3D spheroid growth in gastric cancer cells.....	45
Figure 3.2: Selinexor and eltanexor and normal gastric tissues.....	47
Figure 3.3: Physiologic function of SINEs in <i>vitro</i> .....	48
Figure 3.4: XPO1 inhibition induces cell cycle arrest .....	50
Figure 3.5: Apoptotic analysis of gastric cancer cells treated with SINEs.....	51
Figure 3.6: Scheme of XPO1 activity in gastric cancer.....	53
Figure 4.1: In <i>vitro</i> assessment of selinexor and paclitaxel in gastric cancer.....	60
Figure 4.2: Cell cycle arrest analysis of SNU-1 and SNU-16 cell line.....	62
Figure 4.3: In <i>vivo</i> assessment of nab-paclitaxel and selinexor in SNU-1 xenograft.....	65
Figure 5.1: Chemical structures of compounds used.....	68
Figure 5.2: XPO1 activity is altered in response to chemotherapeutics.....	79
Figure 5.3: Cell viability analysis of selinexor, 5-FU and oxaliplatin.....	81
Figure 5.4: DNA damage is upregulated in gastric cancer treated cells.....	84
Figure 5.5: Inhibition of DNA damage is a mechanism of action.....	86
Figure 5.6: XPO1 downregulation suppresses one carbon metabolism.....	88

<b>Figure 5.7: WBP5 expression is relevant to 5-FU resistance.....</b>	<b>90</b>
<b>Figure 5.8: WBP5 knockdown sensitizes gastric cancer cells to 5-FU.....</b>	<b>91</b>
<b>Figure 5.9: Selinexor down regulates WBP5 in gastric cancer.....</b>	<b>92</b>
<b>Figure 5.10: Selinexor enhances cell death of oxaliplatin and 5-FU specifically in gastric cancer cells.....</b>	<b>94</b>
<b>Figure 5.11: In vivo study of triple combination with SNU-16 xenograft.....</b>	<b>96</b>
<b>Figure 5.12: Schematic of synergy mechanism for selinexor plus oxaliplatin and 5FU.....</b>	<b>99</b>
<b>Figure 6.1: Baseline expression of miR-7974 and miR-129-1-3p in normal and gastric cancer cell lines.....</b>	<b>117</b>
<b>Figure 6.2: Upregulation of miR-7974 enhances cell viability.....</b>	<b>118</b>
<b>Figure 6.3: Downregulation of miR-129-1-3p enhances cell viability.....</b>	<b>120</b>
<b>Figure 6.4 RASGEF1A is activated by miR-7974 and miR-129-1-3p.....</b>	<b>123</b>
<b>Figure 6.5: RASGEF1A controls gastric cancer proliferation .....</b>	<b>124</b>
<b>Figure 6.6: miRNAs Alter selinexor sensitivity in gastric cancer.....</b>	<b>126</b>
<b>Figure 6.7: Selinexor can overcome aberrantly expressed microRNAs.....</b>	<b>127</b>

## LIST OF ABBREVIATIONS

African American	AA
Base pair	BP
Bicinchoninic acid	BCA
Caucasian American	CA
Chromosome Instability	CIN
Confidence Interval	CI
Chromosome Region Maintenance 1	CRM1
Epstein Barr Virus	EBV
Genomically Stable	GS
Human Epidermal Growth Factor 2	HER2
LMB	Leptomycin B
Microsatellite Instability	MSI
NES	Nuclear Export Sequence
PKIs	Protein Kinase Inhibitors
Phosphate Buffered Saline	PBS
Polyvinylidene fluoride	PVDF
RanGTPs	Ras-related nuclear proteins

Radio Immunoprecipitation Assay	RIPA
Sodium Dodecyl Sulfate	SDS
Selective Inhibitors of Nuclear Export	SINEs
Thymidylate synthase	TYMS
United States	US
Untranslated Region	UTR
WW domain binding protein 5	WBP5
XPO1	Exportin 1
XPO5	Exportin 5
XPO7	Exportin 7
World Health Organization	WHO
7-Aminoactinomycin D	7AAD

## **CHAPTER 1- GASTRIC CANCER**

### **1.1 Gastric cancer is a heterogeneous disease**

Gastric cancer is a complex and highly heterogeneous disease. In the United States (US), ~25,000 new cases are diagnosed each year whereas throughout the world around one-million are diagnosed per year [Rawla et al., 2019]. Interestingly, the 5-year survival rate differs between the US and the rest of world (32% vs 25%) [Rawla et al., 2019]. The disproportional survival rates remain a mystery but some reports have indicated that better food sanitation practices in the US contribute to these statistics [Rawla et al., 2019; Wang et al., 2009]. Although there is a clear survival disparity, the survival rate remains relatively low due to the highly heterogeneous nature of this disease. Heterogeneity remains distinct at the tumor level, at the cellular level and at the molecular level.

#### **1.1.1 Inter-tumor heterogeneity**

Inter-tumor heterogeneity in gastric cancer is distinct and different subtypes of this disease can be classified in a variety of ways based on pathology, molecular structure, mutational status or invasive properties. The Lauren classification is the oldest subtyping, described in 1965, and has characterized gastric cancer into three subtypes: well-differentiated, poorly differentiated and mixed subtype [Ma et al., 2016]. The sub typing is based on biological tumor characteristics including, but not limited to, adhesive properties, infiltration and the clustering ability of tumor cells [Berlth et al., 2014]. In 1992, the Goeski classification subtyped gastric cancer based on metastatic patterns, local growth rates and tubular differentiation (with or without mucus) [Berlth et al., 2014]. Around this time, the Ming classification was also proposed which used growth patterns



of tumors, specifically the expanding or infiltrating type, for sub-typing and is referred to as the simplest classification system [Berlth et al., 2014]. In 2010, the World Health Organization (WHO) created a new classification system which was the most detailed based on pathohistological characteristics and encompasses several subgroups: papillary, tubular, mucinous, mixed, uncommon and signet ring cell carcinoma [Berlth et al., 2014]. Finally in 2013 an analysis of gastric cancer cases in The Cancer Genome Atlas (TCGA) led to a classification system based on genomic and molecular characterization markers: Epstein Barr Virus positive tumors (EBV), microsatellite instable (MSI), genomically stable (GS) and chromosomal instability (CIN) [Zhang et al., 2014].

All of the above classification systems are used throughout the world and are at the discretion of the oncologist and/or pathologist. Most recently a single cell analysis was performed on gastric cancer tumors and found differences in transcriptomics, genotyping, molecular and phenotypic functions that led to a two-part classification system with prognostic ability [Wang et al., 2021]. Another subtle distinction of gastric cancer in the US, compared to other regions of the world, is the inclusion of gastroesophageal junction (GEJ) cancer. GEJ cancer is any malignancy at the junction where the esophagus and stomach meet and is caused by gastric reflux (GERD) and *H. Pylori* infection, which leads to further complexity [Odze 2005].

### **1.1.2 Intra-tumor heterogeneity**

In many cases of gastric cancer, *H. Pylori* can initiate disease in a stepwise manner by altering the molecular landscape of normal gastric cells specifically inducing chronic inflammation by the influx of CD4 Th1 cells which produce high levels of reactive nitrogen oxygen species. This increased oxidative stress results in inflammation leading to DNA

damage and cellular changes [Ishaq and Nunn, 2015]. Not only can *H. Pylori* induce gastric cancer but also a high salt and low fiber diet and exposure to chemical carcinogens like N-nitroso compounds or alcohol can induce inflammatory responses that result in the progression to gastric cancer [Lee and Derakhshan, 2013]. Although inflammation is a driving factor for gastric cancer, not all gastric cancer cells are identical and mutations within a tumor frequent occurs and adds another layer of complexity to this disease.

For example, human epidermal growth factor receptor 2 (HER2) positivity is variable in tumors and this diversity can be visualized pathogenically in dual block detection versus paraffin block detection [Zhang et al., 2020]. The differing HER2 expression in a tumor can produce clones resistant to the HER2 antibody (trastuzumab) leading to disease progression and poor prognosis [Zhang et al., 2020]. Cancer stem cells (CSCs) are present in gastric cancer and these tumor clones have unlimited self-renewal, differentiation and tumor generating capacities. Various studies have suggested that some populations of gastric cancer cells have increased expression of CD44, SOX2, Oct4 and Musashi-1 leading to aggressive and chemotherapeutic resistant disease [Fu et al. 2018]. Finally, a genetic component to gastric cancer occurs in the form of E-cadherin (CDH1) and/or alpha-E-catenin (CTNNA1) mutations, referred to as hereditary diffuse gastric cancer (HDGC) [Lobo et al., 2021]. HDGC comprises 1%-3% of all gastric cancer cases and is extremely rare but variability between family members with these mutations is evident regardless of histopathological findings [Gullo et al., 2018].

## **1.2 Gastric cancer treatments**

There is no worldwide-accepted gold standard of treatment for gastric cancer but rather it is physicians choice. In the section below, we will discuss various treatment

strategies used within the clinic to treat this disease.

### **1.2.1 First generation treatment strategies**

Until recently, acceptable treatment strategies normally consisted of treatment based on known molecular aberrations. For example, first line treatment depended on HER2 tumor status. If the patient exhibited HER2-positivity, treatment consisted of trastuzumab (HER2 monoclonal antibody) plus a platinum-based regimen (DNA damaging agent) but if the patient was HER2 negative, treatment consisted of a platinum-based regimen or clinical trial [Mitani et al., 2020]. Second line treatment depended on whether the tumor has low or high microsatellite instability. If the tumor had high microsatellite instability (was mismatch repair deficient), treatment consisted of pembrolizumab, Programmed Death Ligand 1 (PD-L1) immunotherapy, but if the tumor had low microsatellite instability (mismatch repair proficient) treatment consisted of ramucirumab (VEGF2 monoclonal antibody) and paclitaxel (microtubule inhibitor) [Hui et al., 2017; Chau et al., 2020]. Finally, third line treatment depended on PDL1 status. If PDL1 expression was high, greater than 1%, treatment included pembrolizumab but if PDL1 expression was absent the antimetabolite tipiracil/trifluridine (TAS-102) was recommended [Hogner et al., 2021 and Brar and Shaw, 2019; Arai and Nakajima et al., 2020].

Many oncologists have also chosen to use combinatory therapy including FOLFOX or CAPOX which consists of a DNA damaging agent (platinum), an anti-metabolite (5-fluorouracil/capecitabine) and folinic acid as well as giving treatment with or without radiation [Arai and Nakajima et al., 2020]. Currently, the only curative treatment available for gastric cancer is surgical resection at an early stage of disease, which is uncommon

[Weledji 2017]. Many gastric cancer patients are elderly, making treatment decisions somewhat complex. Older patients are unable to tolerate some of the combination therapies due to high toxicity profiles. A recent study showed that patients over 80 years old with gastric cancer who underwent surgery had more co-morbidities related to the surgery, lower overall survival and lower disease specific survival [Fujiwara et al., 2017]. A comparison of different treatment strategies suggested combination therapy with platinum and fluoropyrimidines is recommended for elderly patients who are not frail where as monotherapy is recommended for frail and/or elderly patients [Kim et al., 2016].

### **1.2.2 New treatment outlooks**

Recently, new treatment options have been successfully debated and mainly include different immunotherapy combinations. For example PD-L1 immunotherapy (pembrolizumab) can be used as a first line therapy for patients with or without chemotherapy, based on the PDL1 expression score [Ahn and Kim, 2021]. Trastuzumab deruxtecan (DS-8201), a dual-combination HER2 monoclonal antibody and drug conjugate topoisomerase I inhibitor, has been approved for second line treatment in HER2 positive gastric cancer cases based on results from the DESTINY-Gastric01 trial in Japan [Kotani and Shitara, 2021]. Pembrolizumab or nivolumab in combination with an anti-metabolite (fluoropyrimidines) and DNA damaging agent (platinum) was FDA approved for unresectable gastric cancer that is HER2 over expressing based on results from the randomized phase 2 INTEGA trial [Tintelnot et al., 2020]. Finally, nivolumab was FDA approved after initial chemoradiotherapy for esophageal-gastric junction cancer [Schena et al., 2019]. There are 2,070 registered gastric cancer clinical trials investigating targeted treatments, including various tyrosine kinase inhibitors, or modifications of the

current treatment options available but studies available with results show that many of these clinical trials had lackluster responses. These results highlight that novel targeted agents need to be investigated in gastric cancer. In the following chapter, the role of protein transporters in relation to gastric cancer is discussed.

## CHAPTER 2- HISTORY OF THE NUCLEAR EXPORT PATHWAY

### 2.1 Initial discoveries

Nuclear export is the scientifically coined term for a complex and dynamic process that occurs in all cells. The term “nuclear export” refers to the controlled and dynamic shuttling of cellular proteins (tumor suppressors, oncogenes, some RNA, and small non-coding RNAs) from the nucleus to the cytoplasm. The family of proteins that carries out nuclear export, known as exportins, are part of the broader family of Karyopherin proteins [Pemberton and Paschal, 2005]. The most recognizable exportin protein is Exportin 1 (XPO1), referred to as such since the 1990s. XPO1 was previously referred to as Chromosomal Region Maintenance Protein 1 (CRM1) [Evgeneva et al., 1964]. Discovered initially by Russian researchers, CRM1 expression was linked to the metastasis of rhabdomyoblastoma tumors but its function was unknown [Evgeneva et al. 1964]. Further research revealed that CRM1 is highly conserved across eukaryotes and is found in *Schizosaccharomyces* and other higher-order eukaryotic organisms. CRM1 is cold sensitive and is involved in the organization of cell cycle dependent centromeres [Adachi et al., 1989; Funabiki et al., 1993; Toda et al., 1992]. Earlier on it was found that CRM1 localizes mainly within the nucleus but did show some activity within the periphery [Funabiki et al., 1993] suggestive of a dynamic, broad and largely unknown cellular protein.

#### 2.1.1 Leptomycin B

Although there were initial discoveries into CRM1 activity, it was largely unknown how to harness this protein as a target for cancer therapy. In 1983, the anti-fungal antibiotic, Leptomycin B (LMB) (2E,5S,6R,7S,9R,10E,12E,15R,16Z,18E)-17-ethyl-6-

hydroxy-3,5,7,9,11,15-hexamethyl-19-[(2S,3S)-3-methyl-6-oxo-2,3-dihydropyran-2-yl]-8-oxononadeca-2,10,12,16,18-pentanenoic acid), was identified as a potent compound that inhibits the growth of eukaryotic organisms *Schizosaccharomyces* and *Mucor* [Hamamoto et al., 1983]. LMB was initially synthesized as a byproduct of the fermentation process of *Streptomyces* for Kazusamycin production, a potent antibiotic with potential anti-tumor activity [Hamamoto et al., 1983]. LMB was effective in treating Lewis lung carcinoma and lymphocytic leukemia but the mechanism of action was unknown [Komiyama et al., 1985] and no significant toxicities were observed *in vivo* in preclinical studies.

Between 1989 and 1993 critical discoveries into LMB activity were made including uncovering the ability of LMB to inhibit cell cycle arrest, control cellular checkpoints and inhibit yeast cell fission [Yoshida et al., 1990; Abe et al., 1991; Yoshida et al., 1993]. Following this, in 1994 it was found that LMB targets CRM1 activity in yeast [Nishi et al., 1994]. These discoveries along with two important previous findings: (1) CRM1 activity is involved in cancer progression and (2) CRM1 activity is highly conserved throughout the eukaryotic kingdom, paved the way for the beginning of a phase I clinical trial studying LMB in advanced refractory cancers (ovarian, colon, melanoma, glioma, sarcoma, pancreas) [Newlands et al., 1996]. Unfortunately, the phase I clinical trial had surprisingly poor results. Although LMB (elactocin) was effective in preclinical models, the associated toxicities were too great in humans to proceed. These findings eliminated LMB for future use in patients [Newlands et al., 1996].

### **2.1.2 Leptomycin B as an *in vitro* tool to study nuclear export**

Regardless of the failed clinical trial, critical scientific discoveries were

made in subsequent years using LMB as a tool to study nuclear export. Not only was LMB an effective inhibitor of tumor growth but it was found to inhibit the action of viral proteins, specifically the human immunodeficiency virus type 1 (HIV-1) Rev protein. Due to the correlation between LMB and CRM1 activity, it was suggested that inhibition of CRM1 might cause the retention of viral or cellular proteins within the nucleus [Wolff et al., 1997].

Structural studies into the LMB-CRM1 interaction revealed CRM1 contains a residue that recognizes specific leucine-rich sequences on proteins [Fornerod et al., 1997]. These sequences, referred to as nuclear export sequences (NESs), are located on proteins such as Rev, Protein Kinase Inhibitors (PKIs). The NESs directly interact with XPO1 resulting in binding. After binding, Ras-related nuclear proteins (RanGTPs) are involved in dynamically transporting the complex (CRM1-protein) from the nucleus to the cytoplasm independent of nuclear import activity [Askjaer et al., 1999]. CRM1 was found to interact with nuclear pore components such as NUP214 and Nup88 leading to the idea that CRM1 activity was broad and extended well beyond structural maintenance in cells [Fornerod et al., 1997]. In 1997, the identifier CRM1 was replaced with nuclear export protein-1 (XPO1) based on the rationale that this protein did much more than only maintain the centromere region of cells (**Figure 1.1**) [Stade et al., 1997; Yano et al., 1994].

### **2.1.3 Nuclear export is upregulated in several malignancies**

Although it was known that XPO1 activity has a connection to cancer development, it was not until 2009 that scientific evidence suggested that XPO1 overexpression naturally occurs in malignant cells [van der Watt et al., 2009]. XPO1 overexpression has since been identified in virtually all solid and liquid cancer types including breast, ovarian,



gastric, pancreatic and leukemia's [Cheng et al., 2014; Noske et al., 2008; Sexton et al., 2019; Azmi et al., 2017; Boons et al., 2021]. XPO1 overexpression has been linked to perturbations in cellular signaling pathways such as activation of the RAS/MEK/ERK pathway [Azizian and Li, 2020] and alterations in inflammatory pathways related to NF- $\kappa$ B activation [Kashyap et al., 2016].

#### **2.1.4 Nuclear export is a complex process**

Within the 30-year period since discovering CRM1/XPO1, other members of the nuclear export family were uncovered including nuclear export protein 5 (XPO5). Identified in 2002, XPO5 was found to predominantly interact with double stranded RNA-binding proteins, tRNAs and elongation factors with the capacity to synergize with other nuclear transport pathways [Brownawell et al., 2002; Bohnsack et al., 2002; Calado et al., 2002]. Nuclear export protein 7 (XPO7) was discovered in 2000. Originally referred to as RanBP16, it was found to be overexpressed in the testis and pancreas and was highly conserved in other eukaryotic organisms [Koch et al., 2000]. Although other proteins of the nuclear export protein family have been discovered, XPO1 has gained significant and widespread attention mainly due to its ability to transport a variety of cancer related proteins (oncogenes and tumor suppressors) as well as the ease of targeting this protein with readily available inhibitors.

#### **2.2 Strategies to safely inhibit nuclear export**

With proof of concept studies showing LMB could target XPO1, there have been improved efforts to create more effective and less toxic inhibitors of XPO1 using differing chemical strategies. Below I will discuss the brief history and origins of nuclear export inhibitors in which there are currently three categories: bacterial, herbal and synthetic,

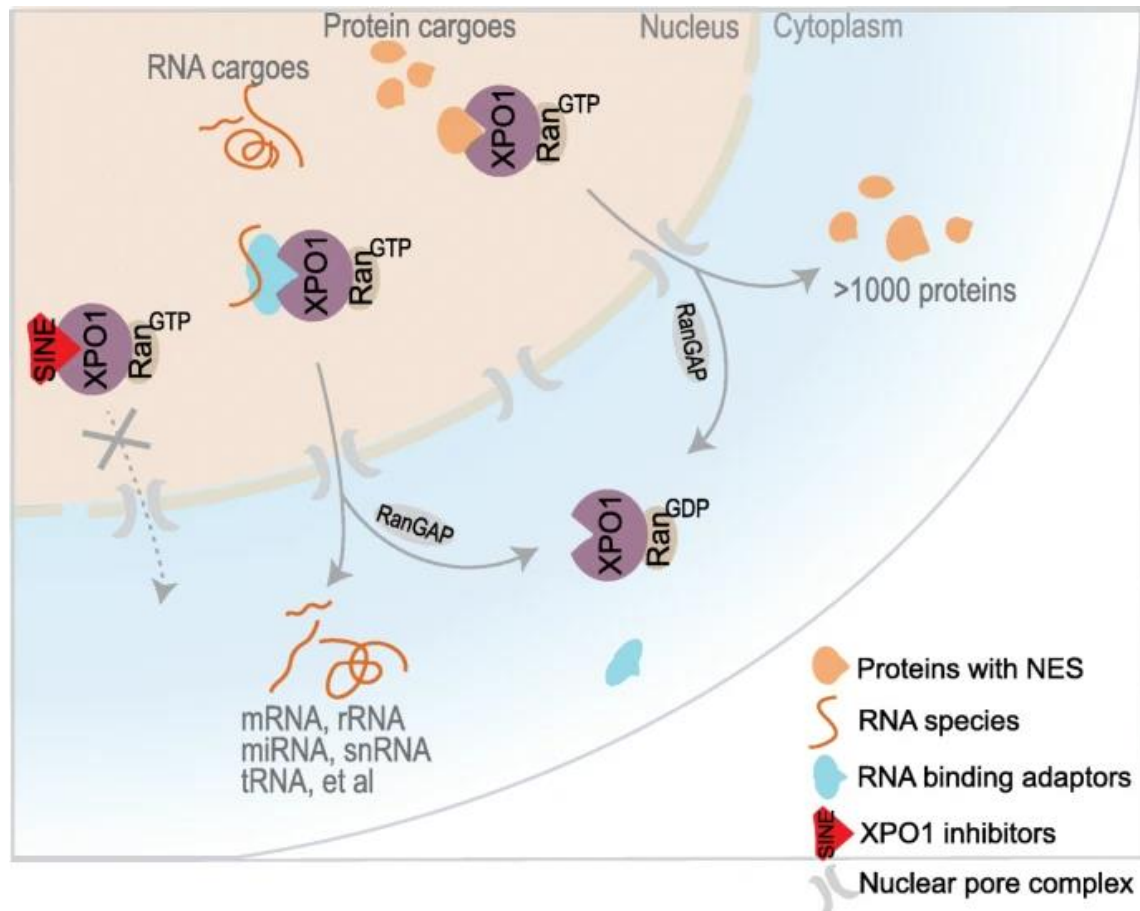


**Figure 1.1: Overview of the nuclear export process via XPO1/CRM1.** Nuclear export occurs through the nuclear pore in all cells. XPO1 and RANGTPs bind to a cargo protein through the leucine rich NES forming a tricyclic complex. XPO1 binds to a cargo protein through the leucine rich NES that is aided by RANGTPs. Once this complex forms it travels through the nuclear pore to the cytoplasm where the RAN-GTP is hydrolyzed to RAN-GDP and the cargo protein is released into the cytoplasm. The dissociation causes XPO1 to go back to the nucleus for another round of transport. XPO1 inhibitors, such as LMB, bind to the NES region where proteins normally bind and block nuclear transport. Adapted from [Azizian and Li, 2020] which is an open access article distributed under the terms of the Creative Commons CC BY license, which permits unrestricted use, distribution, and reproduction in any medium.

all of which have shown anti-cancer properties in pre-clinical investigations.

### 2.2.1 Bacterial nuclear export inhibitors

The bacterial nuclear export inhibitors includes Leptomycin B (LMB) and Ratjadone c [Meissner et al., 2004]. LMB, as discussed above, is a potent inhibitor of XPO1 that binds covalently to the NES recognizing the Cys528 amino acid residue located within the XPO1 binding groove. However, due to substantial toxicities associated with its permanent covalent interaction with XPO1, this compound cannot be used safely in humans. LMB is a large molecule with polyketide chains and hydrophobic binding regions which sequesters the NES sequence (at cysteine 528 residue) on XPO1, allowing for the inhibition of this protein (**Figure 1.2**). It was discovered that the functional groups on LMB, when bound to XPO1, re-oriented in a way that caused a covalent and irreversible inhibition of XPO1 through hydrolysis of tetrahedral intermediates [Kudo et al., 1998]. Ratjadone C ((2R)-2-[(1E,3Z,5R,7E,9E,11S)-11-hydroxy-11-[(2R,4S,5R,6R)-4-hydroxy-5-methyl-6-[(E)-prop-1-enyl]oxan-2-yl]-3,5,7-trimethylundeca-1,3,7,9-tetraneyl]-2,3-dihydropyran-6-one) is a natural compound that is derived from the mycobacterium *Sorangium cellulosum* and is similar in structure to LMB (**Figure 1.2**) [Meissner et al., 2004]. As with LMB, Ratjadone C inhibits the growth of multiple myeloma cells [Theodoropoulos et al., 2020] but no further testing was performed *in vivo* and whether its toxicity profile is similar to LMB remains unknown.

### 2.2.2 Herbal nuclear export inhibitors

Herbal XPO1 inhibitors include the active agent in turmeric (1E,6E)-1,7-Bis(4-hydroxy-3-methoxyphenyl)hepta-1,6-diene-3,5-dione) (curcumin), and hydroxyl-1,4-naphthoquinone (plumbagin) (**Figure 1.2**). Curcumin has shown effectiveness in

preclinical *in vitro* and *in vivo* investigations [Jin 2018]. The mechanism of action of this compound is a Michael addition reaction where the curcumin acts as a Michael acceptor reacting with the Cysteine 528 residue of XPO1 to eliminate its ability to be exported to the cytoplasm [Niu et al., 2013]. Although this natural compound is effective, it has been shown to have poor bioavailability and has several off target effects making it an undesirable clinical compound [Lopresti 2018]. Plumbagin, a compound found in the carnivorous plants *Drosera* and *Nepenthes*, has been found to inhibit XPO1 activity both *in vitro* and *in vivo* through modulating AMPK and the RAS/MEK/ERK pathway [Liu et al., 2017].

### 2.2.3 Synthetic nuclear export inhibitors

Various synthetic inhibitors were identified on drug screening assays for their ability to inhibit XPO1 activity. Some of these synthetic *in vitro* compounds includes selective inhibitors of nuclear export (SINE): KPT-185 (propan-2-yl (Z)-3-[3-[3-methoxy-5-(trifluoromethyl)phenyl]-1,2,4-triazol-1-yl]prop-2-enoate) and KPT-251 ((Z)-2-(2-(3-(3,5-bis(trifluoromethyl)phenyl)-1H-1,2,4-triazol-1-yl)vinyl)-1,3,4-oxadiazole), CBS9106 (N-[(S)-1-carbethoxy-1-butyl]-(S)-alanine) and PKF050-638 (N-azolylacrylate) (**Figure 1.2**). All of these synthetic compounds have a nearly identical mechanism of action to LMB, that is binding to the cysteine 528 residue within the XPO1 binding groove, which inhibits the natural function of XPO1 [Sun et al., 2016; Muqbil et al., 2018; Daelemans et al., 2002, Sakakibara et al., 2011]. Synthesized *in vitro* tool compounds KPT-185 and KPT-251 are structurally similar to LMB but differing chemical properties on the functional side chains made these compounds tolerable. Further, these compounds lack the side chain structures found on LMB, which causes irreversible inhibition of XPO1 [Sun et

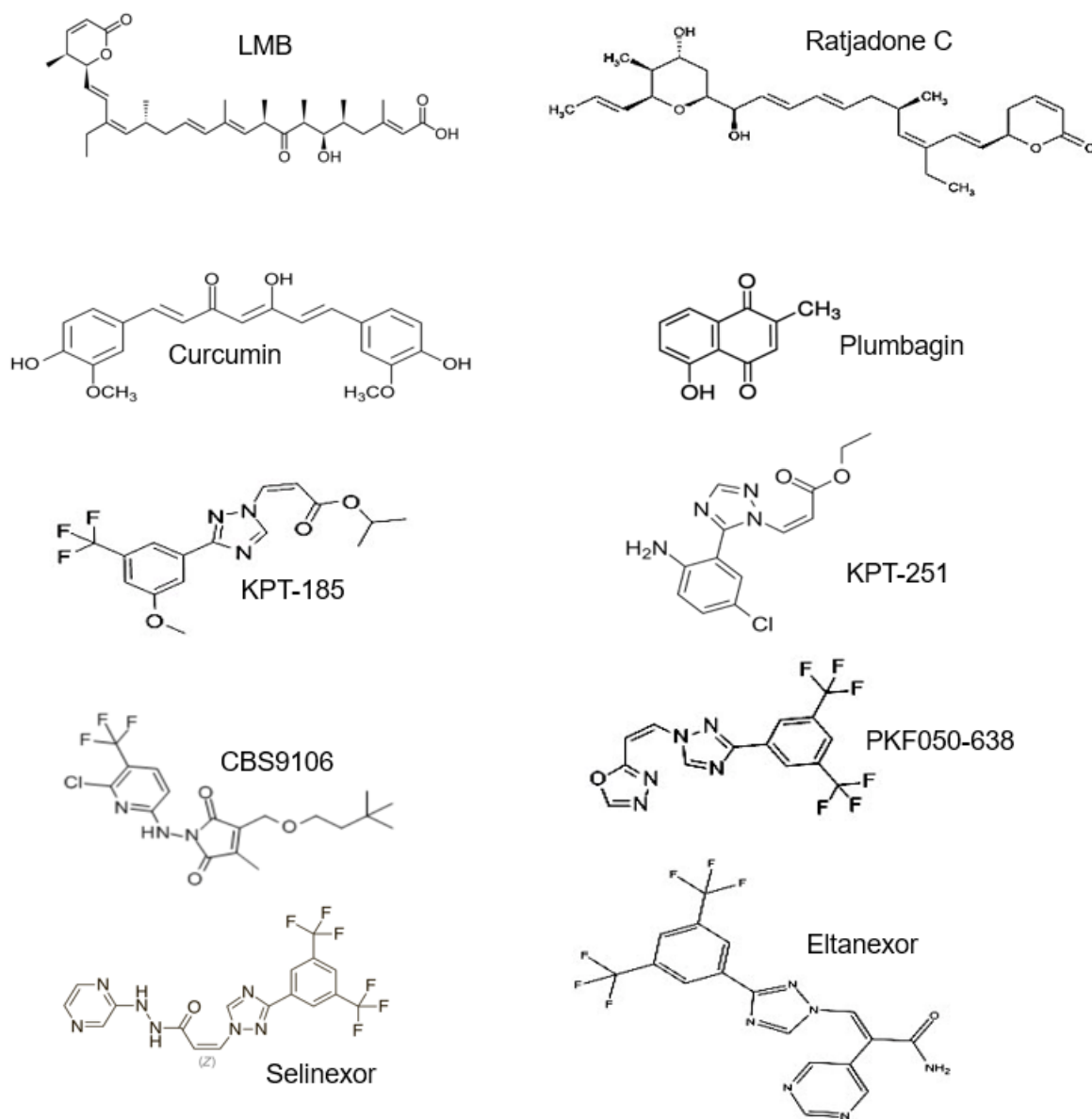


**Figure 1.2: Inhibitors of XPO1 activity.** The three classes of XPO1 inhibitors include bacterial (LMB and Ratjadone C), herbal (Curcumin and Plumbagin) and synthetic *in vitro* inhibitors (KPT-185, KPT-251, CBS9106 and PKF050-638). All inhibitors target cysteine 528 residue on XPO1 allowing for the blocking of XPO1 to cargo protein.

al.,2013]. The lack of identical side chain on the SINEs results in no occupation of the space below the NES helix leading to a reversible inhibition of XPO1, a distinctive difference.

KPT-185 and KPT-251 occupy the space above the Cysteine 528 residue (cysteine 539) which is unoccupied by LMB, suggesting SINE shift upward within the NES binding groove and interact exclusively through hydrophobic interactions unlike LMB which interacts with electrostatic and hydrophobic interactions [Lapalombella et al., 2012]. These subtle but critical differences suggested that further modifications on these side chain functional groups were possible to allow for further refinement of the SINE compounds to reduce toxicities and enhance efficacy.

#### **2.2.4 First and second-generation selective inhibitors of nuclear export (SINE)**

Modifications of KPT-185 and KPT-251 led to the first and second-generation reversible XPO1 inhibitors KPT-330 (selinexor) ((Z)-3-[3-3,5-bis(trifluoromethyl)phenyl]-1,2,4-triazol-1-yl]-N'-pyrazin-2-ylprop-2-enehydrazide) and KPT-8602 (eltanexor) ((E)-3-[3,5-bis(trifluoromethyl)phenyl]-1,2,4-triazol-1-yl]-2-pyrimidin-5-ylprop-2-enamide)

**(Figure 1.2).** Selinexor is structurally similar to KPT-251, has potent pre-clinical and clinical efficacy in a variety of cancer cell models by reducing growth, inducing cell cycle arrest and stimulating apoptosis [Rosen et al., 2021; Marijon et al., 2021; Galinski et al., 2021]. In 2019, the FDA approved oral selinexor for use in penta-refractory multiple myeloma and in 2020 for use in combination with R-CHOP chemotherapy in diffuse large B-cell lymphoma [Kasamon et al., 2021]. Compared to LMB, selinexor is a better tolerated compound with some anticipated toxicities, including gastrointestinal symptoms and hyponatremia that are manageable and reversible with supportive care [Gavriatopoulou

et al., 2020]. KPT-8602 (eltanexor) is the second-generation SINE compound which is currently undergoing clinical testing in a Phase I/II clinical trial for relapsed cancer patients and has shown tolerability and reduction of toxicities that have been seen previously with selinexor [Clinical Trial Identifier: NCT02649790].

### **2.3 Clinical progress of selinexor**

As mentioned above selinexor has been FDA approved for use in certain hematological malignancies. Below we will detail some of the safety and efficacy studies that have been performed with not only the two clinical trials in multiple myeloma and diffuse large B-cell lymphoma but others that have studied in depth the pharmacology parameters of this compound. Future studies are looking at the pharmacologic profile of the second-generation SINE compound eltanexor.

#### **2.3.1 Pharmacokinetic properties of selinexor**

As mentioned above selinexor has been investigated in clinical trials with favorable results including a complete investigation into its pharmacology profile [Karyopharm Therapeutics Inc, 2019]. According to the ADME (Absorption, Distribution, Metabolism, and Excretion) pharmacokinetic parameters, selinexor absorption is orally bioavailable occurring between 2-6 hours of ingestion [Karyopharm Therapeutics Inc, 2019, Bader et al., 2021]. The plasma protein binding has been measured at greater than 95% and has little interaction with the red blood cells [Karyopharm Therapeutics Inc, 2019; Bader et al., 2021]. Further, the volume of distribution ranged between 1.5 and 2 liters per kilogram suggesting its ready distribution into tissues. The metabolism of selinexor occurs mainly within the liver and occurs via cytochrome enzymes, resulting in a half-life of ~6 hours. During selinexor metabolism, the trans-isomer KPT-375 is a common metabolite

[Karyopharm Therapeutics Inc, 2019; Bader et al., 2021]. Selinexor is excreted through the hepatobiliary route via the feces and minimally through the urine. The total recovery of this compound was 93 percent, suggesting there is minimal long-term retention of this compound or any of its metabolites, such as KPT-375, and a clearance ratio (CL/F) of 17.7 liters/hour [Garzon et al., 2017; Karyopharm Therapeutics Inc, 2019; Bader et al., 2021].

### **2.3.2 Pharmacodynamic properties of selinexor**

The pharmacodynamic parameters of selinexor were also measured in clinical trials. Primary pharmacology studies revealed *XPO1* mRNA levels after selinexor treatment were induced in peripheral blood cells with the maximum effect being observed at 4 hours and was sustained up to 48 hours. Secondary pharmacology of selinexor was assessed for potential effects on the heart QTc interval prolongation after *XPO1* inhibition, which was hypothesized to interfere with hERG potassium current channel conduction. Studies found no differences in the toxicity and cardiovascular system of primates and no QT prolongation is anticipated at the upper dosing of selinexor [Karyopharm Therapeutics Inc, 2019; Tremblay et al., 2021].

### **2.3.3 Patient demographics and selinexor**

Various patient populations were studied to identify whether a subgroup would have adverse reactions from selinexor. Patients with renal function impairment showed no impact on the pharmacokinetics of selinexor regardless of their baseline creatine status but those with impaired hepatic function did have some effect on clearance (14.1% lower levels compared to hepatic competent patients) [Karyopharm Therapeutics Inc, 2019; Tremblay et al., 2021]. Interestingly, the volume of distribution, clearance and half-



life were independent of dosing, where as the plasma export was proportional across a wide range of dosing > 85 mg/m<sup>2</sup> [Karyopharm Therapeutics Inc, 2019; Tremblay et al., 2021]. Since patients vary in gender, race and body composition, these factors were taken into account. It was found that there were little clearance differences between males and females (17.7 vs. 14.3 liters per hour respectively). There were no significant differences found between drug elimination and race, but one glaring issue of this comparison is the significantly diminished variability in populations that were assessed (607 Caucasian vs 46 (African American)/15 (Asian) /35 (other) respectively) [Karyopharm Therapeutics Inc, 2019; Tremblay et al., 2021]. Body mass did show differences in drug clearance where the leaner population (based on body mass index ratios) showed lower clearance ability than obese patients (76% vs 38%) [Karyopharm Therapeutics Inc, 2019; Tremblay et al., 2021].

## **2.4 Conclusions**

The inhibition of XPO1 has been studied since the 1960s and has gained monumental attention in recent years with improvements in technology and drug design strategies. Not only is XPO1 inhibition feasible but it has already been tested in a number of malignancies with favorable results. An in-depth investigation into gastric cancer is needed to identify novel treatment strategies for this deadly disease.

## CHAPTER 3- XPO1 IS UPREGULATED IN GASTRIC CANCER

### 3.1 Introduction

As mentioned in **Chapter 1**, gastric cancer is a deadly disease with high heterogenic intra and inter tumor variability. Disease development is due to many causes including biological changes, such as HER2 amplifications, genetic components (*CDH1* downregulation) and environmental factors (high salt diet, poor refrigeration, and smoking). Within the field, the bulk of the research is focused on developing more effective HER2 targeted treatments and identifying subsets of gastric cancer patients that will respond favorably to immunotherapy. These patient populations are somewhat small, ~10% to 30%, and due to the high heterogeneity of this disease, it is difficult to find treatment strategies that will be effective across large gastric cancer populations. Within this chapter, we will present data suggesting XPO1 is overexpressed in gastric cancer cell lines and tissues. We will also show that XPO1 overexpression is a pathogenic cellular event that can perpetuate gastric cancer disease.

### 3.2 Materials and methods

#### 3.2.1 Cell lines, culture conditions and reagents

In this study, the NCI-N87, SNU-1 and SNU-16 cells, purchased from American Type Culture Collection (ATCC, Manassas, VA, USA), were used (**Table 1**). Cell lines were maintained in RPMI-1640 (hereafter referred to as RPMI) (Invitrogen, Carlsbad, CA, USA) supplemented with 10% fetal bovine serum (FBS) and 1% penicillin/streptomycin (P/S) in 5% CO<sub>2</sub> atmosphere at 37 °C. Cell lines were purchased in 2017 and were tested and authenticated most recently on August 28, 2018. Primary antibody against XPO1, primary antibody against  $\beta$ -actin and siRNA constructs (targeting XPO1 or silenced

	<b>NCI-N87</b>	<b>SNU-1</b>	<b>SNU-16</b>
Histology	Metastatic	Poorly-differentiated	Poorly-differentiated
Stage	IV	I	IV
Pre-Treated	No Treatment	No Treatment	No Treatment
Major Genetic Aberrations	HER2 amplification	E-cadherin ( <i>CDH1</i> ) methylation (silenced), Downregulation of MutL Homolog 1 protein ( <i>hMLH1</i> ), <i>COX2</i> absence	Fibroblast growth factor ( <i>FGF</i> ) amplification, keratinocyte growth factor ( <i>KGF</i> ) amplification, Myc Proto-oncogene ( <i>Myc</i> ) amplification,

**Table 1: Descriptive Characteristics of Gastric Cancer Cell Lines.** The NCI-N87, SNU-1 and SNU-16 cell lines were obtained from ATCC. The initial lab in which the cells were isolated and characterized provided descriptive characteristics [Park et al., 1990; Park et al., 2005].

control) were purchased from Santa Cruz Biotechnology (Santa Cruz, CA, USA). Anti-Mouse secondary antibody was purchased from Cell Signaling (Danvers, MA, USA). XPO1 overexpression vectors (XPO1, NM\_003400 Human Tagged ORF Clone pCMV6-Entry) or empty vector (pCMV6-Entry) was purchased from OriGene (Rockville, MD, USA) and Lipofectamine 3000 was purchased from Thermo Fisher (Waltham, MA, USA).

### **3.2.2 XPO1 silencing**

$5.0 \times 10^4$  NCI-N87 cells were plated in 24-well plates with RPMI only and incubated for 24 h. The following day siXPO1 or siControl (10  $\mu$ M) was mixed with Lipofectamine (1 mg/mL) according to the manufacturer's protocol (Thermo Fisher (Waltham, MA, USA)) for a final concentration of 2.5  $\mu$ g per well and added individually to the cells in medium containing RPMI + 10% FBS. Cells were incubated for 72 h with siRNA/Lipofectamine complexes. After incubation, the cells were trypsinized and either re-plated for a subsequent MTT assay (see section **3.2.5**) or underwent protein collection (see section **3.2.8**).

### **3.2.3 XPO1 transient overexpression**

$3.0 \times 10^5$  NCI-N87 cells were plated in 24-well plates with RPMI plus FBS only (~70% confluence). The following day 1  $\mu$ g of empty vector or XPO1 vector (NM\_003400 Human Tagged ORF Clone pCMV6-Entry) were mixed with Lipofectamine (1 mg/mL) according to the manufacturer's protocol for a final concentration of 2.5  $\mu$ g and added individually to the cells in medium containing RPMI + 10% FBS. Cells were incubated for 72 h with siRNA/Lipofectamine complexes then trypsinized and were either re plated for MTT assay or underwent protein collection. For colony formation assays, cells were initially transfected for 72 h, as explained above, then the media was aspirated, the cells

were washed and the cells were again transfected for another 72 h, according to the above methods. Immediately after the double transfection, the cells were trypsinized, collected and re-plated on 10 mm dishes and subjected to the protocols mentioned in

#### **3.2.4.**

#### **3.2.4 Colony formation**

NCI-N87 cells were plated at a density of 75% confluency in complete medium. The following day fresh complete media along with siXPO1 or siControl at 5 uM was added to the cells at the indicated concentration along with Lipofectamine 3000. Cells were incubated for 72 h washed and re-silenced for another 72 h. After incubation, cells were washed, trypsinized and plated at very low density ( $1 \times 10^3$  cells/mL) in complete media and incubated until sufficient visible colonies (50 cells per colony) were detected, fifty cells per colony visualized under the microscope, in any of the plates. Plates were then fixed with 100% methanol for 5 min and stained with Coomassie blue.

#### **3.2.5 MTT assay**

SiControl, siXPO1, empty vector or XPO1 vector transfected NCI-N87 cells (section 3.2.2) were seeded at a density of  $1 \times 10^4$  cells per well in 96-well micro-titer plate in complete media. After 72 h of incubation the MTT assay was performed by adding 20  $\mu$ L of 3-(4,5-dimethylthiazol-2-yl)-2,5-diphenyltetrazolium bromide (MTT) (Sigma, St. Louis, MO, USA) solution (0.5 mg/mL in PBS) to each well and incubated for 2 h. After the supernatant was aspirated, cells were lysed in 100  $\mu$ L of 100% 2-propanol leading to the dissolving of the formazan crystals within the cells. The plates were rocked for 30 min in a gyratory shaker and absorbance was measured at 570 nm via a plate reader.

### 3.2.6 Trypan blue cell viability assay

After transfection or treatment suspension SNU-1 cells, (empty vector or XPO1 transfected vector) or SNU-16 cells (siControl, siXPO1, empty vector or XPO1 transfected vector) were seeded at a density of  $2.5 \times 10^4$  cells/well in a 24-well plate in complete RPMI. After 72 h of incubation, the cells were mixed well with a pipette, collected and diluted 1:1 with Trypan blue, 20  $\mu$ L each. The cells were counted using a hemocytometer.

### 3.2.7 Immunohistochemistry

Under a DMC IRB approved protocol: (1608015145A002) gastric tissues including normal dysplastic (7 tissues), primary intestinal (3 tissues), primary diffuse (4 tissues), and lymph node metastasis (17 tissues) were obtained from the Karmanos Cancer Institute Biobank. The Karmanos Cancer Institute BioBanking core performed staining of XPO1. IHC assays were performed on a Biogenex i6000 automated stainer using a Cell Marque Hi-Def Polymer Detection Kit. Anti-XPO1 antibody was obtained from Abcam (Waltham, MA, USA) and used at a dilution of 1:100 for staining the tissue. The staining score for IHC was calculated by a semi-quantitative assessment of both the staining intensity (graded as: -, negative; +, weak; ++, moderate; or +++, strong) and the percentage of positive cells over the total cells. The calculation formula was: Staining score = (% stained cells at 1+)  $\times$  1 + (% stained cells at 2+)  $\times$  2 + (% stained cells at 3+)  $\times$  3. For the retrospective analysis and according to the IRB approved protocol (20-09-2719-M1) normal gastric tissue (172) and gastric cancer tissues (182), matched and unmatched, were obtained from the Karmanos Cancer Institute Biobank with a record of race and stage in a smaller subset of cases (**Table 2**). The demographics consisted of 58 African American and 77 Caucasian Americans. Tissues were stained for XPO1

Diagnosis Year	African American (# of patients)	Caucasian (# of patients)	Stage	African American	Caucasian
2009	13	36	0	_____	_____
2010	15	27	I	23	35
2011	25	30	II	15	29
2012	9	22	III	31	35
2013	16	24	IV	45	92
2014	8	17	Unknown	_____	_____
2015	10	17			
2016	11	20			
2017	12	11			
Total	119	204			
Patients					

**Table 2: Patient demographics for XPO1 IHC study.** The tissues were obtained from Karmanos Biobank and were deposited between 2009 and 2017. The breakdown of the number of specimens as well as the stage of disease are provided for reference.

expression as above. After staining, a pathologist scored the tissues based on XPO1 expression and were graded between 0-4 and a sum expression of the tissues was calculated, as described above. After scoring, we compared the matched gastric cancer and normal tissues to calculate fold change.

### **3.2.8 Western blotting**

Normal human gastric epithelial cells (Cell Applications Inc, San Diego, CA) and gastric cancer cell lines SNU-1, SNU-16 and NCI-N87 were plated at a density of  $2.5 \times 10^5$  cells/ml in 24-well plate in complete media. Normal human gastric epithelial media was purchased from Cell Applications (San Diego, CA, USA) and the cancer cell lines were cultured in RPMI-1640 media supplemented with 10% Fetal Bovine Serum and 5% Penicillin-Streptomycin for 24 h. Cells were then collected, and protein was extracted using Radio-immunoprecipitation assay (RIPA) Buffer and western blotting was performed by running proteins in 10% SDS-page bis-acrylamide gel (BioRad, Hercules, CA). Proteins were transferred from SDS-page gel to PDVF membrane and transferred at 100 V for 2 hours at 4 degrees Celsius. After transfer, the PDVF membrane was incubated in 5% milk dissolved in PBS + 0.01% Tween 20 (PBS-T) (Thermo Fisher, Waltham, MA) for one-hour at room temperature. Primary antibody was added at 1:2500 dilution in 5% milk-PBST and incubated overnight at 4 degrees Celsius. The following day the membranes were washed three times, 15-minutes each, in PBS-T with gentle agitation. The membranes were then incubated in 5%-milk-PBST with secondary antibody (either mouse or rabbit depending on initial host species of primary antibody) at a concentration of 1:5000 at room temperature. After secondary antibody addition, the membranes were washed with PBS-T, three times for 15-minutes each, and developed



using chemiluminescence through interaction with the HRP tag found on the secondary antibody (Thermo Fisher, Waltham, MA, USA). Detection was performed using the BioRad ChemiDoc Imaging system (BioRad, Hercules, CA, USA). Housekeeping genes were used to assess the loading of protein within the gel (Beta-Actin). Densitometry was calculated using ImageJ software. The blots were loaded to the software for analysis. The background was first subtracted from the blot and the image was then inverted. Densitometry was taken using the mean grey analysis and calculated by the ImageJ software. ImageJ assessed the protein bands of interest and the housekeeping genes.

Normalization of the protein bands of interest were made by comparing to the housekeeping gene (Beta-actin) with the following calculation (protein of interest/housekeeping gene) for each individual band and its corresponding housekeeping gene. The individual bands were then normalized to the control, or untreated, lane by the following calculation (experimental band value/control band value). Statistics of the western blotting were found using GraphPad PRISM software plotting the intensity values of the three independent experiments and using two-tailed t-test at 95% confidence interval to verify. Independent validation was performed using Excel software as well.

### **3.2.9 Statistics**

Statistics was performed using GraphPad Prism, excel (where denoted), or F-distribution calculator using two-tailed t-test with 95% confidence interval.

## **3.3 Results**

### **3.3.1 XPO1 Overexpression occurs in gastric cancer cell lines and patient tissues**

*In vitro* XPO1 overexpression was found using western blot comparison of normal

primary epithelial gastric cells and three distinct gastric cancer models: SNU-1, SNU-16 and NCI-N87 (**Figure 2.1**). We wanted to assess whether XPO1 overexpression was found in gastric cancer tissues. Using immunohistochemistry, we stained for XPO1 and found overexpression of XPO1 ( $p < 0.05$ ) significantly within a small gastric cancer cohort compared to normal tissue and XPO1 expression was prominent in the primary stage of disease (**Figure 2.2**). We observed XPO1 overexpression within dysplastic tissue as well as in different subtypes of disease (**Figure 2.2**). This finding confirms other observations within the literature suggesting XPO1 is overexpressed in the gastric cancer tumor tissues compared to normal [Subhash et al., 2018].

### **3.3.2 XPO1 expression and survival disparities**

African Americans face a disproportional risk of gastric cancer development, 1.8 to 2.2 times higher, within both men and women respectively in comparison to the Caucasian population [Ashktorab et al., 2017]. A recent comparison between surveillance, survival and epidemiological results between 1997 and 2010 suggested the African American population had an increased diagnosis of non-cardia gastric cancer (poorly-differentiated gastric cancer located within the upper stomach and/or esophagus), with squamous histology (92% to 48%) [Ashktorab et al., 2017]. Furthermore a lack of early interventions occurs more so within the African American gastric cancer population. This is due to a variety of socioeconomic factors including prevalence within the bottom income bracket (43.6% African American vs 13.9% Caucasian) and more prevalence of no insurance (5.8% African American vs. 2.1% Caucasian) which leads to reduced survival outcomes [Merchant et al., 2014; Bliton et al., 2020]. P53 mutations are disproportionately found within African American gastric cancer cohort (89%) compared to

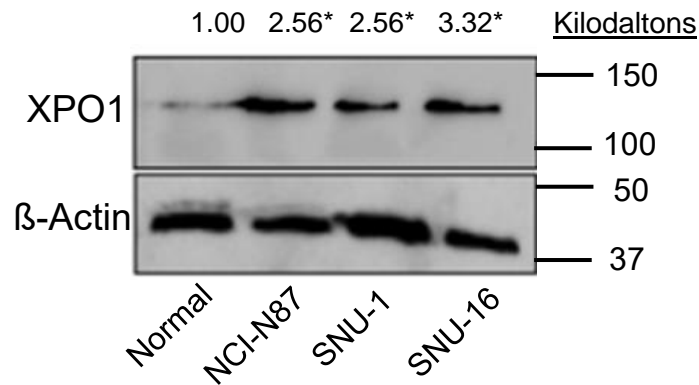


**Figure 2.1: XPO1 expression is upregulated in gastric cancer cell lines.** Normal epithelial gastric cells, NCI-N87, SNU-1 and SNU-16 cells were lysed for protein and assessed for XPO1 expression (Beta-Actin was used as a loading control) with western blotting and is representative of two independent experiments. Densitometry (mean) provided of two independent experiments. Standard error is as follows from left to right: 0.00172, 0.1754, 0.102, and 0.0888. Statistics was performed using GraphPad Prism software using two-tailed t-test at 95% confidence interval, we assessed the changes between normal cells and the gastric cancer cell lines (NCI-N87, SNU-1 and SNU-16) with \* indicative of a p-value < 0.05.

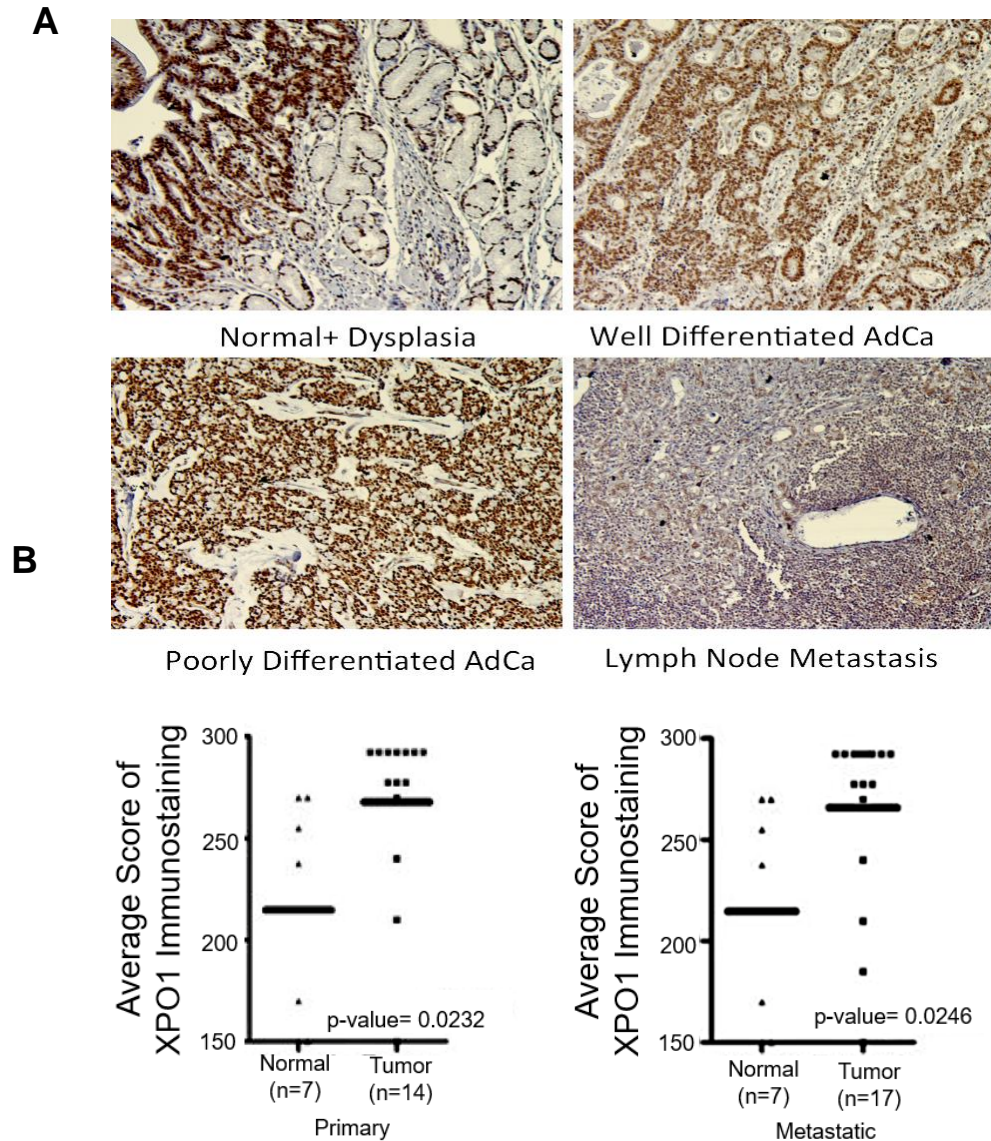


**Figure 2.2: XPO1 is overexpressed in gastric cancer patients.** [A] Patient tissues: normal/dysplastic, primary and metastatic gastric cancer tissues were stained for XPO1 and scored and the representative images are provided. Scoring results were plotted using GraphPad Prism and statistical analysis was performed to evaluate differences between normal and primary tissues [B] or normal versus metastatic tissues [C] p-values < 0.05 are considered statistically significant using two-tailed 95% confidence interval t-test.

Caucasians with TP53 mutations ( $p$ -value= 0.012) and are directly involved in the pathogenesis of this disease [van Beek et al., 2018]. P53 is a prominent tumor suppressor, which harbors an NES sequence and is involved in the pathogenesis of a variety of cancers. Since a loss of P53 is a common phenotype within African American gastric cancers, we hypothesized that this demographic may have higher levels of XPO1 compared to Caucasian gastric cancer patients, which in turn leads a more aggressive disease state. Furthermore, we hypothesize a higher frequency of XPO1 overexpression within the African American population may contribute to the racial disparity seen among patients with gastric cancer.

There is a lack of publicly available datasets to investigate this topic so we performed a large scale immunohistochemistry screen on 221 gastric cancer tissues and 138 normal gastric tissues of various stages of disease and contained near equal numbers of specimens from African American and Caucasian gastric cancer patients (119 vs 204) (**Table 2**). Following XPO1 immunohistochemistry staining, we found an increased expression of XPO1 in gastric cancer tissues compared to normal tissue and an increased rate of XPO1 expression within the African American gastric cancer cohort (**Table 3**). These results confirm our initial findings that XPO1 expression is upregulated in gastric tumors, but is dependent on stage of disease, and shed light on a demographic disparity among patients in relation to XPO1 expression. As mentioned above, gastric cancer disproportionately affects the African American community in regard to overall survival. XPO1 overexpression within this demographic may explain why this group has poorer overall survival rates and chemotherapeutic resistance.

	<b>Stage I</b> (AA n=15) (CA=21)	<b>Stage II</b> (AA n=9) (CA=15)	<b>Stage III</b> (AA n=19) (CA=18)	<b>Stage IV</b> (AA n=15) (CA=23)
African American Fold Change	2.16* (p-value=0.0342)	1.30* (p-value=0.0367)	1.50 (p-value=0.0646)	3.13** (p-value=0.00760)
Caucasian Fold Change	1.00 (p-value=0.500)	2.15 (p-value=0.0521)	1.98* (p-value=0.0165)	1.68* (p-value=0.0248)

**Table 3: XPO1 expression from gastric cancer patient tissues (AA vs CA).** Fold Change was determined by comparing the total expression scores (sum) of gastric cancer tissues (either African American or Caucasian) and normal tissues for each stage of disease. Statistics were assessed using Excel by first calculating the F-statistic ( $F = s_1^2 / s_2^2$  where s refers to sum of data). The f-value was then put into the F-distribution calculator (Statology) to obtain p-values. Significance was denoted based on p-value where \* < 0.05, \*\* < 0.01 and \*\*\* < 0.001.

### 3.3.3 XPO1 upregulation is pathogenic in gastric cancer

Literature reports have shown that XPO1 overexpression is a cancer promoting process [Rashid et al., 2018; Galinski et al., 2018] but there have been no reports directly investigating the role of XPO1 overexpression in gastric cancer. To understand the functional role of XPO1 overexpression in gastric cancer, we performed transient *in vitro* validation of XPO1 overexpression using XPO1 constructs transfected with lipofectamine 3000 in three separate gastric cancer models as a proof of principle study. Within the SNU-1, SNU-16 and NCI-N87 cell lines, we have found that XPO1 overexpression causes sustained increases in gastric cancer growth, indicative by cell viability, MTT assay and colony formation assay (**Figure 2.3**). Further, using the SNU-1 cells as a model, western blotting revealed increases in KRAS expression suggestive of increased growth signaling and viability pathways related to gastric cancer growth and proliferation were observed including stimulation of the RAS/MEK/ERK pathway (**Figure 2.3**). Together these results suggest that (1) XPO1 overexpression occurs within gastric cancer relative to normal gastric tissues and (2) overexpression of XPO1 leads to increases in gastric cancer cell viability and proliferative potential. Based on these initial results we hypothesize knockdown of XPO1 should be beneficial in reducing gastric cancer viability. Furthermore, targeting XPO1 is a targeted treatment strategy that will target gastric cancer cells more specifically than gastric tissue as a whole.

### 3.3.4 XPO1 knockdown reduces gastric cancer viability

To investigate the cellular impact of XPO1 knockdown in gastric cancer, we began by knocking down XPO1 in the SNU-16 and NCI-N87 gastric cancer cell lines with siRNA. After XPO1 knockdown, we found that there was a decrease in cell viability and colony

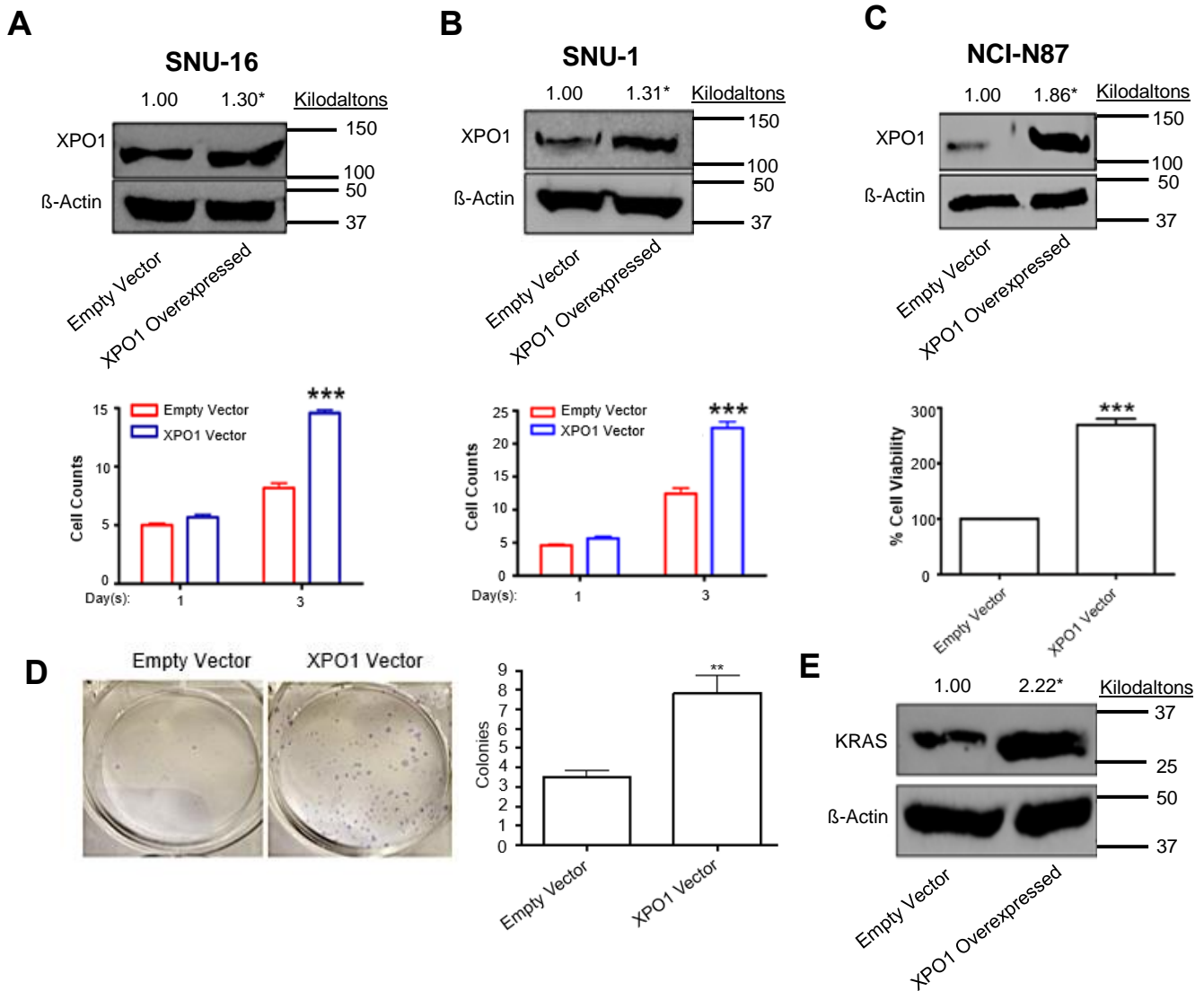


**Figure 2.3: XPO1 overexpression induces gastric cancer proliferation.** SNU-16 [A], SNU-1 [B] and NCI-N87 [C] cells were transfected with 5  $\mu$ M XPO1 vector or empty vector for 72 hours. Validation of XPO1 overexpression was done via western blot and showed statistically significant increases in cell viability in all cell lines where E.V. is referring to empty vector control. Images and graphs (mean) are representative of three independent experiments and densitometry (mean) is provided with error bars depicting standard deviation. Standard error is as follows from left to right for SNU-16: 0.0515, 0.0831, SNU-1: 0.0559, 0.0406, NCI-N87: 0.0707, 0.0434. Statistics were done using GraphPad Prism software using two-tailed t-test at 95% confidence interval where p-value \* < 0.05, \*\* < 0.01 and \*\*\* < 0.001. [D] Colony formation within the NCI-N87 cell line showed increased colony formation in the overexpressed cells with quantification provided as a representative of three independent experiments Error bars indicate standard deviation between experiments. [E] Western blotting showed increased KRAS expression in the XPO1 overexpressed SNU-1 cells compared to empty vector control. Provided image is representative of three independent experiments as well as densitometry (mean). Standard error is as follows from left to right: 0.0974, 0.14. Statistics were done using two-tailed t-test at 95% confidence interval with \* indicative of p-value < 0.05.



formation suggesting that XPO1 is a critical cellular protein and intervention of this protein may be a therapeutic approach that can be exploited to treat gastric cancer (**Figure 2.4**).

### **3.4 Conclusions**

Based on these results, XPO1 overexpression is prominent in gastric cancer patient tissues and cell lines and the consequence of this phenotype is the promotion of a pro-cancerous cellular state. Low XPO1 expression was found in primary gastric tissues, which further confirms our hypothesis of XPO1 overexpression. XPO1 overexpression was also found to be upregulated differentially (via fold-change) in gastric tissues dependent on patient demographic. Finally, we have found XPO1 knockdown is beneficial in targeting gastric cancer by reducing growth and proliferation. Based on these results, it is clear that targeting XPO1 in gastric cancer is a rational and feasible strategy to treat this deadly disease.

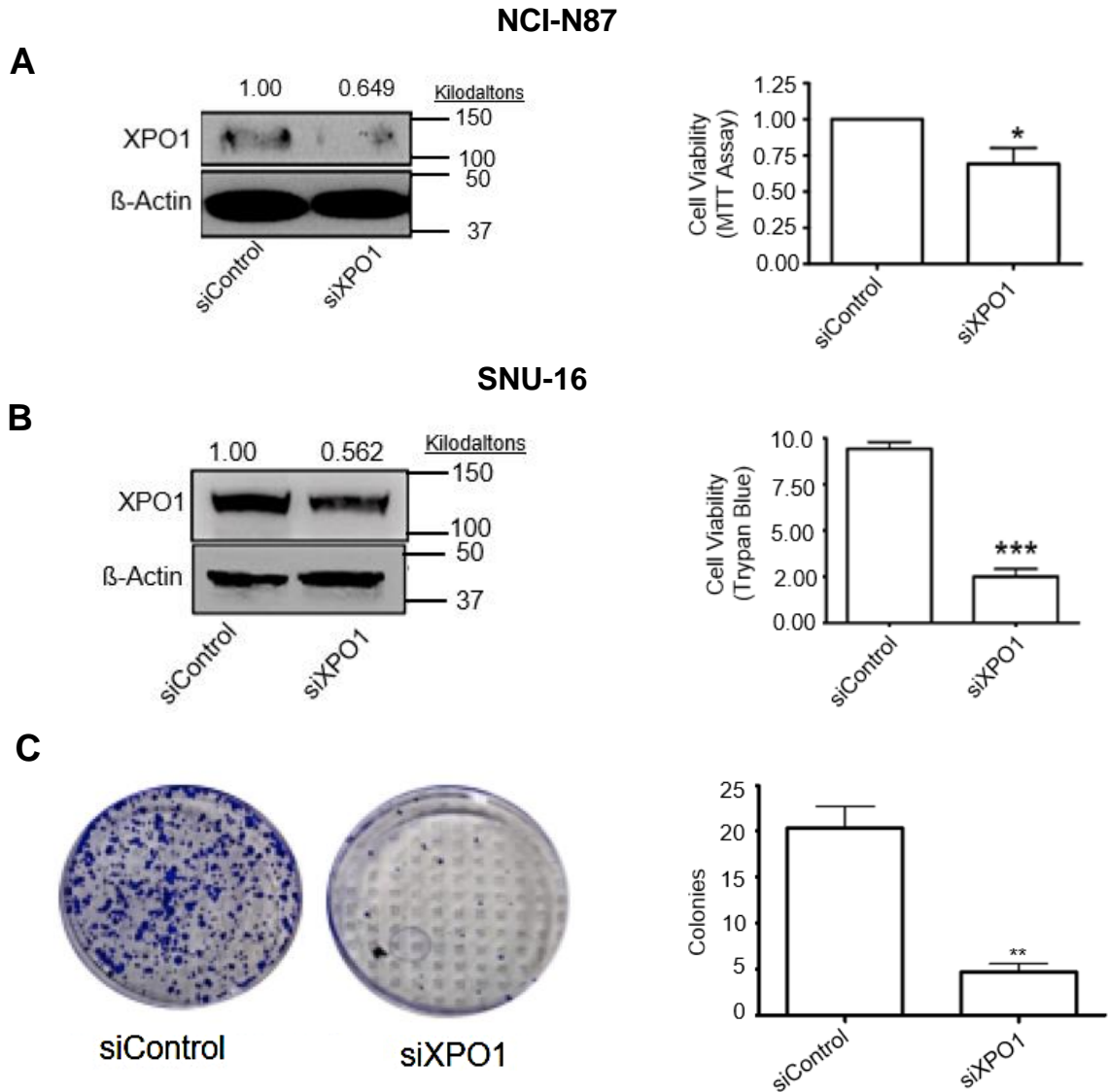


**Figure 2.4: Knockdown of XPO1 causes reduction in gastric cancer cell viability.** NCI-N87 [A] and SNU-16 [B] cells were transfected with 5  $\mu$ M siRNA targeted to XPO1 for 72 hours. Validation of XPO1 knockdown was done using western blot. Graph (average) is representative of three independent experiments and error bars denote standard deviation (n=3). Statistics were done using GraphPad software using two-tailed t-test with 95% confidence interval where p-value \* < 0.05 and \*\* < 0.01. [C] Cell viability was significantly decreased in the siControl versus knockdown NCI-N87 XPO1 inhibited cells. Colony formation is representative of three independent experiments and graph provided is an average of three independent experiments. Error bars denote standard deviation (n=3).

## **CHAPTER 4- TARGETING XPO1 IN GASTRIC CANCER**

### **4.1 Introduction**

We have found that gastric cancer exhibits high expression of XPO1 in primary tumor samples as well as cell lines compared to normal tissues (**Figure 2.1-2.2**) and that knockdown of XPO1 with siRNA reduces cellular growth and colony formation (**Figure 2.4**). This suggests that XPO1 is a bona fide therapeutic target in gastric cancer that needs further exploration. In this chapter we will describe the phenotypic changes induced after XPO1 inhibition with the XPO1 SINE inhibitors in three gastric cancer cell line models: SNU-1 (primary poorly differentiated), SNU-16 (metastatic poorly differentiated) and NCI-N87 (metastatic well-differentiated). We also assessed the impact of SINE inhibitors on normal gastric cells. Our results suggest that targeting XPO1 with SINE is beneficial in reducing disease burden both in *vitro* and in *vivo*.

### **4.2 Materials and methods**

#### **4.2.1 Cell lines, culture conditions and reagents**

For this study the NCI-N87, SNU-1 and SNU-16 cells (purchased from ATCC) were used and maintained in RPMI-1640 (Invitrogen) supplemented with 10% fetal bovine serum (FBS) and 1% penicillin/streptomycin (P/S) in 5% CO<sub>2</sub> atmosphere at 37 °C. Normal adult human epithelial cells were purchased from Cell Applications (San Diego, CA, USA) and maintained in epithelial growth media (provided by Cell Applications). Before plating, the wells of the plates were coated in collagen solution (Cell Applications) for 2 minutes. All normal cells were used up to 6 passages as recommended by the company. Cell lines were purchased in 2017 and were tested and authenticated most recently on August 28, 2018, and used up to 28 passages. Primary antibody against

XPO1 was purchased from Santa Cruz Biotechnologies (Santa Cruz, CA, USA). Cyclin D1 and p53 antibodies were purchased from Cell Signaling Technologies (Danvers, MA, USA).  $\beta$ -actin was purchased from Sigma (St. Louis, MO, USA). Anti-rabbit secondary antibody was purchased from Santa Cruz Technologies (Santa Cruz, CA, USA) and anti-mouse secondary antibody was purchased from Thermo Fisher (Waltham, MA, USA). The Annexin V FITC apoptosis kit was purchased from Biovisions (Milpitas, CA, USA) and 7-Aminoactinomycin D (7AAD) was purchased from Thermo Fisher Scientific (Waltham, MA, USA). SINEs (selinexor, eltanexor, tran (-ve control)) were provided by Karyopharm Therapeutics (Newton, MA, USA) and LMB was purchased from Santa Cruz Biotechnology (Santa Cruz, CA, USA).

#### **4.2.2 Apoptosis analysis**

NCI-N87, SNU-1 and SNU-16 cells were seeded at a density of  $5 \times 10^5$  cells/mL. The subsequent day SINE compounds were added to the NCI-N87 cells at indicated concentrations where SINEs were taken from 1 mM stock in DMSO: selinexor (1  $\mu$ M), eltanexor (1  $\mu$ M), tran (1  $\mu$ M). SINE compounds were added at the indicated concentration to SNU-1 and SNU-16 cells where SINEs were taken from 1 mM stock in DMSO: selinexor (150 nM), eltanexor (150 nM), KPT-301 (150 nM). After 72 h of incubation, the cells were assessed using 7AAD reagent according to the manufacturer's protocol. All cells were analyzed by flow cytometry via the flow cytometry core facility at Karmanos Cancer Institute using the BD-SLR II flow cytometer. The gastric cancer cells, suspended in PBS, were put through the BD-SLR II flow cytometer and assessed using laser beam, which detects different wavelengths of light emitted by the cells (either with 7AAD reagent uptake or not). The 7AAD reagent emits at a maximum wavelength of 647

nm and can be excited at 488 nm. The cells are then sorted based on the detected wavelength. Loss of membrane integrity is a hallmark of cell death and those gastric cancer cells that have taken up the 7AAD dye is considered dead (apoptotic or necrotic). Cells that do not uptake the 7AAD or Annexin V dye are viable and thus healthy and can be assessed using software to differentiate the different cellular states.

#### **4.2.3 Cell Cycle Arrest**

NCI-N87 cells were plated at a density of  $5 \times 10^5$  cells/mL in RPMI without FBS. The following day fresh complete media along with either selinexor or eltanexor was added to the cells at the indicated concentration. Cells were incubated for 72 h then collected and fixed with 70% cold ethanol. Propidium iodide (stock 1 mg/mL) and RNase A, to a final concentration of 21.5 ug/mL of propidium iodide and 0.470 ug/mL of RNase A, was then added to the cells, incubated, and submitted to the flow cytometry core at Karmanos Cancer Institute for processing using the BD SLR-II flow cytometer.

#### **4.2.4 Colony formation assay**

NCI-N87 cells were plated at a density of 75% confluency in complete medium. The following day fresh complete media along with SINE (KPT-185, selinexor, eltanexor, tran) (500 nM) or LMB (+ ve control, 250 nM) was added to the cells. Cells were incubated for 72 h, trypsinized and collected. After collection, cells were plated at very low density ( $1 \times 10^3$  cells/mL) in complete media and incubated until colonies were visualized (~50 cells/colony) was reached in any of the plates. Plates were then fixed with 100% methanol for 5 min and stained with Coomassie blue.

#### **4.2.5 MTT assay**

NCI-N87 cells or normal gastric cells were seeded at a density of  $1 \times 10^4$  cells per

well in 96-well micro-titer plate in complete media. The following day the medium was removed and replaced with medium containing SINE compounds at the indicated concentrations (0-500 nM) taken from 1 mM stock dissolved in DMSO. After 72 h of incubation, the MTT assay was performed by adding 20  $\mu$ L of 3-(4,5-dimethylthiazol-2-yl)-2,5-diphenyltetrazolium bromide (MTT) (Sigma, St. Louis, MO, USA) solution (0.5 mg/mL in PBS) to each well and incubated for 2 h. After the supernatant was aspirated, cells were lysed in 100  $\mu$ L of 100% 2-propanol to dissolve the formazan crystals produced within the cells. The plates were rocked for 30 min in a gyratory shaker and absorbance was measured at 570 nm via a plate reader. The normal cells were plated at a density of  $5 \times 10^3$  cells/well in a 96-well plate. The following day, cells were supplemented with fresh media and increasing concentrations (0-5  $\mu$ M) of selinexor or eltanexor and incubated for 72 hours. Following incubation, MTT dye was added for 2 hours and after incubation and processed as described above.

#### **4.2.6 Trypan blue cell viability assay**

SNU-1 and SNU-16 cells were seeded at a density of  $2.5 \times 10^4$  cells/well in a 24-well plate in complete medium. After subsequent acclimation (3-5 h) in 37<sup>o</sup>C incubator, single agent SINE compounds (selinexor, eltanexor, KPT-185, tran) were added to the medium (0-150 nM). SINE compounds were diluted from 1 mM stock dissolved in DMSO to 1:100 in PBS. After 72 h of incubation, the cells were mixed well with a pipette, collected and diluted 1:1 with Trypan blue, 20  $\mu$ L each. The cells were counted using a hemocytometer.

#### **4.2.7 Immunofluorescence assay**

NCI-N87 cells were grown on glass chamber slides overnight to a confluency of

~50% and exposed to KPT-185 at 1  $\mu$ M for 2h. SNU-16 cells were treated for 2 h with 50 nM selinexor then spun down on a microscope slide using a Cytospin. At the end of treatment, the cells were fixed with 4% paraformaldehyde for 10 min (NCI-N87) or 100% cold acetone for 5 min (SNU-16) and all were permeabilized with PBS plus 0.05% Triton X 100. The fixed slides were then blocked in 5% Bovine Serum Albumin (BSA) and probed with anti-p53 primary antibody (Cell Signaling) and incubation with secondary antibody (Alexa Flour 448 conjugated secondary antibody (Thermo Fisher, Waltham, MA, USA)) for one hour at room temperature. The slides were washed with PBS and ProLong Antifade mounting medium (Thermo Fisher, Waltham, MA, USA) was added to the slides before placing the coverslips. The slides were analyzed with an inverted fluorescent microscope (EVOS, Thermo Fisher, Waltham, MA, USA).

#### **4.2.8 Spheroid formation assay**

NCI-N87 cells maintained in RPMI-1640, 10% FBS and 1% P/S were trypsinized and collected. Cells were resuspended in spheroid growth medium [Lee et al., 2018] in  $1 \times 10^3$  cells per well in a 6-well low attachment plate using a cell strainer to get single cell suspensions (Corning, Durham, NC, USA). Media was changed every 4 days and spheroid growth was monitored visually using inverted microscope. For drug treatments, spheroids were transferred to a 24-well low attachment plate (Corning, Durham, NC, USA) in spheroid culture media and treated the following day. Selinexor and eltanexor were taken individually from 1 mM stock dissolved in DMSO and used at a final concentration of 500 nM.  $IC_{50}$  values were found for selinexor and eltanexor in 2D culture separately and were 862.70 nM and 403.9 nM respectively. Selinexor  $IC_{50}$  was 800 nM and eltanexor  $IC_{50}$  was 500 nM. We wanted to use the same lower concentration of both

drugs with the rationale being cells in 3D culture behave differently than in a 2D culture and found a response at this lower concentration. Growth was monitored for 10 days and images were captured using inverted microscopy assessing spheroid disruption only and the presence of intact versus dispersed spheroids.

#### **4.2.9 Western blotting**

$1 \times 10^6$  SNU-1 and SNU-16 cells were plated in complete medium and treated with 150 nM SINE (for cyclin D1 blotting) or treated with 50 and 100 nM of selinexor, eltanexor or tran. Drugs were prepared from a 1 mM stock of drug dissolved in DMSO and further diluted 1:100 in PBS (for XPO1 blotting). Cells were incubated for the indicated times, collected and lysed using RIPA lysis buffer with protease inhibitors. Cellular lysates were prepared, clarified and protein concentrations ( $\mu\text{g}$ ) were determined using the bicinchoninic acid (BCA) protein assay. Proteins were run on SDS-PAGE gel and transferred to PVDF membrane. Membranes were incubated overnight with primary antibodies (1:2500) in 3% milk at 4 °C and secondary antibodies were incubated (1:5000) in 3% milk for 1 h room temperature (RT) both with intermediate washes with PBS + Tween-20 (0.1%) 5 min each, three times. Densitometry was taken using the mean grey analysis and calculated by the ImageJ software. ImageJ assessed the protein bands of interest and the housekeeping genes.

Normalization of the protein bands of interest were made by comparing to the housekeeping gene (Beta-actin) with the following calculation (protein of interest/housekeeping gene) for each individual band and its corresponding housekeeping gene. The individual bands were then normalized to the control, or untreated, lane by the following calculation (experimental band value/control band value).



Statistics of the western blotting were found using GraphPad PRISM software plotting the intensity values of the three independent experiments and using two-tailed t-test at 95% confidence interval to verify. Independent validation was performed using Excel software as well.

#### 4.2.10 Statistics

Statistics were provided by GraphPad Prism software using two-tailed t-test at 95% confidence interval.

### 4.3 Results

#### 4.3.1 SINE inhibits gastric cancer cellular proliferation

As mentioned above, the synthetic small molecule inhibitors, which target XPO1 (SINE) are potent reversible inhibitors of XPO1 activity. In order to assess whether SINE compounds are effective in reducing gastric cancer disease we first assessed cell growth in the presence of these compounds. The SNU-1 and SNU-16 cell lines have substantial sensitivity to selinexor and eltanexor characterized by low nanomolar IC<sub>50</sub> values compared to the NCI-N87 cell line (**Table 4**). Sensitivity to the *in vitro* tool compound KPT-185 also was observed suggestive of sensitivity of gastric cancer to XPO1 inhibition (**Table 4**). This observation is clearly not due to any altered expression of baseline XPO1 (**Figure 2.1**) as all cell lines have similar expression profiles but rather may be attributed to their growth patterns where suspended cell lines, like lymphoid cancer cell models, have high sensitivity to selinexor *in vitro* [Muqbil et al., 2016]. Although the NCI-N87 cell lines have higher IC<sub>50</sub> values for selinexor and eltanexor, the doses are pharmacologically relevant. A recent phase I clinical trial showed that selinexor was present in the tumor after 6-hour treatment suggestive of the potency and ability of these compounds to

Compound	Cell Line	IC <sub>50</sub> (nM)	St. Dev
KPT-185			
	SNU-1	50.13	11.24
	SNU-16	73.18	12.45
	NCI-N87	696.30	0.652
selinexor			
	SNU-1	47.58	5.56
	SNU-16	33.68	17.18
	NCI-N87	862.70	0.405
eltanexor			
	SNU-1	52.13	18.40
	SNU-16	21.86	8.80
	NCI-N87	403.9	0.162

**Table 4: IC<sub>50</sub> values of SINE compounds in gastric cancer cell lines.** IC<sub>50</sub> values are representative of an average of three independent experiments either done by MTT assay (NCI-N87) or Trypan blue cell viability assay (SNU-1 and SNU-16). The experiments were performed as above in sections 4.2.5 and 4.2.6. Standard deviations are representative of three independent experiments.

penetrate tumors.

Further experimental validation of the effects of SINEs in gastric cancer was seen with the colony formation assay (**Figure 3.1**). Quantification revealed a significant number of colonies were reduced following treatment with KPT-185 (~30%), selinexor (~60%) and eltanexor (~60%) compared to control. The positive control showed superior reduction in colony formation (~90-100%). Using a negative analog tran (KPT-301), an isomer of the *in vitro* tool compound KPT-185, we saw no reduction of colony formation after treatment (**Figure 3.1**). Finally, a 3D culture model was used to visualize the penetrative ability of selinexor and the second-generation compound eltanexor in a more realistic 3D tumor-like condition. The results show that spheroid integrity was disrupted after 10 days indicative of the compounds ease of penetrating tumors and disrupting cancer structures (**Figure 3.1**). Due to the differing growth pattern of NCI-N87 cells (monolayer vs detached spheroid) we could treat with less selinexor to achieve phenotypic effect, as can be observed between the IC50 values of SNU-1 and SNU-16 (suspended growth pattern) compared to NCI-N87 monolayer (**Figure 3.1**).

#### **4.3.2 SINE treatment in normal gastric cells**

When making any preclinical assessment of a compound understanding the therapeutic benefit versus toxicity of a drug it is of the utmost importance. To better understand whether the benefit, the reduction in tumor burden, also impacts normal gastric tissues we utilized epithelial adherent normal cells to assess drug sensitivities. Gastric tissues, specifically the epithelial lining, can be highly sensitive to non-specific chemotherapeutic agents because these compounds target rapidly dividing cells. For the multiple myeloma clinical trial a reported side effect of selinexor was more gastrointestinal

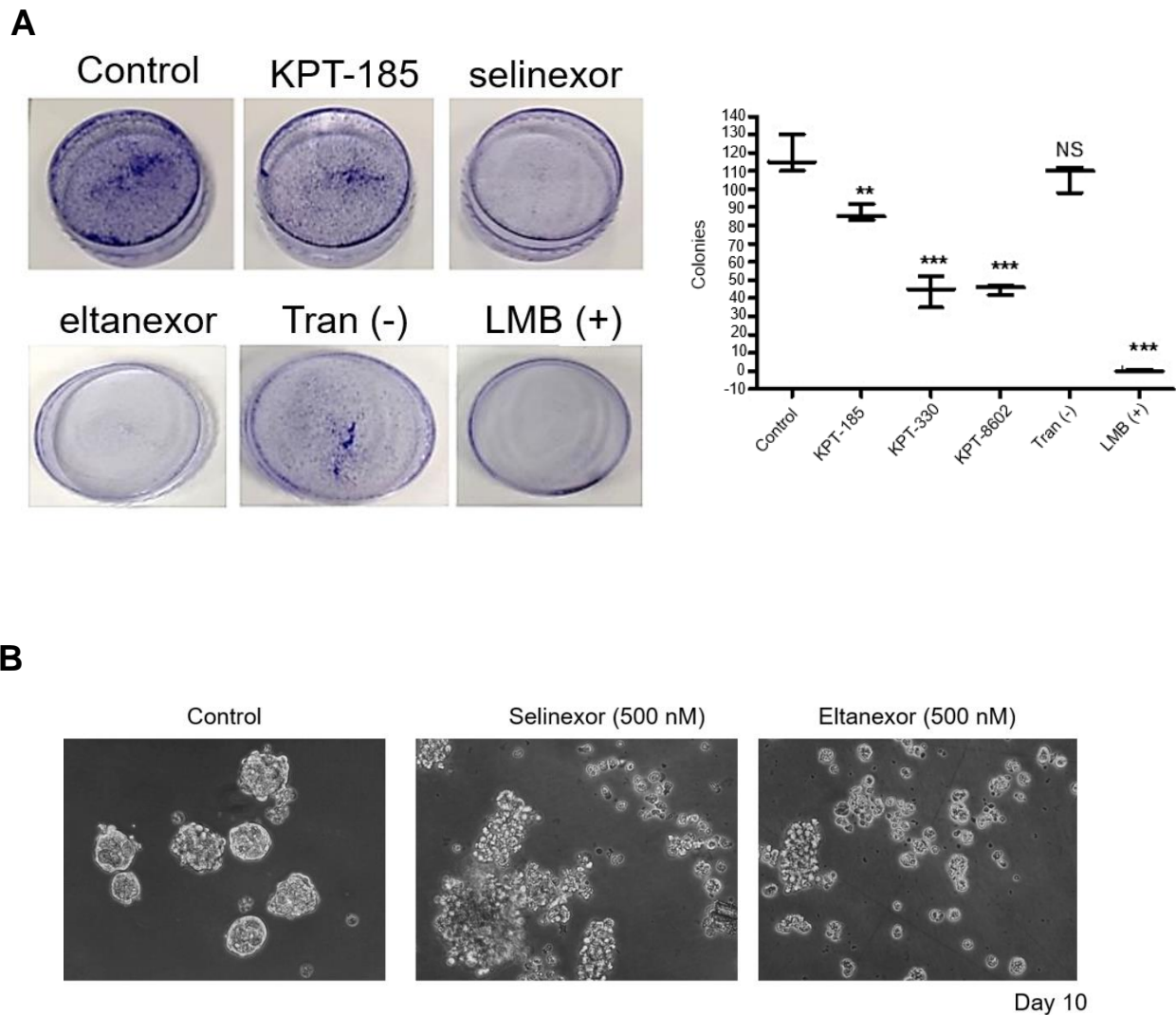


**Figure 3.1: SINEs reduce colony formation and 3D spheroid growth in gastric cancer cells.** [A] Colony formation assay showed significant decreases in colony formation with the *in vitro* tool compound KPT-185 (500 nM), first generation SINE selinexor (500 nM), second generation SINE eltanexor (500 nM) and LMB (250 nM) (+ control). Control (no-treatment) and tran (500 nM) (-ve) showed no statistical significant reduction in growth. Experiments were performed three times and quantification is representative of three independent experiments using two-tailed 95% confidence interval t-test where \*\*  $p < 0.001$  and \*\*\*  $p < 0.001$ . Graphical depiction shows standard deviations between the three experiments. [B] Spheroid formation suggests SINE disrupt gastric cancer spheroid after 10 days of treatment with either selinexor (500 nM) or eltanexor (500 nM). Results and images are a representative figure of three independent experiments.

discomfort. To test whether the normal cells of the gut can be targeted by either selinexor or eltanexor, we performed cell viability assay on normal adult epithelial stomach cells at increasing concentrations. After 72-hour treatment with either selinexor, we found no significant loss in cell survival at the highest doses (2.5  $\mu$ M) (**Figure 3.2**). Thus, the effective doses we have observed (within the nanomolar range) found to alter gastric cancer cell growth (**Table 2**), suggest that this treatment is potent and highly selective towards gastric tumors versus normal stomach epithelium.

#### **4.3.3 Physiological role of XPO1 knockdown in gastric cancer cells**

XPO1 knockdown with LMB causes a sustained suppression of XPO1 due to an irreversible inhibition. Thus, this causes indefinite dose-dependent retention of XPO1 within the nucleus [Crochiere et al., 2015]. Since SINE compounds are slowly reversible inhibitors, we wanted to test the phenotypic changes that occur after XPO1 inhibition with SINEs over time. Unlike treatment with LMB [Crochiere et al., 2015], both selinexor and eltanexor resulted in a reduction of XPO1 expression at 24 and 48 hours (**Figure 3.3**). Further, there was no altered expression of XPO1 with the negative control KPT-301 confirming the selectivity of the active analogs. The reason for this protein degradation is due to an interaction between XPO1 and the ubiquitin proteasome system (UPS) [Zheng et al., 2014; Kim et al., 2016]. After treatment with SINE compounds, unlike LMB, XPO1 is not irreversibly inhibited so dissociation of this protein from SINE leads to XPO1 traveling to the cytosol and becoming degraded by the UPS. The degradation is hypothesized to be due to a protein modification or damage to XPO1 after treatment but further investigation is needed to elucidate the exact mechanism. To experimentally validate SINE treatment hits the intended cellular target (XPO1) and causes observable

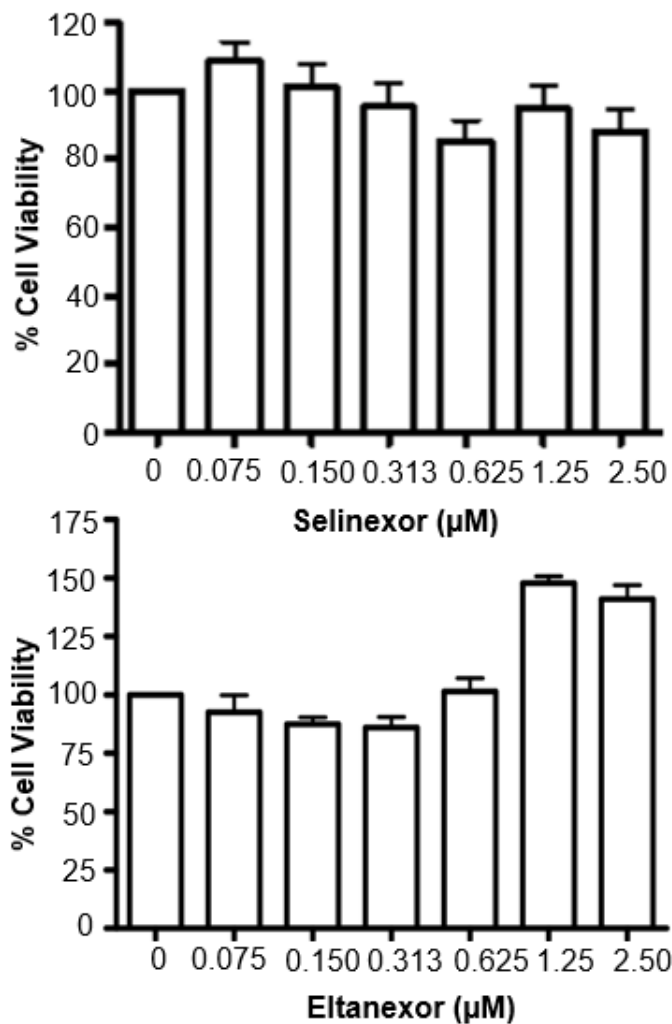


**Figure 3.2: Selinexor and Eltanexor Inhibition of Normal Gastric Cell Growth.** Normal gastric epithelial cells were treated with increasing concentrations of either selinexor or eltanexor and cell viability (MTT assay) was assessed after 72 hours. Cell viability assays shows that there is no significant cell death with either treatment. Relevant  $IC_{50}$  values from gastric cancer cell lines fall within the nM range (Table 4) and results with normal gastric cells show little to no losses in cell viability. Results are representative of three independent experiments. Graphs were generated by GraphPad PRISM software where the bars represent standard deviation between experiments.

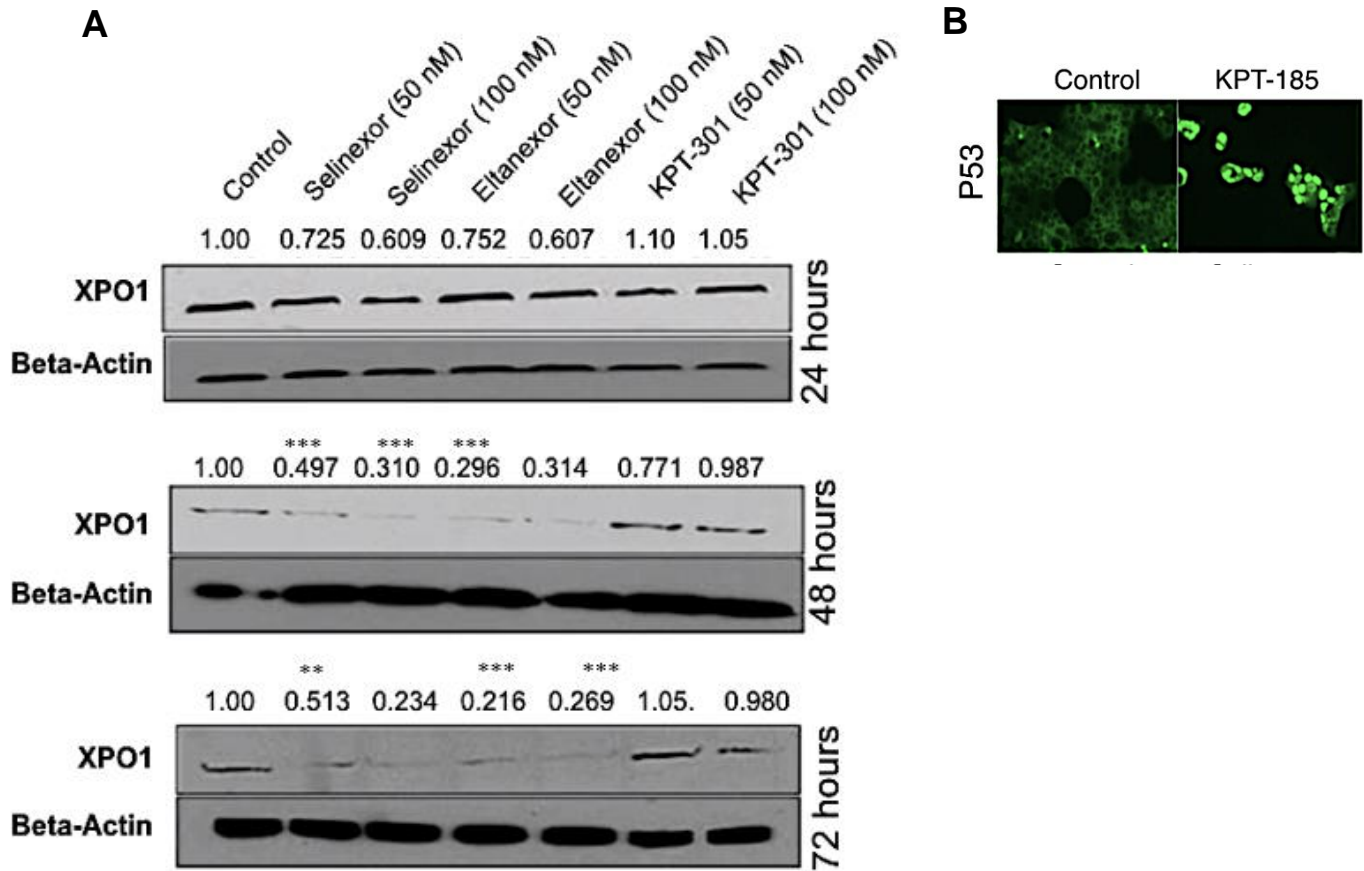


**Figure 3.3: Physiologic function of SINEs *in vitro*.** **[A]** Treatment with selinexor or eltanexor showed decreased protein expression after 24-hour treatment, each at two concentrations, suggestive of a degradation mechanism of XPO1 after inhibition with SINE. No significant downregulation was observed with negative analog tran (KPT-301). Western blots and densitometry (mean) are representative of three independent experiments. Standard error for western blots are as follows for 24 hour from left to right: 0.321, 0.277, 0.285, 0.348, 0.218, 0.278, 0.245, 48 hour: 0.369, 0.259, 0.267, 0.195, 0.231, 0.287, 0.298, 72 hour: 0.0524, 0.0686, 0.0550, 0.0471, 0.0403, 0.0651, 0.156. Significance was found using two-tailed t-test at 95% confidence interval using GraphPad PRISM software where \*\* p-value < 0.01 and \*\*\* p-value < 0.001. **[B]** Upregulation of p53 after 3-hour treatment with SINE resulted in nuclear retention. Immunofluorescence is representative of three independent experiments.

phenotypic effects we utilized immunofluorescence to visualize these cellular changes using downstream proteins directly transported by XPO1. P53 is a known tumor suppressor that has an NES sequence and was the first marker we visualized [Stommel et al., 1999]. After a 3-hour incubation with KPT-185, there was significant retention of p53 into the nucleus suggesting that XPO1 inhibition was directly retaining tumor suppressors (**Figure 3.3**).

#### **4.3.4 Cell cycle arrest induces apoptosis after SINE treatment**

LMB inhibits cell cycle at both the G2/M and G1/S phase [Mutka et al., 2009]. We wanted to see whether XPO1 inhibition with SINEs also showed similar effects in gastric cancer models. We found after 48 hours with NCI-N87 cells, there was a clear G1 phase cell cycle arrest indicative of a mechanism similar to LMB but no true G2 phase arrest (**Figure 3.4**). To experimentally validate these findings we probed for Cyclin D1, a prominent cell-cycle protein involved in stimulating the transition from G1 to S, in the SNU-1 and SNU-16 cell lines. Absence of cyclin D1 after treatment with SINEs confirms our cell cycle analysis observations of a G1/S phase arrest (**Figure 3.4**). Since we have observed that SINE treatments result in the retention of tumor suppressors and cell cycle arrest, we wanted to identify whether these events led to cell death. Using flow cytometry, we tested SINE efficacy in the three gastric cancer cell lines. Using Annexin V, which binds to the membrane-localized phosphatidylserine residues within apoptotic cells [Koopman et al., 1994], or 7-AAD, which binds to double stranded DNA by intercalating between base pairs, and undergoes a spectral shift within apoptotic cells [Zembruski et al., 2012], selinexor, eltanexor and KPT-185 all induced significant apoptosis (**Figure 3.5**)



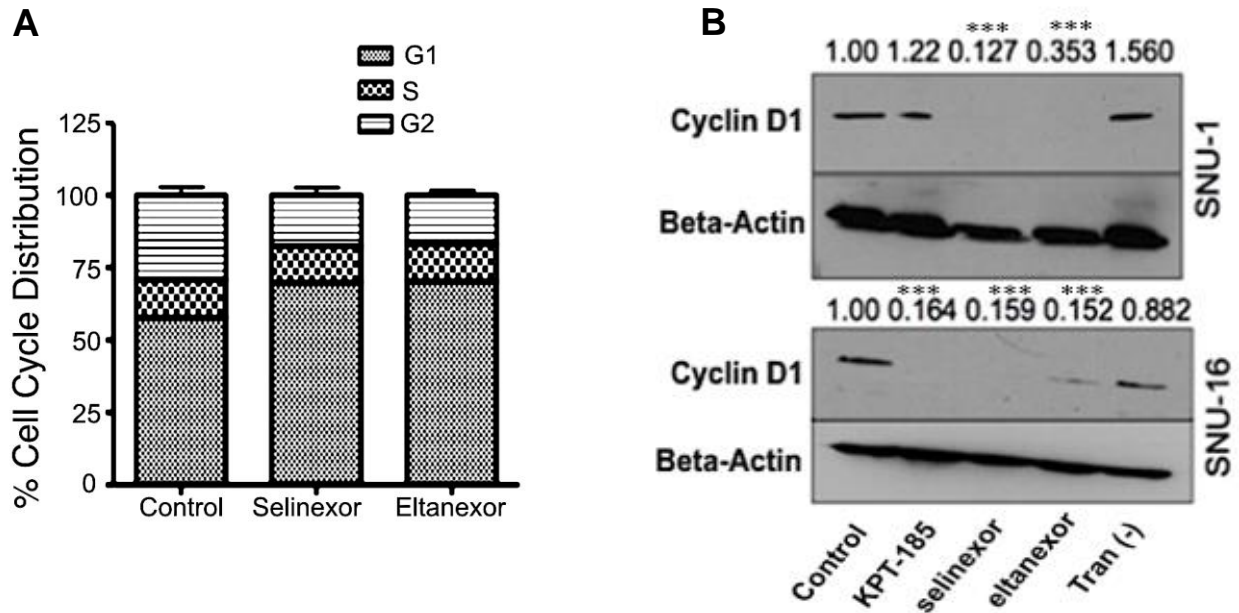


**Figure 3.4: XPO1 inhibition induces cell cycle arrest.** **[A]** Flow cytometry analysis of cell cycle in the NCI-N87 cell line showed an increase in a cell population exhibiting G1 phase cell cycle arrest after treatment with selinexor or eltanexor compared to control after 48 hours. All experiments were performed with three independent replicates with error bars representing standard deviation between experiments. **[B]** Western blotting in the SNU-1 and SNU-16 cell line showed after 72-hour treatment with KPT-185, selinexor or eltanexor that there was a loss of the cyclin D1 protein, a prominent protein involved in the transition between the G1 and S phase of the cell cycle. No significant changes in the cells treated with the negative control, KPT-301; provide further confidence in our results. All experiments were performed with three independent replicates and densitometry (mean) is representative of an average of the three independent experiments. Standard error is as follows from left to right for SNU-1: 0.164, 0.0959, 0.00584, 0.0789, and 0.0923, SNU-16: 0.0873, 0.0114, 0.0148, 0.0183, and 0.105. Significance was calculated using two-tailed t-test at 95% confidence interval using GraphPad PRISM software where \*\*\* p-value < 0.001.

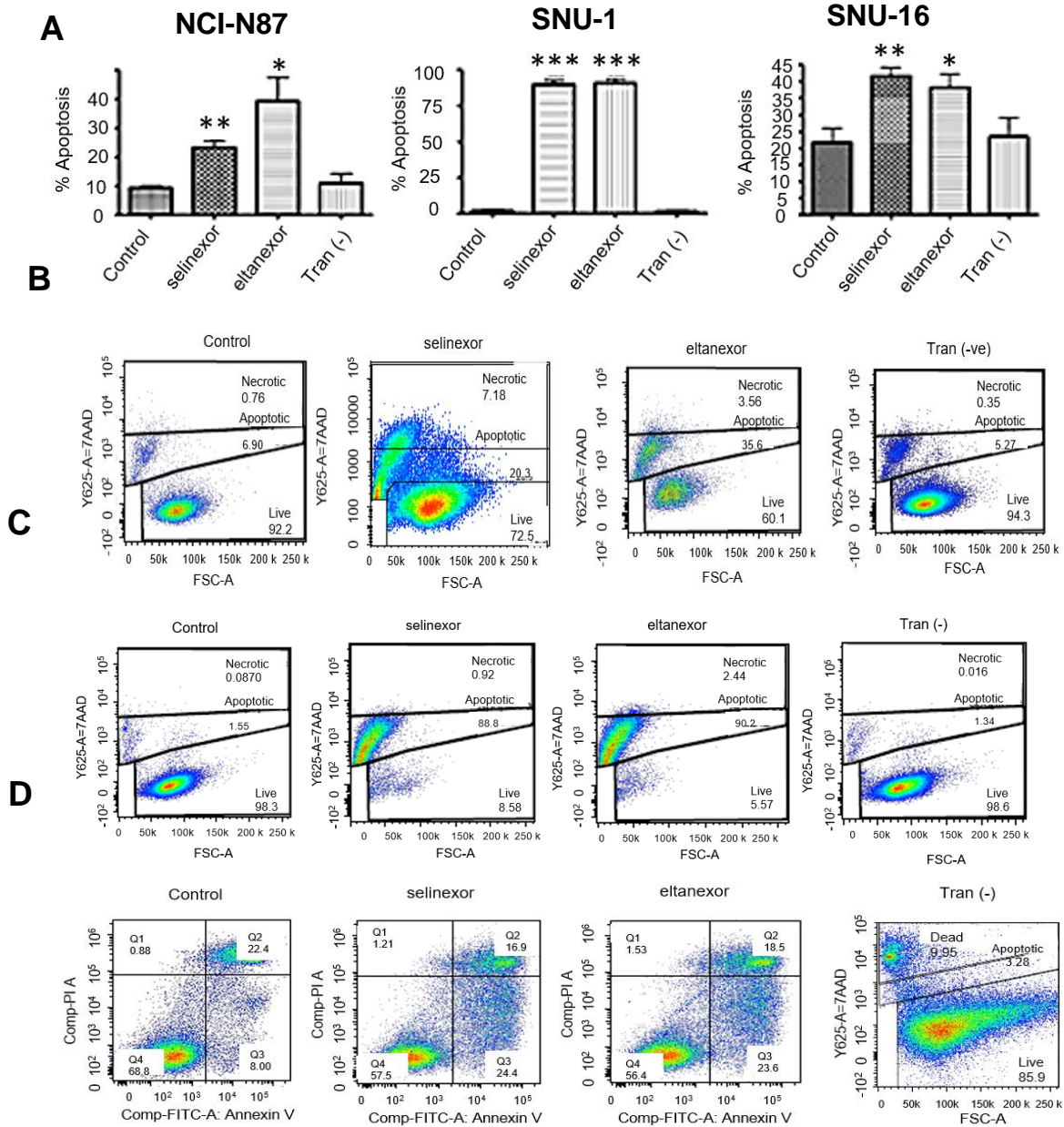


**Figure 3.5: Apoptotic Analysis of gastric cancer cells treated with SINE compounds. [A]** NCI-N87, SNU-1, and SNU-16 cells were treated with SINE compounds (see methods) for 72 hours. Apoptotic analysis revealed significant cell death with selinexor or eltanexor treatment compared to untreated control and negative control. Results are representative of three independent experiments using two-tailed t-test at 95% confidence interval where \* indicates p value < 0.05, \*\* p value < 0.010 and \*\*\* p value < 0.005 and error bars are indicative of standard deviations. **[B]** Representative image of SNU-16 apoptosis results from Flow Cytometry core showing necrotic, apoptotic and viable cells after treatment with SINE (150 nM). **[C]** Representative image of SNU-1 apoptosis results from Flow Cytometry core showing necrotic, apoptotic and viable cells after treatment with SINE (150 nM). **[D]** Representative image of NCI-N87 apoptosis results from Flow Cytometry core showing necrotic, apoptotic and viable cells after treatment with SINE (500 nM).

#### 4.3.5 Conclusions

Altogether, these results suggest that XPO1 knockdown with SINE compounds block gastric cancer growth, colony formation, cell cycle arrest and apoptosis. In addition, the lack of prominent cell death in normal gastric cells indicates that this targeted treatment could be cancer cell specific and effective for managing gastric cancer disease *in vitro* while sparing normal and critical tissue functions. A schematic diagram of the mechanism of action and observations of this single agent study is provided (**Figure 3.6**).

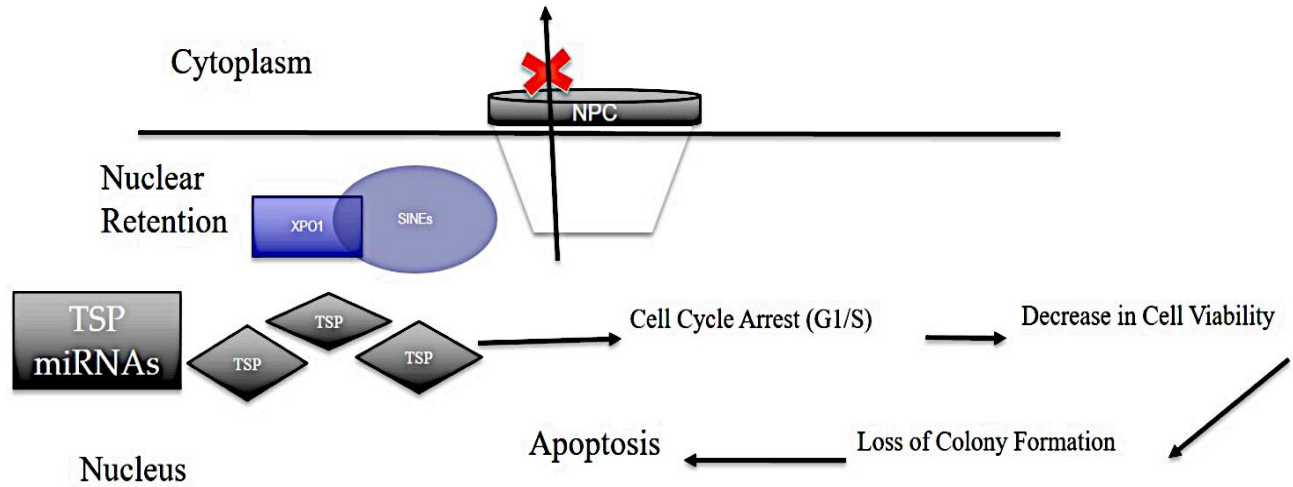


**Figure 3.6: Scheme of XPO1 Activity in Gastric Cancer.** XPO1 activity is aberrantly expressed in gastric cancer leading to a hyperactive influx of cellular proteins and tumor suppressor proteins from the nucleus to the cytoplasm. Through inhibition of XPO1, SINE compounds reduce the relative efflux of these proteins leading to nuclear retention of tumor suppressor proteins and cell cycle arrest leading to a decrease in cell viability and colony formation ultimately resulting in apoptosis [Adapted from Sexton et al., 2019].

## CHAPTER 5- SELINEXOR ENHANCES THE THERAPEUTIC EFFICACY OF COMMONLY USED CHEMOTHERAPEUTICS

### 5.1 Introduction

Although there is no gold standard of treatment for gastric cancer, a variety of chemotherapeutics are used to treat this disease including microtubule inhibitors, topoisomerase inhibitors and DNA damaging agents. Microtubule inhibitors, such as paclitaxel and docetaxel, have shown some clinical efficacy in reducing gastric cancer disease burden especially in doublet or triplet combination with other chemotherapeutics such as fluoropyrimidines, DNA damaging agents and monoclonal antibodies [Gadgeel et al., 2003]. Currently, paclitaxel or the nanoparticle albumin-bound paclitaxel (nab-paclitaxel (Abraxane)), is used as a common standard of care treatment in combination with the VEGFR-2 antibody ramucirumab as a second line therapy after initial combinations of either fluoropyrimidines or trastuzumab (HER2 monoclonal antibody) has failed [Wilke et al., 2014]. These recommendations were made after results of the Rainbow trial, which showed paclitaxel and ramucirumab were as effective and manageable in patients (11.4 months versus 7 months) [Wilke et al., 2014].

We hypothesized that XPO1 inhibition with SINEs could enhance the therapeutic effect of paclitaxel *in vitro* through a dual cell cycle arrest at both the G1/S phase (attributed to selinexor) and G2/M phase (attributed to paclitaxel). In this chapter, we aim to describe the *in vitro* evidence that suggests selinexor can enhance the therapeutic efficacy of paclitaxel in gastric cancer.

### 5.2 Paclitaxel's mechanism of action

Paclitaxel is a chemotherapeutic which belongs to the larger class of taxane drugs. Taxanes work by inhibiting microtubule formation, inducing G2/M phase cell cycle arrest

and ultimately inhibiting cell division. Initially, paclitaxel was derived and extracted from the bark of the Pacific yew (*Taxus brevifolia*) tree. Currently there are two forms of paclitaxel: free paclitaxel and nab-paclitaxel (Abraxane). Nab-paclitaxel is albumin bound paclitaxel, which has better tolerability in patients including less neutropenia, but there still are other side effects such as fatigue and sensory neuropathy [Vishnu and Roy, 2011]. Paclitaxel targets rapidly dividing cells non-specifically through inhibition of microtubules while inducing cell cycle arrest at the G2/M phase resulting in apoptosis. Paclitaxel is administered at a dose of 175 mg/m<sup>3</sup> over an infusion of 3 hours. Unfortunately, there is notable paclitaxel resistance leading to progression of disease. *In vitro* attempts to understand paclitaxel resistance in gastric cancer have led to the following conclusions, (1) non-coding RNA expression is involved in paclitaxel resistance, (2) diffuse gastric cancer patients have higher percentage of taxane resistance and (3) gain of function mutations in cytoskeletal proteins, such as dynamins and kinesins, can contribute to taxane resistance [Staff et al., 2020; Sakamoto et al., 2009; Zhu and Chen., 2019]. Due to the problems that gastric cancer patients face with taxane resistance, we aim to understand whether selinexor can enhance the therapeutic efficacy of paclitaxel and other taxane compounds in gastric cancer.

## **5.3 Materials and methods**

### **5.3.1 Cell lines, culture conditions and reagents**

The SNU-1 and SNU-16 cell lines used for these studies were purchased from ATCC, (Manassas, VA, USA) in 2017 and were maintained in RPMI-1640 (Invitrogen, Carlsbad, CA, USA) supplemented with 10% fetal bovine serum (FBS) and 1% penicillin/streptomycin (P/S) in 5% CO<sub>2</sub> atmosphere at 37°C. Paclitaxel was purchased

from Selleckchem (Pittsburg, PA), the Annexin V FITC apoptosis kit was purchased from Biovisions (San Francisco, CA, USA) and 7AAD was purchased from Thermo Fischer Scientific (Waltham, MA, USA).

### **5.3.2 Trypan blue cell viability assay**

Suspension SNU-1 and SNU-16 cells were seeded at a density of  $2.5 \times 10^4$  cells/well in a 24-well plate in complete medium. After subsequent acclimation (3-5 h) single agent SINE, paclitaxel, or combination SINE plus paclitaxel was added to the medium at the indicated concentrations. SINE and paclitaxel compounds were diluted from 1 mM stock dissolved in DMSO to 1:100 in PBS. After 72 h of incubation, the cells were mixed well with a pipette, collected and diluted 1:1 with 20  $\mu$ L of trypan blue. The cells were counted using a hemocytometer. To assess for synergy we utilized the cell counts. The counts were calculated for % cell viability (relative to control) and put into the CalcuSyn software with their respective concentrations. Synergy was calculated where the confidence integer (CI) value is less than 1.00. The synergies reported are from the average of three independent experiments where the CI values were less than 1.00. The isobologram figures are generated by the CalcuSyn software and is a plotted representation of the two drugs being tested, in this case paclitaxel and selinexor, and if the generated points are below the indicated line then they are considered synergistic [Chou, 2010].

### **5.3.3 Cell cycle analysis**

SNU-1 and SNU-16 cells were plated at a density of  $5 \times 10^5$  cells/mL in RPMI without FBS. The following day, fresh complete media along with selinexor (50 nM) or paclitaxel (25 nM) was added to the cells. Cells were incubated for 24 h, then collected

and fixed with 70% cold ethanol. Propidium iodide (stock 1 mg/mL) and RNase A, to a final concentration of 21.5 ug/mL of propidium iodide and 0.470 ug/mL of RNase A, was then added to the cells, incubated, and submitted to the flow cytometry core at Karmanos Cancer Institute for processing using the BD SLR-II flow cytometer.

#### **5.3.4 Xenograft studies**

Under our Wayne State University 2016 approved Institutional Animal Care and Use Committee (IACUC) protocol, 24 ICR-SCID female mice (Taconic Biosciences, Rensselaer, NY, USA) IACUC protocol (16-03-059) were unilaterally and subcutaneously transplanted with about 50–70 mg SNU-1 previously established tumor fragments. One week post implantation, all animals were checked for engraftment. Once engraftment was confirmed (20 out of 24 mice), they were randomly assigned to four cohorts each with five mice: untreated, KPT-330 orally treated (10 mg/kg q3d), nab-paclitaxel intravenously treated (30 mg/kg q3d) and their combination. All mice were followed daily and their body weights, tumor volumes ( $L \times W^2/2$ ) and conditions were recorded every three days. The experiment was terminated when tumor burden reached 5-10% of total body weight.

Tumor volumes were estimated from two-dimensional caliper measurements, where tumor mass (in mg) =  $(a \times b^2)/2$ , and a and b are the tumor length and width in mm, respectively. Quantitative endpoints include: (i) tumor growth delay [T-C, where T is the median time in days required for the treatment group tumors to reach a predetermined size (e.g., 1000 mg), and C is the median time in days for the control group tumors to reach the same size; tumor-free survivors are excluded from these calculations]; and (ii) gross log<sub>10</sub> cell kill (LCK) [determined by the formula,  $LCK = (T-C)$ ; tumor growth delay in



days)/3.32 x Td (tumor doubling time in days)]. Further analysis included determinations of T/C values (in percent) on all days of tumor measurement using the median total tumor burden for treatment (T) and control (C) groups. Mouse body weight, percent body weight loss were used, along with daily health monitoring, to gauge drug effects and potential toxicity.

### 5.3.5 Statistics

Statistics were assessed using GraphPad PRISM software with two-tailed t-test at 95% confidence interval.

## 5.4 Results

### 5.4.1 Selinexor enhances the therapeutic efficacy of paclitaxel in *vitro*

Utilizing the SNU-1 and SNU-16 cell lines, we first determined the IC<sub>50</sub> value of paclitaxel (**Table 5**). Utilizing treatment combination doses that were below the IC<sub>50</sub> values of selinexor, eltanexor and paclitaxel, we found that there was significant synergy with the paclitaxel/selinexor and paclitaxel/eltanexor than single agent treatment after 72 hours. This was determined by a significant reduction in cell growth (**Figure 4.1**). Analysis of the cell cycle initially revealed behavior differences in either diploid or tetraploid cellular composition. The SNU-1 cell line (primary) is a near diploid model [Park et al., 1993] and this was observed in cell cycle analysis (**Table 6**). We observed changes to ploidy (**Table 6**) based on drug treatment (either paclitaxel, selinexor or combination of both). Treatment with paclitaxel induced more tetraploid behavior, or 4N chromosomal events (**Table 6**). This suggests the SNU-1 cells are undergoing mainly DNA replication but due to software limitations, we cannot know whether it is G2/M or G0/S phase arrest.

This observation is consistent with the literature suggesting paclitaxel inhibits the

	Paclitaxel IC <sub>50</sub>	Standard Deviation	Paclitaxel + Selinexor (nM)	CI Value	Fa Value	Standard Deviation
SNU-16	12.17	4.23				
			25 : 50	0.560	0.905	0.328
SNU-1	10.38	5.99				
			12.5 : 25	0.645	0.765079	0.214
			50 : 25	0.797	0.930159	0.155
SNU-1			Paclitaxel + Eltanexor (nM)	CI Value	Fa Value	Standard Deviation
			37.5 : 75	0.0433	0.999999	0.0325

**Table 5: Synergy analysis of paclitaxel and SINE.** Varying concentrations of paclitaxel, in combination with either selinexor or eltanexor, in 1:2 ratio on cell growth inhibition were assessed for synergy. Synergy analysis of the data obtained by MTT assay was performed using CalcuSyn software with two-tailed 95% confidence interval. Results suggest significant synergy at the indicated concentrations in both the SNU-1 and SNU-16 cell lines, where CI values less than 1.00 indicate synergy; CI values at 1.00 indicate additive effect and CI values greater than 1.00 indicate antagonism. Results are representative of three independent experiments.

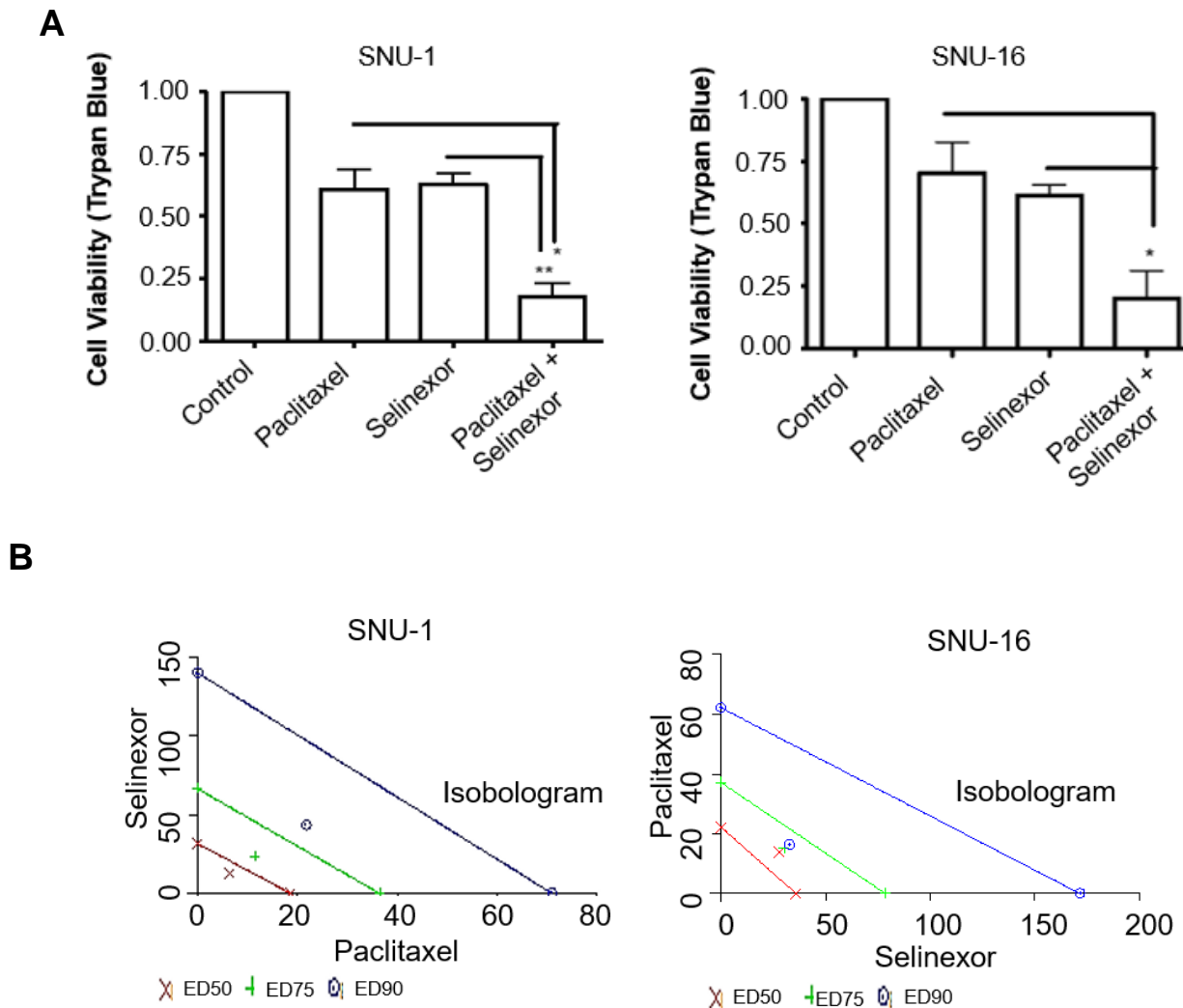


**Figure 4.1: In vitro assessment of selinexor and paclitaxel in gastric cancer. [A]** Cell viability assay after treatment with paclitaxel, selinexor or combination in the SNU-1 and SNU-16 cell line. Graph is representative of three independent experiments and statistics were provided by GraphPad PRISM software using two-tailed 95% confidence interval where \*\* p-value < 0.05 and \*\*\* p-value < 0.01 with the error bars representing standard deviation. **[B]** Isobologram was created using the CalcuSyn program in which synergy with paclitaxel and selinexor in the SNU-1 and SNU-16 cell lines was observed.

G2/M phase of the cell cycle so thus after replication and before mitotic division [Wang et al., 2000]. Normally, diploid characteristics are not highly associated with enhanced tumorigenesis compared to tetraploid cell characteristics [Lim et al., 2014]. Treatment with selinexor alone showed a retention of diploid status (2N chromosomal events) (**Table 6**). It is understood that selinexor inhibits the cell at the G1/S phase of the cell cycle and these results further confirm that the SNU-1 cells remain in their natural diploid state, i.e. before chromosomal replication [Nakayama et al., 2016]. Treatment with paclitaxel and selinexor induced changes to both the diploid and tetraploid status of the SNU-1 cells suggesting a halting of the cell cycle at both the G1/S and G2/M phases resulting in decreased cellular growth (**Figure 4.1, Table 6**).

Assessment of the cell cycle characteristics in the SNU-1 and SNU-16 cell lines revealed trending patterns of alterations to the cell cycle (**Figure 4.2**). As we have observed above with differences in ploidy, we found the SNU-1 cells to have increased G1 phase cell cycle arrest, and loss of S phase, between the paclitaxel treatment alone and paclitaxel plus selinexor in both the diploid and tetraploid cells (**Figure 4.2**). Between the tetraploid cell conditions, we found a decrease in the G2 phase of the cell cycle comparing paclitaxel alone to combination treatment (**Figure 4.2**). Paclitaxel is known to arrest in the G2/M phase of the cell cycle [Wang et al., 2000] indicative of the G1-phase cell cycle arrest being the dominant phenotype within the paclitaxel/selinexor combination in the SNU-1 cell line. In SNU-16 cell line, we observed similar arrest patterns between the diploid and tetraploid cells indicative of a dominant G1 phase cell cycle arrest, caused by the addition of selinexor, across differing gastric cancer cell types (**Figure 4.2**).

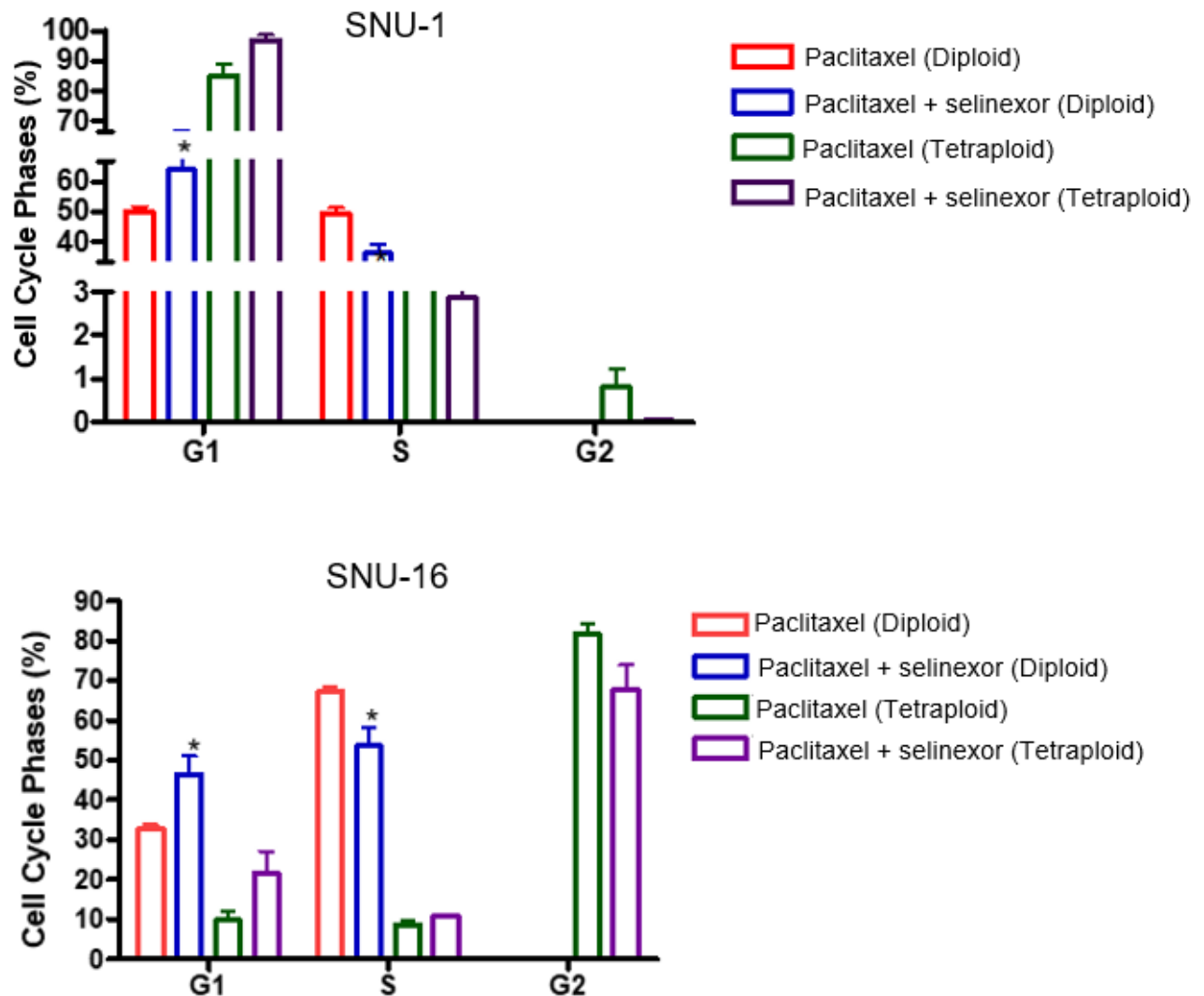


**Figure 4.2: Cell cycle arrest analysis of SNU-1 and SNU-16 cell line.** SNU-1 and SNU-16 cells underwent cell cycle analysis (flow-cytometry) after treatment with paclitaxel (12.5 nM), selinexor (25 nM) or combination. The cells were found to have differences in cell cycle arrest patterns between the diploid and tetraploid phases as well as differences between treatments. Graphs are representative of three independent experiments and statistics were provided by GraphPad software using two-tailed t-test at 95% confidence interval. Error bars are representative of standard deviation and p-value  $* < 0.05$ .

SNU-1 Cell Line								
	Control (%)	Standard Deviation	Paclitaxel (%)	Standard Deviation	Selinexor (%)	Standard Deviation	Paclitaxel + Selinexor (%)	Standard Deviation
Diploid	93.96	0.276	18.38***	3.26	88.94***	0.813	36.05***	10.8
Tetraploid	6.07		81.61***		11.05***		64.94***	

**Table 6: Ploidy status of SNU-1 and SNU-16 cell line after treatment with SINE and/or paclitaxel.** Flow cytometry analysis revealed a dramatic shift in ploidy in the SNU-1 cell line after treatment with either SINE and/or paclitaxel after 24 hours. Table is representative of the averages of three independent experiments (average percentage). Statistics were provided by Excel and are indicative of a comparison between control and individual treatments. Individual p-values are as follows: paclitaxel  $2.34 \times 10^{-6}$ , selinexor  $5.52 \times 10^{-4}$ , and paclitaxel plus selinexor  $7.03 \times 10^{-4}$ . Asterisks are indicative of statistical significance where \*\*\* p-value < 0.001. Comparison between paclitaxel and paclitaxel plus selinexor had p-value of 0.0627.

#### 5.4.2 Selinexor enhances the therapeutic efficacy of nab-paclitaxel *in vivo*

Since we found evidence of synergy *in vitro* in gastric cancer cell lines, we then performed an *in vivo* assessment of synergy in an animal xenograft model. Our results show that selinexor and paclitaxel in the SNU-1 xenograft showed superior reduction in tumor growth compared to single agent treatment (**Figure 4.3, Table 7**).

#### 5.4.3 Conclusions

Based on these results, we can conclude that selinexor does enhance the therapeutic efficacy of paclitaxel/nab-paclitaxel in gastric cancer. Although the effect we see within the *in vivo* studies are modest, it can be partially explained by the fact that these doses are being used at lower than the maximum tolerated dosing concentrations to minimize anticipated toxicities from this drug combination. Although the study was designed to identify whether selinexor can improve therapeutic responses to paclitaxel, we have found encouraging results that warrant further investigation. We have found that selinexor does improve therapeutic responses *in vitro* and does reduce tumor burden significantly *in vivo* while producing little toxicities. Although the tumor weights we observed at the end of the experiment are modest in growth reduction, moving forward, further investigation is necessary to identify the optimal dosing that would elicit the best therapeutic response *in vivo*.

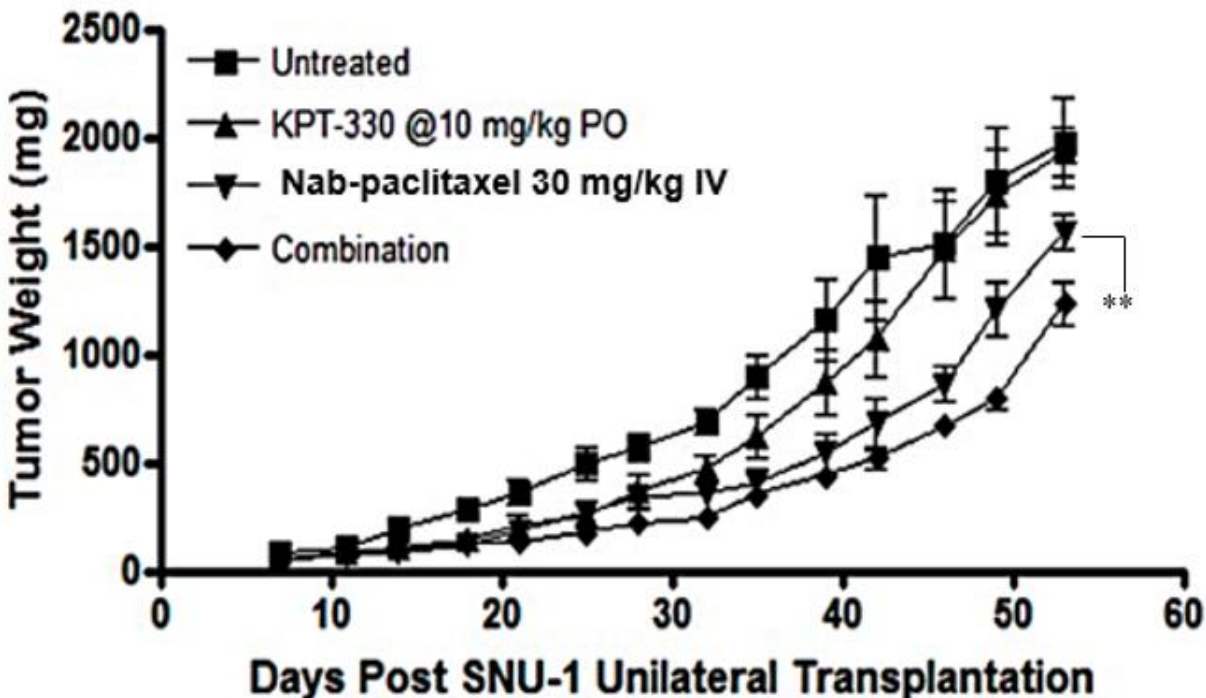


**Figure 4.3: *In vivo* assessment of nab-paclitaxel and selinexor using SNU-1 xenografts.** SNU-1 cell fragments were implanted subcutaneously on the inner thigh into ICR SCID mice cohort (n=5 mice per group) and treated with either single agent nab-paclitaxel (IV), selinexor (oral gavage) or a combination of both at the indicated concentrations for two weeks while tumor burden was measured as described in materials and methods. To reduce anticipated toxicities with this combination the drug concentrations used were below the maximum tolerated dosing that we have previously found for both nab-paclitaxel and selinexor. Measurements occurred both during and after treatments in a 20 mice cohort. These results suggest that there is some therapeutic benefit to adding selinexor to treatment than single agent nab-paclitaxel or single agent selinexor alone as indicated by the lower tumor weight observed in the combination cohort. Statistics were calculated on GraphPad PRISM software using two-tailed t-test at 95% confidence interval between nab-paclitaxel and nab-paclitaxel plus selinexor at the final day of measurement where \*\* p-value < 0.01.



Treatment	Route	Schedule	Total Dosage (mg/kg)	T/C (%)	Time to 1000 mg in days (range)	Tumor Growth Delay (days)
No Treatment	_____	_____	_____	_____	37 (35-39)	_____
Selinexor	Oral Gavage	Q3d Start Day 7	70	14.96	42.5 (39-46)	5.5
Nab- paclitaxel	IV	Q3d Start Day 7	210	37.13	49.5 (49-53)	12.5
Selinexor + Nab- paclitaxel	Oral Gavage/ IV	Q3d Start Day 7	280	52.20	53 (53-53)	16

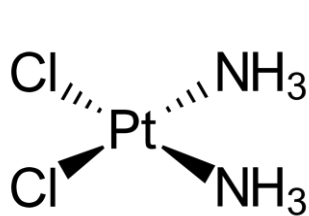
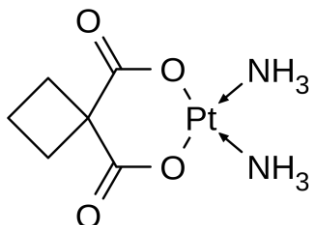
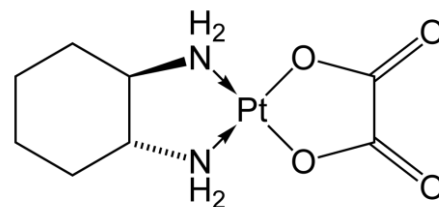
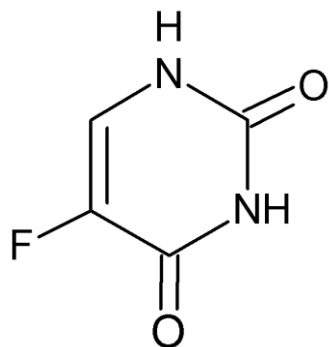
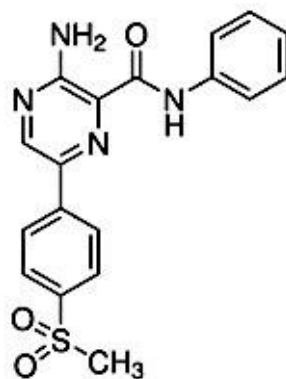
**Table 7: *In vivo* efficacies of nab-paclitaxel and selinexor toward the SNU-1 xenografts. Female ICR-SCID mice (4-6 weeks old) were subcutaneously implanted with human SNU-1 tumor fragments on day 0. Beginning on day seven the mice were dosed intravenously (IV) as follows: **nab-paclitaxel**, Q3dx3 at 30 mg/kg injection, total dose 210 mg/kg; and **selinexor** Q3dx3 at 10 mg/kg/injection, total dose 70 mg/kg. Mice were weighted periodically and health conditions were assessed daily; tumors were measured by caliper two-to-three times weekly. Mice were sacrificed when the cumulative tumor burden reached 5-10% of body weight (1-2 g). Tumor volumes were estimated from two-dimensional caliper measurements, where tumor mass (in mg) =  $(a \times b^2)/2$ , and a and b are the tumor length and width in mm, respectively. Quantitative endpoints include: (i) tumor growth delay [T/C, where T is the median time in days required for the treatment group tumors to reach a predetermined size (e.g., 1000 mg), and C is the median time in days for the control group tumors to reach the same size; tumor-free survivors are excluded from these calculations]. Mouse body weight, percent body weight loss were used, along with daily health monitoring, to gauge drug effects and potential toxicity. Percent body loss was assessed with each individual mouse and each individual treatment.**

## CHAPTER 6- SINE ENHANCES DNA DAMAGING CHEMOTHERAPEUTICS

### 6.1 Introduction

Platinum agents (cisplatin, carboplatin, oxaliplatin) and anti-metabolites are other types of chemotherapeutics used in combination to treat gastric cancer (Bozkurt et al., 2017). Platinum agents work by intercalating in the DNA of rapidly dividing cells, and inducing DNA damage. **(Figure 5.1)**. Antimetabolites interfere with one or more enzymes involved in one-carbon metabolism and pyrimidine synthesis that are necessary for DNA synthesis and replication. 5-Fluorouracil (5-FU) is the most common anti-metabolite compound used to treat gastric cancer [Miura et al., 2010] **(Figure 5.1)**.

Cisplatin, or cis-[Pt(NH<sub>3</sub>)<sub>2</sub>Cl<sub>2</sub>], was discovered in the mid-1800s and referred to as Peyrone's salt which showed anti-bacterial properties [Joyce et al., 2010]. In the 1970s, Dr. Rosenberg at Michigan State University discovered this compounds anti-cancer properties [Lippard, 1982]. In the 1970's carboplatin was synthesized by Drs. Connors and Herrap of Michigan State University through a collaboration with the National Institute of Cancer Research as an alternative and better tolerated cisplatin [Newell et al, 2003]. In 1976 oxaliplatin was synthesized and discovered for its anti-cancer properties by Dr. Kidani in Japan [Graham et al, 2004]. Since the discovery of platinum compounds, clinical trials have revealed that oxaliplatin, fluorouracil and folinic acid (FOLFOX) showed superior survival benefit compared to single agent therapies or combinations with other platinum compounds in GI cancers due to the frequent cisplatin resistance seen in patients [Hosoda et al., 2019; Masuishi et al., 2017]. Oxaliplatin mechanism of action differs somewhat from cisplatin and carboplatin leading to a different platinum-based treatment [Schoch et al, 2020]. 5-FU, fluoro-substitute pyrimidine compound, was

**CISPLATIN****CARBOPLATIN****OXALIPLATIN****5-FLUOROURACIL****VE-821**

**Figure 5.1: Chemical structures of compounds used.** The chemical structures of platinum compounds: cisplatin, carboplatin and oxaliplatin, and the anti-metabolite 5-FU used in this study for combination studies with SINE compounds. VE-821 is an ATR/ATM inhibitor used within the study to validate the DNA damage repair response in subsequent experiments.

synthesized in 1957 based on the principle that, uracil, is more readily found within tumor tissues and is more readily taken up into the tumor than analogs of other pyrimidine bases [Shirasaka, 2009].

Although these compounds are used frequently within the clinic, there is sufficient evidence indicating the development of resistance to these agents that is visible in the poor overall 5-year survival rates [Masuishi et al., 2017]. In this section we show sufficient evidence that selinexor sensitizes gastric cancer cells to a combination of oxaliplatin and 5-FU *in vitro* and *in vivo*.

## **6.2 Materials and Methods**

### **6.2.1 Cell lines, culture conditions and reagents**

The SNU-1 and SNU-16 cell lines used for these studies were purchased from ATCC (Manassas, VA, USA) in 2017 and were maintained in RPMI-1640 (Invitrogen, Carlsbad, CA, USA) supplemented with 10% fetal bovine serum (FBS) and 1% penicillin/streptomycin (P/S) in 5% CO<sub>2</sub> atmosphere at 37 °C. Normal epithelial cells were purchased from Cell applications (San Diego, CA, USA) and maintained in Epithelial growth media (provided by Cell Applications). Before seeding, the wells of the plates were coated with collagen solution (Cell Applications) for 2 minutes. All cells were used up to 6 passages as recommended by the company. All chemotherapeutic compounds (oxaliplatin, 5-fluorouracil) were provided by pharmacy at Karmanos Cancer Institute and are clinical grade. Selinexor (KPT-330) and KPT-301 were provided by Karyopharm Therapeutics (Newton, MA, USA) and Leptomycin B was purchased from Santa Cruz Biotechnology (Santa Cruz, CA, USA). VE-821 was purchased from Sellekchem (Pittsburg, PA, USA). The annexin V FITC apoptosis kit was purchased from Biovisions

(San Francisco, CA, USA) and 7AAD was purchased from Thermo Fischer Scientific (Waltham, MA, USA). Primary XPO1 and NF- $\kappa$ B p65 subunit antibodies were purchased from Santa Cruz Biotechnology. Primary thymidylate synthase (TYMS), p53, PARP antibodies and secondary anti-rabbit and anti-mouse antibodies were purchased from Cell Signaling Technologies (Danvers, MA, USA). Primary WW binding domain protein 5 (WBP5) and  $\gamma$ -H2AX antibodies were purchased from Thermo Fisher (Waltham, MA, USA). For western blotting (below) primary antibodies were used at a concentration of 1:2500 and secondary antibodies were used at a concentration of 1:5000 in 5% milk or BSA ( $\gamma$ -H2AX). siControl or siWBP5 were purchased from Santa Cruz Biotechnology and Lipofectamine 3000 was purchased from Thermo Fisher (Waltham, MA, USA).

### **6.2.2 Trypan blue cell viability assay**

Suspension SNU-1 or SNU-16 cells were seeded at a density of  $2.5 \times 10^4$  cells/well in a 24-well plate in complete medium. After subsequent acclimation (3-5 h) single agent selinexor, double combination oxaliplatin and 5-fluorouracil or triple combination selinexor plus 5-fluorouracil and oxaliplatin were added to the medium at the indicated concentrations. Selinexor was diluted from 10 mM stock dissolved in DMSO to 1:100 in PBS where as oxaliplatin was diluted 1:100 in PBS diluted from a 26.7 mM stock dissolved in PBS (clinical grade) and 5-fluorouracil was diluted 1:1000 in PBS diluted from a 384.4 mM stock dissolved in PBS (clinical grade). VE-821 was diluted 1:100 in PBS from 1 mM stock dissolved in DMSO and used at a final concentration of 26 nM, as indicated by manufacturer as the effective dose for DNA damage inhibition. After 72 h of incubation, the cells were mixed well with a pipette, collected and diluted 1:1 with 20- $\mu$ L Trypan blue. The cells were counted using a hemocytometer. To assess for synergy we utilized the

cell counts. The counts were calculated for % cell viability (relative to control) and put into the CalcuSyn software with their respective concentrations. Synergy was calculated where the confidence integer (CI) value is less than 1.00. The synergies reported are from the average of three independent experiments where the CI values were less than 1.00. The isobologram figures are generated by the CalcuSyn software and is a plotted representation of the two drugs being tested, in this case paclitaxel and selinexor, and if the generated points are below the indicated line then they are considered synergistic [Chou, 2010].

### **6.2.3 MTT assay**

Normal gastric cells were plated at a density of  $5 \times 10^3$  cells/well in a 96 well plate. The following day, cells were supplemented with fresh media and treated with PBS (Control), oxaliplatin (125 nM or 125 nM), 5-FU (125 nM or 375 nM) and/or 12.5 nM selinexor. The cells were treated at differing concentrations for oxaliplatin and 5-FU as a representation of the synergistic concentrations found in the SNU-1 and SNU-16 cell lines. The cells were then incubated for 72 hours. Following incubation, MTT dye was added for 2 hours and after incubation, the formazan formed by metabolically viable cells was solubilized with isopropanol and the plates were agitated for 20 minutes. Optical density (O.D.) was measured at 570 nm using a plate reader and growth was quantified.

### **6.2.4 Apoptotic analysis**

SNU-1 or SNU-16 cells were seeded at a density of  $5 \times 10^5$  cells/mL. The subsequent day single agent selinexor, double combination oxaliplatin and 5-fluorouracil or triple combination selinexor plus 5-fluorouracil and oxaliplatin were added to the medium at the indicated concentrations and diluted in the same way as in section **6.2.2**.

After 72 h of incubation, the cells were assessed using the annexin V kit according to the manufacturer's protocol (BD Biosciences, San Jose, CA, USA). All cells were analyzed using flow cytometry via the flow cytometry core facility at Karmanos Cancer Institute using the BSL-II flow cytometer. The gastric cancer cells, suspended in PBS, were put through the BD-SLR II flow cytometer and assessed using laser beam, which detects different wavelengths of light emitted by the cells (either with 7AAD reagent uptake or not). The 7AAD reagent emits at a maximum wavelength of 647 nm and can be excited at 488 nm. The cells are then sorted based on the detected wavelength. Loss of membrane integrity is a hallmark of cell death and those gastric cancer cells that have taken up the 7AAD dye is considered dead (apoptotic or necrotic). Cells that do not uptake the 7AAD or Annexin V dye are viable and thus healthy and can be assessed using software to differentiate the different cellular states.

### **6.2.5 Cell cycle analysis**

SNU-1 and SNU-16 cells were plated at a density of  $5 \times 10^5$  cells/mL in RPMI without FBS. The following day fresh complete media (RPMI + 10% FBS) along with single agent selinexor or double combination oxaliplatin and 5-fluorouracil or triple combination selinexor plus 5-fluorouracil and oxaliplatin was added to the cells. SNU-16 cells were treated at the following doses: oxaliplatin 125 nM, 5-FU 375 nM, selinexor 12.5 nM. SNU-1 cells were treated at the following doses: cisplatin 250 nM, carboplatin, 25 nM, 5-FU 125 nM and/or selinexor 12.5 nM. Cells were incubated for 24 h then collected and fixed with 70% cold ethanol. Propidium iodide (stock 1 mg/mL) and RNase A, to a final concentration of 21.5 ug/mL of propidium iodide and 0.470 ug/mL of RNase A, was

then added to the cells, incubated, and submitted to the flow cytometry core at Karmanos Cancer Institute for processing using the BD SLR-II flow cytometer.

#### **6.2.6 Database search**

Oncomine Database (Thermo Fisher, Waltham MA) was used to look at gastric cancer cell lines that were treated with and without cisplatin using the Garnett Cell Line dataset (mRNA published in Nature 2012/03/28 using Human Genome U133A Array). Oncomine provided statistics and we interpreted significance where p-values were less than 0.05. Geo2.0 database analysis (PubMed) was used to look at the differences in 5-FU resistant and sensitive gastric cancer organoids (Series GSE154127). The Oncomine software provides statistical analysis of test datasets.

#### **6.2.7 Immunofluorescence assay**

SNU-16 cells were plated at a density of  $2.5 \times 10^5$  cells/well in 24 well plate and exposed to either no treatment (PBS control), oxaliplatin (125 nM) and 5-FU (375 nM), selinexor (12.5 nM) or a combination of the three compounds for 24 hours. After treatment, the cells were collected and centrifuged onto a microscope slide using a Cytospin 4 machine (Thermo Fisher, Waltham, MA). At the end of treatment cells were fixed with 100% cold acetone for 5 min and were permeabilized with 0.05% Triton 100x in PBS. The fixed slides were then blocked in 5% BSA and probed with primary anti-p53 antibody (Cell Signaling, for 1 hour at room temperature: p53 (Cell Signaling). Alexa 448 conjugated rabbit secondary antibody (Thermo Fisher, Waltham, MA, USA) in 3% BSA was added for 1 hour at room temperature. The slides were washed with PBS and ProLong Antifade mounting medium (Thermo Fisher, Waltham, MA, USA) was added and



the coverslip placed over the slides. The slides were analyzed under an inverted fluorescent microscope at 40X magnification.

### 6.2.8 RNA extraction

The SNU-1 and SNU-16 gastric cancer cell lines were plated at a density of  $2.5 \times 10^5$  cells/ml in 24-well plate in complete media for 24 hours. Cells were silenced (see Section 6.2.10) for 24 hours and collected and RNA was extracted using TRIZOL RNA isolation protocol (Thermo Fisher, Waltham, MA, USA). cDNA was synthesized at 1  $\mu$ g for each sample using cDNA Reverse Transcription kit (Thermo Fisher, Waltham, MA, USA). RT-qPCR was performed with diluted cDNA samples (1  $\mu$ g) in 96-well plate with WW-domain box protein 5 (*WBP5*) or thymidylate synthase (*TYMS*) primer where the ribosomal 18s subunit used as housekeeping gene for normalization. SyBR Green Master Mix (Thermo Fisher, Waltham, MA, USA), a double stranded DNA specific dye which binds to the minor groove of double stranded DNA, was used as the fluorescence dye to detect the fluorescent signals (when excited at 480 nanometers (nm) with blue light and emission spectra of 520 nm) to measure expression changes between samples. The primers used within this study are as follows:

WBP5 Forward: 5' TCGATTAACCTTCCAACGCA 3'

WBP5 Reverse: 5' CCCGTGGAAGGAGTCAAAC 3'

TYMS Forward: 5' GAGATATGGAATCAGATCTTCCTCT 3'

TYMS Reverse: 5' CGTGGACGAATGCAGAACAC 3'

18s Forward: 5' GCAATTATTCCCATGAACG 3'

18s Reverse: 5' GGCCTCACTAAACCATCCAA 3'

### 6.2.9 Western blot

For Cisplatin/5-FU Single agent treatment:  $1 \times 10^6$  SNU-1 cells were plated in complete medium and treated with 250 nM of Cisplatin, from 1 mM stock dissolved in DMSO, for 72 hours or 250 nM of 5-FU, from 384.4 mM stock, diluted 1:1000 in PBS for 72 hours. Cells were lysed using RIPA lysis buffer; protein was collected and quantified using BCA quantification kit (Thermo Fisher, Waltham, MA, USA).

For Synergy treatment:  $2.5 \times 10^5$  SNU-16 cells were plated in complete medium in a 24-well plate and treated with 375 nM of 5-FU, diluted 1:1000 in PBS taken from 384.4 mM stock in PBS, 125 nM of oxaliplatin, diluted 1:100 in PBS taken from 26.7 mM stock in PBS, and/or 12.5 nM Selinexor, diluted 1:100 in PBS taken from 10 mM stock in DMSO. Cells were treated for 72 hours and following incubation the cells were lysed with RIPA lysis buffer, the protein was collected and quantified using BCA kit (Thermo Fisher, Waltham, MA, USA).

WBP5 knockdown cells: Cells were treated with siControl or siWBP5 for 72 hours (see section 6.2.10). Following incubation the cells were lysed with RIPA lysis buffer, the protein was collected and quantified using BCA kit (Thermo Fisher, Waltham, MA, USA).

### 6.2.10 WBP5 silencing

A total of  $5 \times 10^5$  SNU-1 or SNU-16 cells were plated in 24-well plates with RPMI only and incubated for 24 h. The following day siWBP5 or siControl (10  $\mu$ M) were mixed with Lipofectamine (1 mg/mL) according to the manufacturer's protocol for a final concentration of 2.5  $\mu$ g of siRNA per well and added individually to the cells in medium containing RPMI + 10% FBS. Cells were incubated for 72 h with siRNA/Lipofectamine

complexes then trypsinized and were either re plated for MTT assay or underwent protein collection.

### **6.2.11 In vivo xenograft**

Under our Wayne State University 2016 approved Institutional Animal Care and Use Committee (IACUC) protocol, 40 ICR-SCID female mice (Taconic Biosciences, Rensselaer, NY, USA) were unilaterally and subcutaneously injected with  $1 \times 10^7$  SNU-16 cells in a 1:1 ratio of cells to matrigel (Corning) per mouse [Zhao et al., 2016]. Two weeks post injection, all animals were checked for engraftment and once confirmed (35 out of 40), they were randomly assigned to four cohorts each with seven mice: untreated, KPT-330 orally treated (7.5 mg/kg two times a week for four weeks), 5 mg/kg oxaliplatin (intravenous three times a week for four weeks) and 5 mg/kg FU (via peritoneal injection twice a week for four weeks) or their combination. All mice were followed daily and their body weights, tumor weights ( $L \times W^2/2$ ) and condition were recorded every three days. The experiment was terminated when tumor burden reached 5-10% of total body weights (IACUC protocol 18-12-0887). Tumor volumes were estimated from two-dimensional caliper measurements, where tumor mass (in mg) =  $(a \times b^2)/2$ , and a and b are the tumor length and width in mm, respectively. Quantitative endpoints include: (i) tumor growth delay [T-C, where T is the median time in days required for the treatment group tumors to reach a predetermined size (e.g., 1000 mg), and C is the median time in days for the control group tumors to reach the same size; tumor-free survivors are excluded from these calculations]; and (ii) gross log<sub>10</sub> cell kill (LCK) [determined by the formula,  $LCK = (T-C; \text{ tumor growth delay in days})/3.32 \times T_d$  (tumor doubling time in days)]. Further analysis included determinations of T/C values (in percent) on all days of tumor

measurement using the median total tumor burden for treatment (T) and control (C) groups.

### 6.2.12 Statistics

Statistics were obtained using GraphPad PRISM software using two-tailed t-test at 95% confidence interval and densitometry was further verified using Excel software.

## 6.3 Results

### 6.3.1 XPO1 sensitizes gastric cancer cells to DNA damaging agents

Many studies have suggested XPO1 sensitizes gastric cancer cells to DNA damaging chemotherapeutics, such as platinum agents and 5-FU, but there has been no direct evidence linking XPO1 activity to a cellular response of DNA damaging chemotherapeutic agents. To address this, we first utilized the Garnett dataset within the Oncomine database and found that in a multi cancer cohort (639 human cancer cell lines) there was upregulation of many genes related to nuclear transport including *XPO1*, *RANBP1* and *NUP* proteins post cisplatin treatment (**Table 8**). An analysis of only the gastric cancer cell lines (28 cell lines) of that cohort, treated with cisplatin, showed significant increased *XPO1* expression, a result we have verified *in vitro* using the SNU-1 gastric cancer cell line (**Figure 5.2**). Further, we have found treatment with 5-FU in gastric cancer cells also induced expression of XPO1 after 72 hours (**Figure 5.2**). These results suggest XPO1 expression occurs in response to exposure of DNA damaging agents, possibly as a survival mechanism. It has been found that inhibition of XPO1 leads to an increase in the stress response through alterations in normal ribosomal biogenesis [Tagoung et al., 2013]. Other publications have suggested the physiological impact of XPO1 inhibition reduces the cellular DNA damage response in a triple negative breast

<b>Gene</b>	<b>P-Value</b>	<b>Fold Change</b>
IPO5	7.09E-6	2.22
Nup160	1.58E-5	1.56
Nup133	2.02E-5	1.39
Nup107	1.20E-4	1.46
Nup54	1.82E-4	1.39
IPO7	3.76E-4	1.35
IPO9	5.46E-4	1.48
NUP153	5.90E-4	1.36
<b>XPO1</b>	<b>6.11E-4</b>	<b>1.30</b>
RanBP1	0.032	1.14
RanBP2	0.0223	1.43
XPOT	0.0275	1.34

**Table 8: Upregulation of genes involved in nuclear transport in multi-cancer cohort.** Adapted from the Garnett dataset available in OncoPrint, after treatment with cisplatin in a multi-panel gastric cancer cell line cohort (639 cell lines), results show statistically significant upregulation of various nuclear transport related genes including *XPO1*. OncoPrint Software provided statistics and we interpreted statistical significance to be p-values less than 0.05.

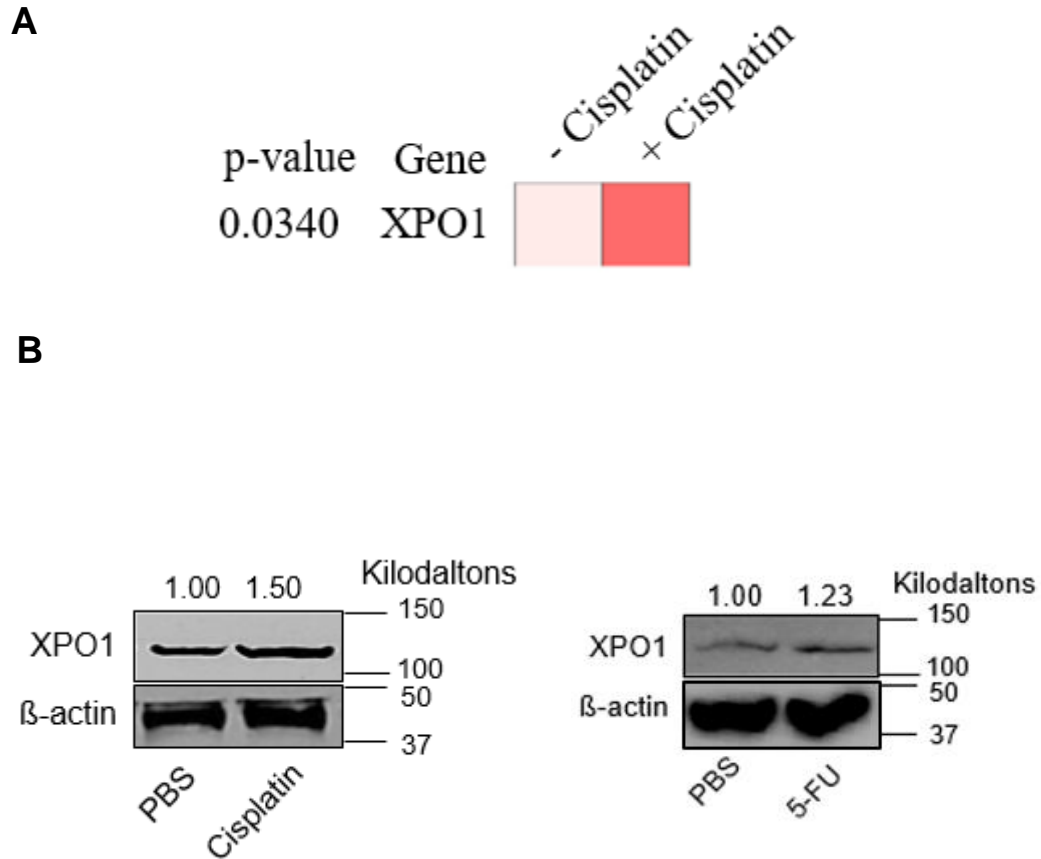


**Figure 5.2: XPO1 Activity is altered in Response to Chemotherapeutics** [A] OncoPrint database shows a statistically significant increase in XPO1 expression in gastric cancer cell lines (n=28) treated with cisplatin. [B] Experimental validation in the SNU-1 cell line showed increased XPO1 expression after a 72-hour treatment with either cisplatin (250 nM) or 5-FU (250 nM). Experiments have been performed three separate times.

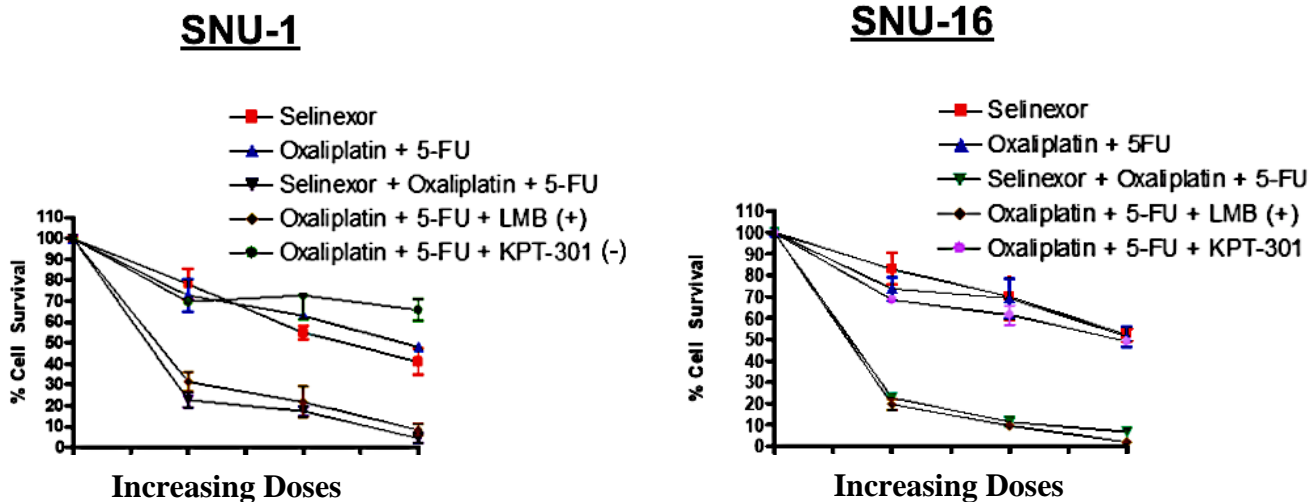
cancer model treated with selinexor [Kashyap et al., 2018]. We provide evidence that DNA damaging agents up regulate the expression of XPO1 activity in gastric cancer (**Figure 5.2**) by increasing growth and proliferative signals. This leads us to the following hypothesis: treatment with selinexor may dampen the survival mechanisms induced by XPO1 in response to chemotherapeutic DNA damaging agents. Furthermore, this alteration in cellular survival processes may lead to cellular death and may overcome resistance mechanisms produced by gastric cancer cells in response to these chemotherapeutic compounds.

The FOLFOX treatment was chosen for study because it is the most common treatment combination used in gastric cancer. Using two distinct gastric cancer cell lines, SNU-1 and SNU-16, we found a significant decrease in cell viability when gastric cancer cells are exposed to oxaliplatin, 5-FU and selinexor (**Figure 5.3A**). The presence of cell death with LMB (+ control)/oxaliplatin/5-FU combination was similar to the cell death patterns from selinexor/oxaliplatin/5-FU treatment where as the cell death with tran (- control)/oxaliplatin/5-FU combination were similar to oxaliplatin and 5-FU alone (**Figure 5.3**). Further assessment revealed a synergistic interaction between selinexor, oxaliplatin and 5-FU in these gastric cancer cell lines, as indicated by CI values less than 1.00 (**Figure 5.3B, Table 9**). The SNU-16 cell line was chosen for further investigation as it is more representative of clinically prominent metastatic gastric cancer cases.

### **6.3.2 XPO1 downregulation suppresses DNA damage repair proteins**

As we have mentioned above, platinum compounds intercalate and create lethal lesions in the DNA. After 24-hour treatment with the SINE KPT-185, we found

A



B

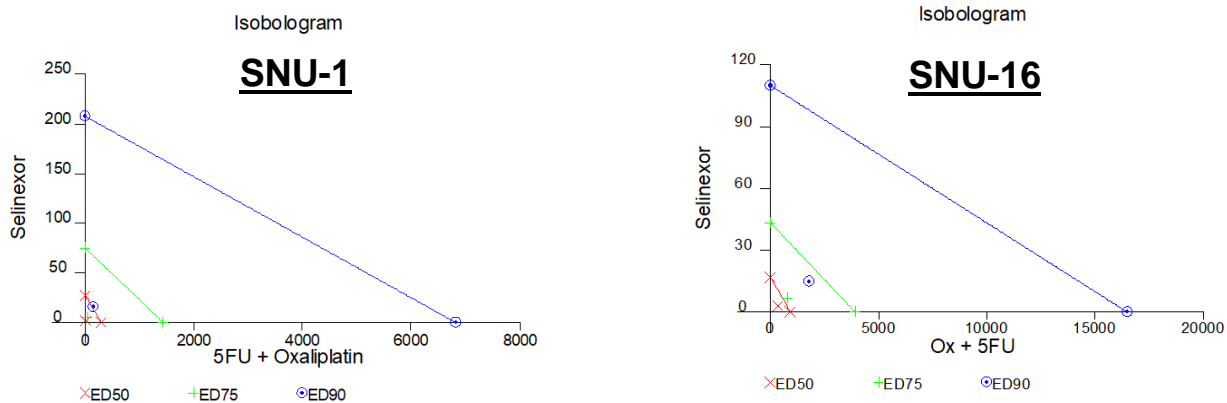


**Figure 5.3: Cell viability analysis of selinexor, 5-FU and oxaliplatin.** [A] SNU-1 and SNU-16 cell lines were treated with oxaliplatin, 5-FU and/or selinexor at the increasing concentrations provided in **Table 9**. LMB and tran were used at the same concentrations as selinexor. Cells were incubated 72 hours the assessed for cell viability. Graphs were created using GraphPad software and is representative of three independent experiments and error bars are representative of standard deviations (n=3). [B] Isobolograms (average) of three independent experiments were included for both the SNU-1 and SNU-16 cell lines to indicate synergistic activity between selinexor and oxaliplatin and 5-FU.



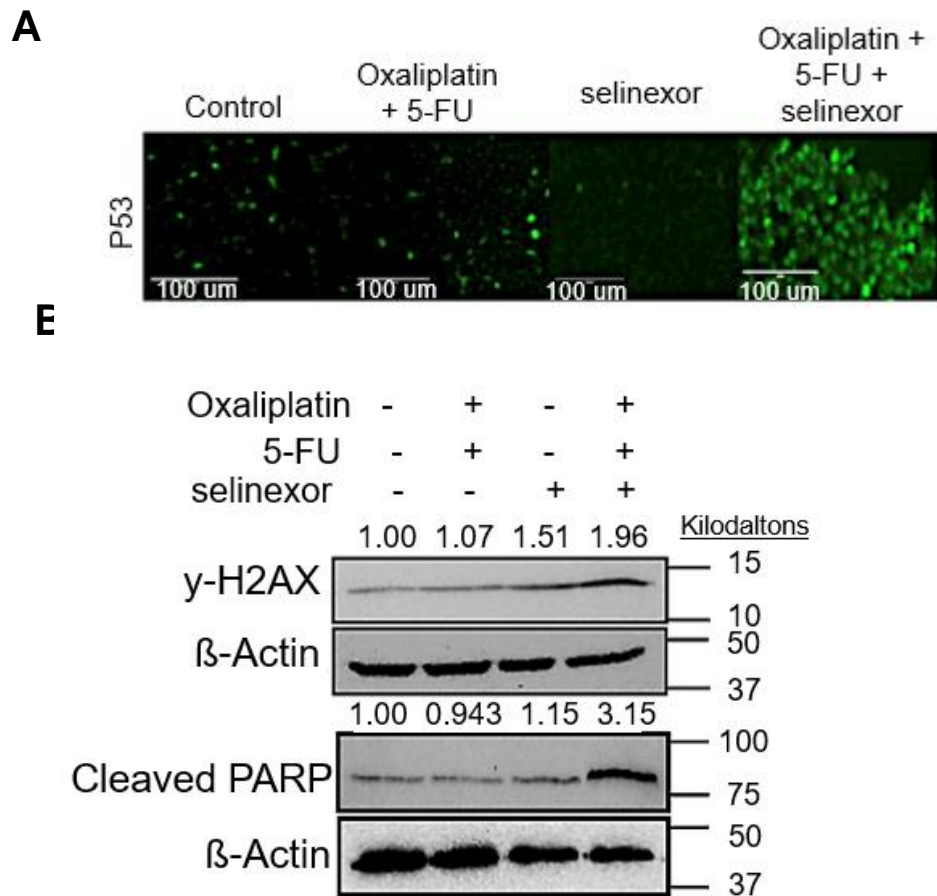
	Oxaliplatin IC <sub>50</sub>	Standard Deviation	5-Fluorouracil IC <sub>50</sub>	Standard Deviation	Oxaliplatin + 5-FU+ Selinexor (nM)	CI Value	Fa Value	Standard Deviation
SNU-16	158.55	1.06	598.9	159.29				
					62.5 : 187.5 : 6.25	0.100	0.773016	0.0407
					125 : 375 : 12.5	0.092	0.885714	0.251
					250 : 750 : 25	0.102	0.931746	0.240
SNU-1	261.7	18.64	134.85	87.37				
					62.5 : 62.5 : 6.25	0.293	0.772283	0.0408
					125 : 125 : 12.5	0.402	0.827025	0.0721
					250 : 250 : 25	0.166	0.955840	0.1155

**Table 9: IC<sub>50</sub> values and synergy calculations for SNU-1 and SNU-16 cell lines with oxaliplatin, 5-fluorouracil and selinexor.** IC<sub>50</sub> values for oxaliplatin and 5-FU were calculated as an average of three independent experiments in both the SNU-1 and SNU-16 cell lines. Standard deviations are provided. The synergy values reported are a mean (average) of three independent experiments with the standard deviations provided between experiments. Synergy was assessed using CalcuSyn software and synergy was determined by CI values were CI < 1.00 is indicative of synergy, CI = 1.00 is indicative of additive effect and CI > 1.00 is indicative of antagonism. The values reported were found to be synergistic within all three individual experiments.

upregulation of p53, a tumor suppressor that is upregulated in response to DNA damage (**Figure 3.4**). Although the ability of selinexor to dampen the DNA damage response has been published previously [Kashyap et al., 2018], this concept has not been studied specifically in gastric cancer. To further explore this, we treated SNU-16 and SNU-1 gastric cancer cells with either oxaliplatin and 5-FU or oxaliplatin, 5-FU and selinexor for 24 hours. The doses administered were selected based on the respective compounds  $IC_{50}$  values for these cell lines (**Table 9**).

24-hour immunofluorescence analysis showed sustained activation of p53 in the triple combination (oxaliplatin, 5-FU and selinexor) compared to oxaliplatin and 5-FU alone (**Figure 5.4A**). As anticipated, there was upregulation of p53 to some extent in the oxaliplatin and 5-FU treated cells but this is much greater with the addition of selinexor (**Figure 5.4A**). Upregulation of p53 is an early cellular event indicative of DNA damage. To verify whether enhanced DNA damage was occurring in the triple combination cells (i.e., cells treated with selinexor, oxaliplatin and cisplatin) compared to the oxaliplatin and 5-FU only treatment, we treated the SNU-16 cells with either oxaliplatin and 5-FU, selinexor only or a combination of selinexor, oxaliplatin and 5-FU and found enhanced DNA damage as visualized by an increase in  $\gamma$ -H2AX expression (**Figure 5.4B**). The enhanced presence of cleaved PARP further suggests an increase in DNA damage within the cells treated with the triple combination (**Figure 5.4B**). To determine whether these cells have the capabilities to repair these genetic lesions induced by the triple combination treatment, we probed for downstream DNA damage repair proteins.

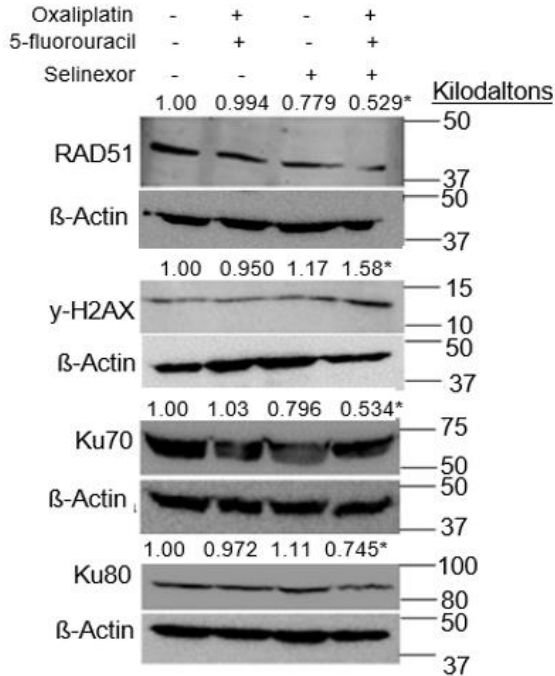
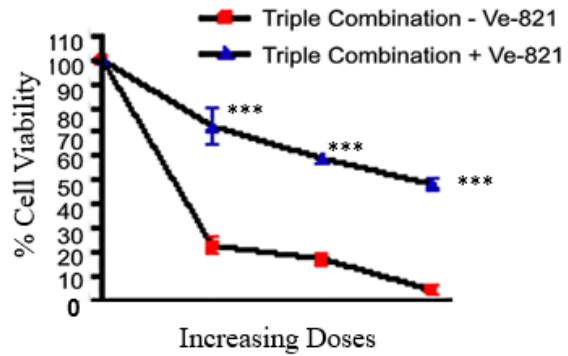
Expression analysis of DNA damage repair proteins downstream of the initial DNA damage signals showed a dampened response to DNA damage repair including



**Figure 5.4: DNA damage is upregulated in treated gastric cancer cells. [A]** SNU-16 cells treated with 125 nM of oxaliplatin and 375 nM of 5-FU, 12.5 nM of selinexor or the combination of these three compounds. Results suggest upregulation of the DNA damage response protein p53 occurs with combination treatment. **[B]** Western blotting of SNU-16 cells treated with 250 nM oxaliplatin, 750 5-FU and/or 25 nM selinexor for 72 hours. Western blotting revealed upregulation of  $\gamma$ -H2AX and PARP, which is indicative of upregulation of cellular DNA damage. Immunofluorescence results are indicative of three independent experiments. Western blotting and densitometry is representative of one experiment.

downregulation of homologous recombination protein enzymes such as Rad51, Ku70 and Ku80 in the cells treated with oxaliplatin, 5-FU and selinexor (**Figure 5.5A**). Downregulation of these repair proteins, as has been observed in other cell models [Kashyap et al., 2018], suggests that the gastric cancer cells cannot repair the DNA damage and thus halting DNA repair could be the mechanism of action.

To validate whether inhibition of the DNA damage response is the only mechanism of action of this triple combination we performed a rescue experiment utilizing the ATM/ATR inhibitor VE-821 (**Figure 5.1**). As part of the DNA damage-signaling pathway, ATM and ATR are protein kinases that are initially phosphorylated in order to signal for the cell to begin repairing DNA lesions [Webber and Ryan, 2015]. ATM is activated, or phosphorylated, by double stranded DNA breaks where ATR is activated, or phosphorylated, by UV lesions or stalled replication forks [Bradbury and Jackson, 2003]. Through inhibition of DNA damage signaling, we hypothesized that treatment with VE-821 would either (1) cause the cells to become completely sensitized to treatment or lead to complete cell death or (2) this would cause the cells to induce a survival mechanism that would suggest there was another mechanism besides DNA damage. To explore this, the SNU-16 gastric cancer cells were treated first with VE-821 for 3-hours and then treated with either oxaliplatin and 5-FU or oxaliplatin, 5-FU and selinexor for 72 hours and assessed for cellular viability. Our results indicate that inhibition of DNA damage response with VE-821 induces enhanced cell viability after treatment with 5-FU, oxaliplatin and selinexor at the three combinations we found to be synergistic (**Table 9, Figure 5.5B**). This indicates that there is a secondary mechanism of action independent of DNA damage.

**A****B**

**Figure 5.5: Inhibition of DNA damage is a mechanism of action. [A]** Inhibition of downstream DNA damage proteins such as RAD51, KU70 and Ku80 after 72-hour treatment. Results and densitometry (mean) are indicative of two or three independent experiments where denoted. Standard error calculations are as follows for the lanes going from left to right on the blot RAD51 (3): 0.108, 0.108, 0.0970, 0.115,  $\gamma$ -H2AX(3): 0.0310, 0.0421, 0.0357, 0.0317, Ku70 (3): 0.0995, 0.00178, 0.09604, 0.148, Ku80(2) 0.0190, 0.0549, 0.0166, 0.00761. \* Notes significance where p-value < 0.05 using two-tailed t-test comparing the double combination (oxaliplatin + 5-FU) to triple combination (oxaliplatin + 5-FU + selinexor). **[B]** SNU-16 cells after 3-hour treatment with/without VE-821 and 72-hour treatment with either the triple combination were assessed using cell viability assay. Graph is representative of three independent experiments. Significance was found using two-tailed t-test at 95% confidence interval where p-value \*\*\* < 0.001. Independent validation found similar trends using Excel software.

### 6.3.3 XPO1 downregulation suppresses one-carbon metabolism

To investigate alternative mechanisms, we first assessed the ways in which inhibition of antimetabolites lead to cellular death. As described above, 5-FUs mechanism of action is to suppress cells from synthesizing the thymidylate enzyme that is used during DNA replication and cell division to synthesize pyrimidine subunits. It is known that 5-FU resistance is due in part to an upregulation of thymidylate synthase (TYMS) [Peters et al., 1995]. Thymidylate synthase is a folate-dependent enzyme that is directly involved in the metabolism of 2'-deoxyuridine monophosphate (dUMP) to deoxythymidine monophosphate (dTMP). Inhibition of this enzyme leads to a perturbation of normal host functions including imbalance of pyrimidine nucleotides (increased dUMP/dTMP) leading to DNA damage [Rose et al., 2002]. Knockdown of XPO1 showed significant downregulation of *TYMS* in gastric cancer cells (p-value < 0.001) (**Figure 5.6A**).

Since treatment with 5-FU induces expression of XPO1 (**Figure 5.2**) and TYMS contains a NES similar to other proteins exported by XPO1 [Bissoon-Haqqani et al., 2006], that supports our initial hypothesis that selinexor overcomes resistance to 5-FU via TYMS inhibition. We probed for TYMS expression after 72-hour treatment with the double combination (oxaliplatin and 5-FU), selinexor single agent, or the triple combination (oxaliplatin, 5-FU and selinexor) and found downregulation of this enzyme in the triple combination more so than the double combination (**Figure 5.6B**). Since inhibition of TYMS mainly induces cell death through DNA damage, we wanted to further investigate alternative mechanisms of action for this triple combination.

Utilizing the Geo2.0 database, we compared patient derived organoids that were

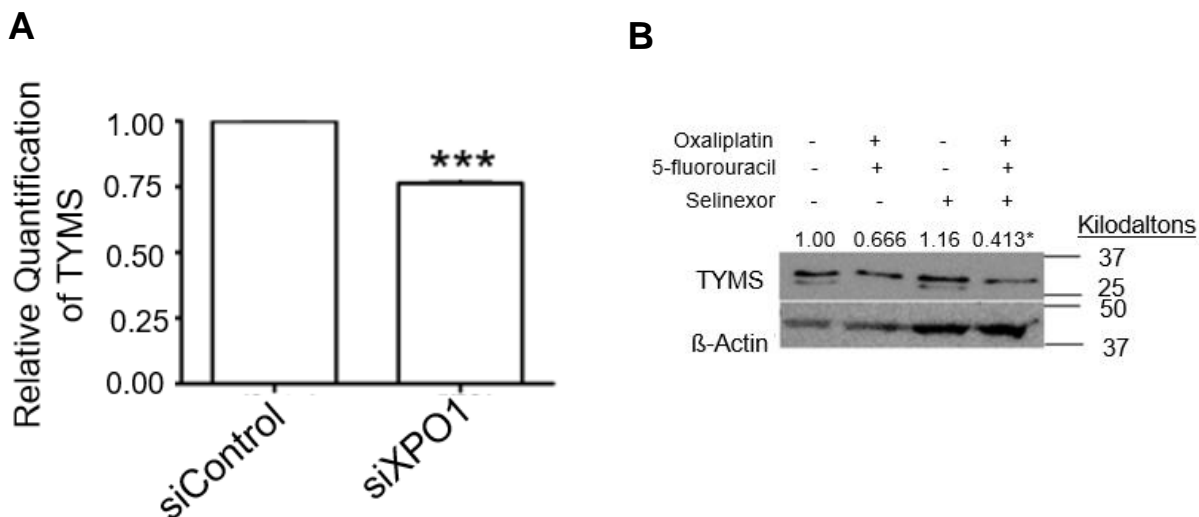


**Figure 5.6: XPO1 downregulation suppresses one carbon metabolism.** **[A]** 72-hour knockdown of XPO1 in the NCI-N87 cell line showed significant downregulation of *TYMS* after normalization to siControl. Results are indicative of three independent experiments where \*\*\*  $p < 0.001$  and statistics and graphs are obtained by GraphPad. Error bar is reflective of standard deviations of three independent experiments. **[B]** Western blotting of *TYMS* in SNU-16 cell line after 72-hour treatment with 125 nM oxaliplatin, 375 nM of 5-FU and 12.5 nM selinexor showed downregulation of this protein compared to either single agent selinexor or double agent oxaliplatin and 5-FU. Standard error is as follows from left to right: 0.373, 0.257, 0.325, and 0.131. Statistics were obtained by GraphPad where  $p$ -value \*  $< 0.05$  comparing double combination (oxaliplatin + 5-FU) to triple combination (oxaliplatin + 5-FU + selinexor). Western blot and densitometry (mean) is representative of three independent experiments. Independent validation found similar trends using Excel software of downregulation more so in the triple combination treatment.

resistant and sensitive to 5-FU. Our analysis revealed an increase in WW Binding Domain 5 (WBP5)/Transcriptional Elongation factor A like 9 (TCEAL9) expression within the 5-FU resistant organoids thus showing downregulation of WBP5 in the 5-FU sensitive organoids (**Figure 5.7A**). WBP5 protein is involved in a variety of cellular processes including maintaining cellular integrity and it is relevant to cancers, specifically papillary thyroid carcinoma [Qian et al., 2019]. Based on database results we hypothesized that WBP5 acts as an oncogene in gastric cancer. We found knockdown WBP5 activity in gastric cancer suppresses gastric cancer growth (**Figure 5.7B-C**) thus confirming our hypothesis. Interestingly, knockdown of WBP5 downregulated *TYMS* at the RNA and protein levels (**Figure 5.8A**) which caused enhanced 5-FU sensitivity in our gastric cancer cells (**Figure 5.8B**).

We evaluated the impact of knockdown of WBP5 in reverses pro-cancerous phenotypes within gastric cancer. Treatment with selinexor (24 hours) down regulated *WBP5* in the triple combination treatment and also decreased inflammatory markers such as the NF- $\kappa$ B p65 subunit and the matrix remodeling protein MMP14 (**Figure 5.9**).

#### **6.3.4 Oxaliplatin, 5-fluorouracil and selinexor induces substantial death**

A recent phase I clinical trial (Sentinel Trial), investigating selinexor in addition to FOLFOX (mFOLFOX6) in colorectal cancer patients was recently performed [Nilsson et al., 2020]. The clinical trial was stopped early due to significant toxicities. It was suggested that a preclinical investigation was needed to identify better dosing schedules [Nilsson et al., 2020]. The dosing schedule for the clinical trial included administering complete doses of 5-FU: (400 mg/m<sup>2</sup> IV Day 1 then 2400 mg/m<sup>2</sup> continuous infusion Day 1-3), complete dose of oxaliplatin (85 mg/kg IV), full dose folinic acid (400 mg/m<sup>2</sup>) and



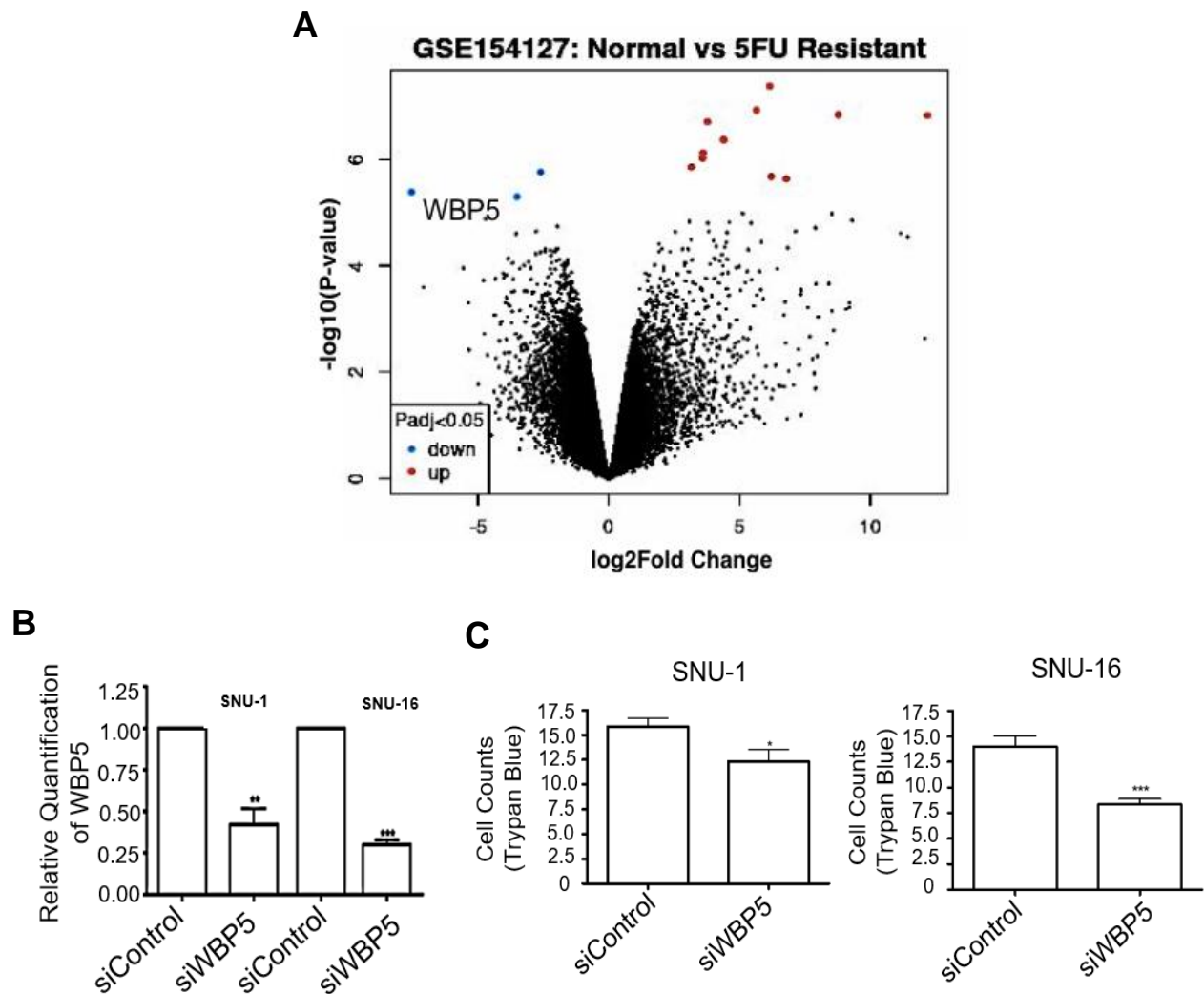
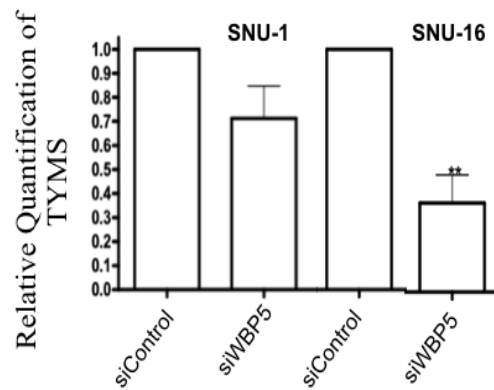


**Figure 5.7: WBP5 expression is relevant to 5-FU resistance.** [A] WBP5 expression was found to be significantly downregulated in 5FU sensitive organoids compared to 5-FU resistant organoids. Statistics were calculated by Geo2.0 analysis and significance was assessed at p-values < 0.05. [B] WBP5 knockdown was performed in the SNU-1 and SNU-16 cell lines and showed decreased cell viability after 24-hour knockdown compared to silenced control using RT-qPCR. Statistics were assessed with GraphPad PRISM software where \*\* p-value < 0.01 and \*\*\* p-value < 0.0001. [C] Cell viability assay after *WBP5* knockdown in SNU-1 and SNU-16 cells. Graph (mean) is representative of three independent experiments and error bars denote standard deviation. Statistics were assessed using GraphPad PRISM software and significance indicated by \* where p-value < 0.05 and \*\*\* where p-value < 0.001.

A



B

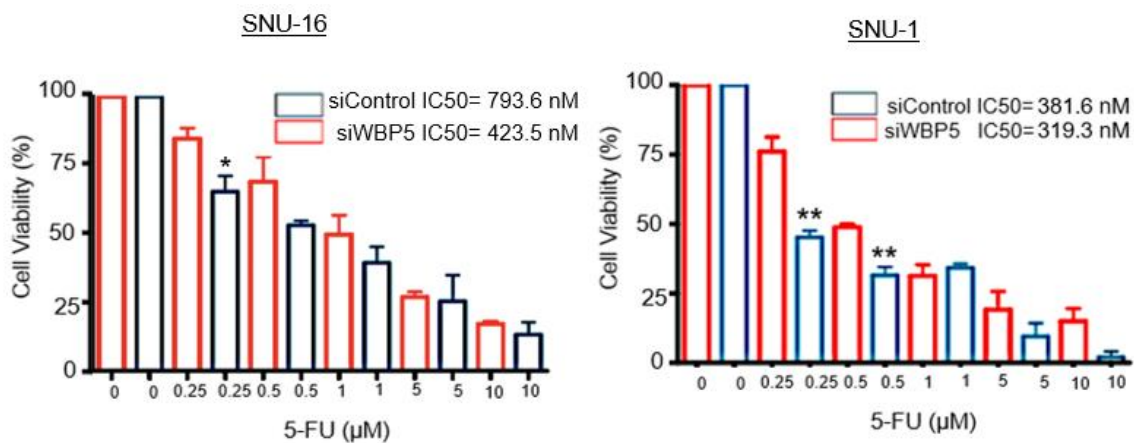


**Figure 5.8: WBP5 knockdown sensitizes gastric cancer cells to 5-FU.** [A] WBP5 knockdown cells (Figure 5.7B) were extracted for RNA. *TYMS* expression was found to be decreased after 24 hour knockdown. Statistics were obtained using GraphPad Software where \*\*  $p < 0.01$ . [B] SNU-1 (right) and SNU-16 (left) cells transfected with either siControl or siWBP5 were treated with 5-FU for 72 hours. After treatment, cell viability was assessed and results show IC<sub>50</sub> values differ between the two groups. Graphs (mean) were created using GraphPad PRISM software and statistics were assessed using two tailed t-test and 95% confidence interval significance is denoted where \*\* indicates  $p$ -value  $< 0.01$ . Error bars represent standard deviation. Standard deviation of the IC<sub>50</sub> values are as follows for SNU-1 cell line siControl .278, siWBP5 0.05561, SNU-16 cell line siControl 0.05155, siWBP5, 0.07834.

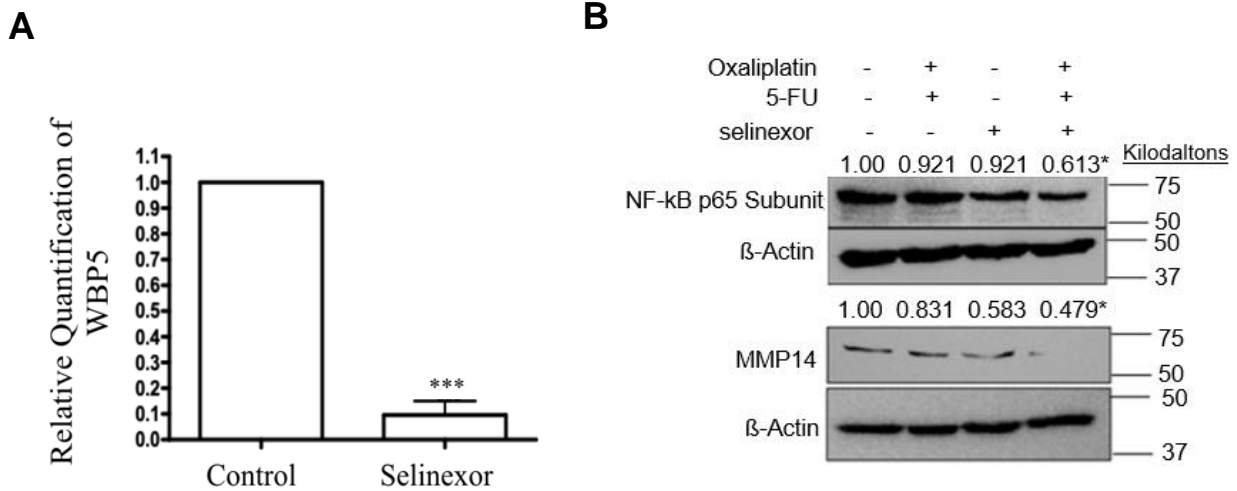


**Figure 5.9: Selinexor downregulates WBP5 in gastric cancer.** **[A]** Treatment with 50 nM of Selinexor for 24 hours caused significant downregulation of *WBP5* expression in the SNU-1 cell line. Results are representative of two independent experiments using two-tailed t-test with 95% confidence interval. Statistics were obtained using GraphPad Software where \*\*\*  $p < 0.001$ . Error bars represent standard deviation. **[B]** Further investigation into downstream processes controlled by WBP5 such as inflammation (NF-kB) and matrix remodeling (MMP14) were suppressed after selinexor (12.5 nM) was added to oxaliplatin (125 nM) and 5-FU (375 nM) in the SNU-16 cell line where \* denotes  $p$ -value  $< 0.05$  calculated by GraphPad PRISM software. Standard error was calculated as follows from left to right, NF-kB: 0.178, 0.201, 0.0752, 0.0985; MMP14: 0.577, 0.467, 0.336, and 0.276.

full dose selinexor, 80 mg/kg [Nilsson et al, 2020]. Dosing of selinexor was at day 1, 3 and 8 with a de-escalation plan from 80 mg to 20 mg. Unfortunately, the study was terminated early, after 40 mg treatment with selinexor, due to intolerable toxicities [Nilsson et al, 2020]. Our results suggest that we can reduce the doses of all three compounds and still obtain meaningful and synergistic results (**Table 9**).

Based on this trial results, we wanted to identify how treatment with this triple combination would affect normal gastric cells at the doses we found to be relevant in gastric cancer (**Table 9**). After 72-hour treatment with selinexor, oxaliplatin and 5-FU, we found no significant reduction in cell viability for the normal epithelial gastric cells (**Figure 5.10A**). Although we expected to not see much cell killing with selinexor because it is a targeted therapeutic, to our surprise we also did not find much cell killing in the double combination (oxaliplatin and 5-FU), which includes non-targeted compounds. A simple explanation for this is because we are using these compounds at sub-optimal doses, i.e., the IC<sub>25</sub> of the gastric cancer cells. Further, the normal gastric epithelial cells are not as rapidly dividing as the gastric cancer cells. The doubling times of normal gastric epithelial cells vary between 20-53 hours [Aziz et al., 2015] whereas the SNU-1 and SNU-16 cell line are more rapidly dividing with a doubling time of 25-30 hours. The mechanisms of oxaliplatin and 5-FU involve targeting rapidly dividing cells to cause DNA damage non-specifically. It would make sense that relative to cancer cells at the low doses administered they are less impacted by these compounds. Clearly, at higher doses there would be indications of cytotoxicity and cell death. Apoptotic analysis of the SNU-16 gastric cancer cells revealed substantial cell death in the triple combination compared to

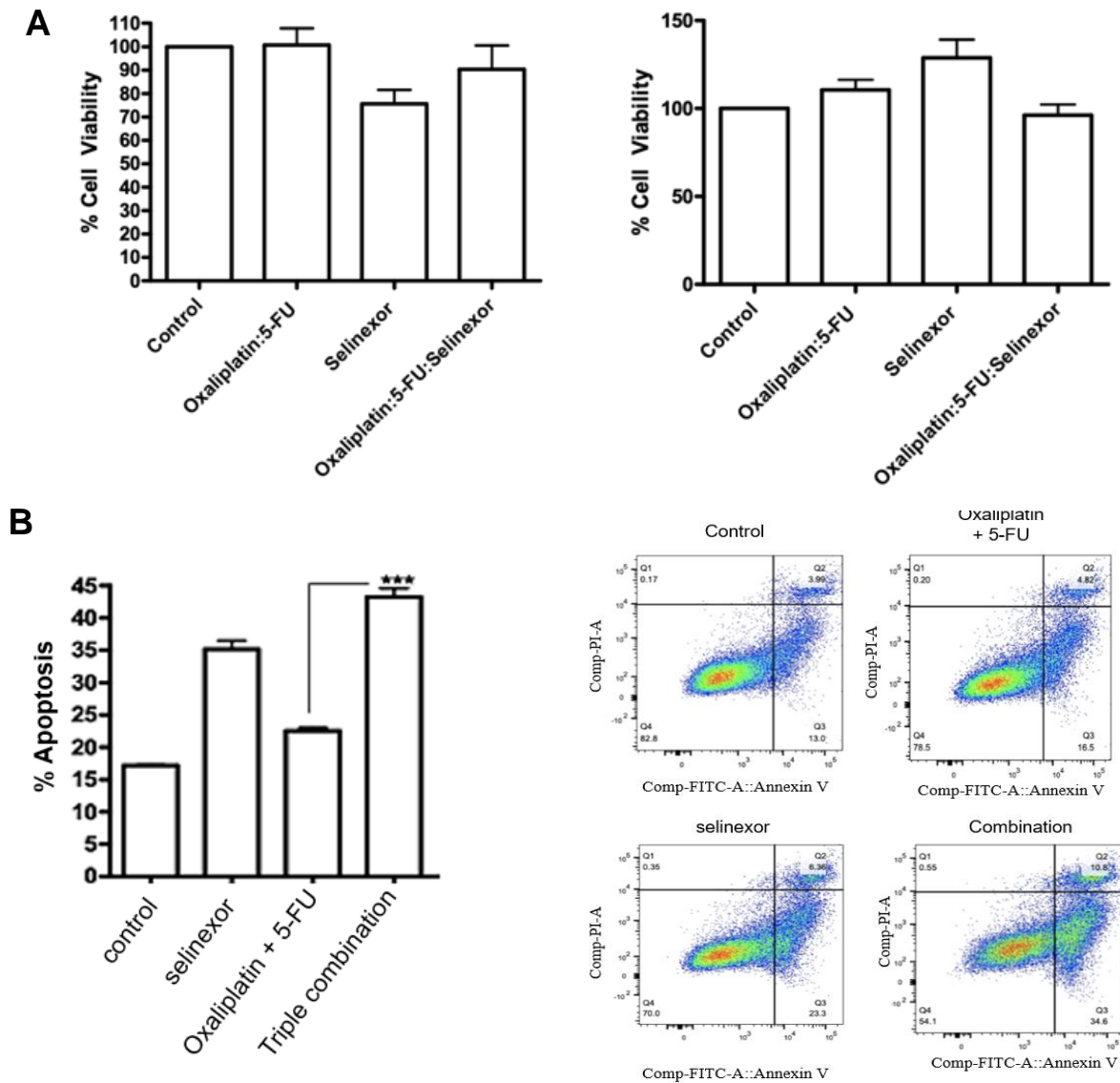


**Figure 5.10: Triple combination efficacy in normal and gastric cancer cells. [A]** Normal epithelial cells were treated at the doses found to be effective for killing SNU-1 and SNU-16 cells for 72 hours. Left diagram depicts epithelial gastric cells being treated at 125 nM oxaliplatin, 125 nM 5-FU and 12.5 nM selinexor (representative of doses for SNU-1 cell line) where the right diagram depicts epithelial gastric cells treated with 125 nM oxaliplatin, 375 nM 5-FU and 12.5 nM selinexor for 72 hours (representative of doses for SNU-16 cell line). The graph is representative of mean values and the error bars represent standard deviation. **[B]** SNU-16 gastric cancer cells were treated with single agent selinexor (12.5 nM), oxaliplatin and 5-FU (125 nM and 375 nM, respectively) or combination for 72 hours. Cells were collected and assessed for apoptosis using flow cytometry and statistics were assessed using GraphPad PRISM software using two-tailed t-test at 95% confidence interval where \*\*\* denotes p-value < 0.0001. Error bars depict standard deviation.

the double treatment or single agent selinexor along with no substantial cell death in the epithelial gastric cells (**Figure 5.10B**). Moving forward with *in vivo* investigation, we tested the oxaliplatin/5-FU/selinexor triple combination in SNU-16 xenografts. Upon completion of the experiment, we observed significant loss in tumor volume in the triple combination (oxaliplatin, 5-FU, and selinexor) compared to double combination (oxaliplatin and 5-FU) (**Figure 5.11A**). Throughout the course of treatment as well as after treatment ended, we found no statistically significant loss of body weight suggestive of the tolerability of this regimen at the indicated concentrations (**Figure 5.11A, Table 10**). For molecular analysis, we isolated the protein from the residual tumors and assessed different markers including TYMS, RAD51 and WBP5 (**Figure 5.11B**).

We found enhanced cleaved PARP in the triple combination compared to double combination indicative of enhanced DNA damage (**Figure 5.11B**). The DNA damage repair protein RAD51 was found to be significantly downregulated, and is in line with the *in vitro* results (**Figure 5.11B**). We further found loss of TYMS expression in the triple combination compared to double combination indicative of a loss of one-carbon metabolism (**Figure 5.11B**). Finally, we observed loss of WBP5, the oncogenic protein found to be prominent in 5-FU resistant gastric organoids (**Figure 5.11B**).

#### **6.4 Conclusions**

Together these results suggest that selinexor enhances the therapeutic efficacy of oxaliplatin and 5-FU in *vitro* and *in vivo*. The mechanism of action between these synergistic interactions is an enhancement of DNA damage, loss of DNA damage repair signaling and additional proteins related to gastric cancer sustenance. Treating SNU-16

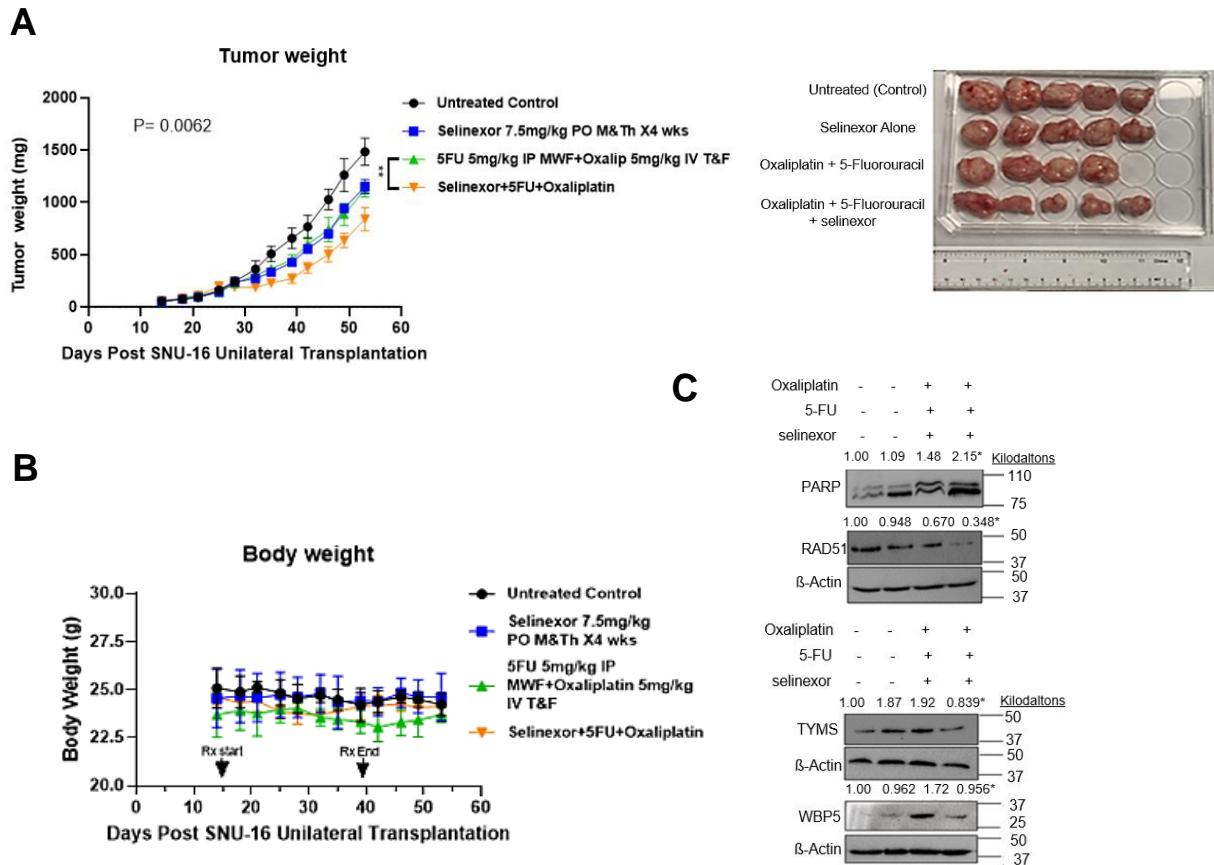


**Figure 5.11: In vivo study of triple combination in SNU-16 xenograft.** [A] In vivo study of SNU-16 xenograft in ICR-SCID mice treated with either oxaliplatin and 5-FU, selinexor alone or combination treatment. After the experiment ended and mice were sacrificed, tumor burden was weighed, calculated and plotted. Error bars denote just standard deviation. Statistics were plotted using GraphPad PRISM software where \*\* denotes p-value < 0.01. Image is representative of the SNU-16 xenograft cohorts. [B] Body weight (toxicity) was measured over the course of the experiment and plotted using GraphPad PRISM. Error bars represent standard deviation where the graph represents a mean value. [C] Western blotting of SNU-16 xenograft tissues probing for DNA damage proteins (PARP) and proteins involved with 5-FU resistance (WBP5, TYMS). Graphical image is a representative image of two or three independent experiments (denoted) with a standard error or the following going from left to right: PARP(2): 0.0257, 0.0966, 0.0475, 0.0336, RAD51(3): 0.0423, 0.0943, 0.0247, 0.0376, WBP5(3): 0.155, 0.227, 0.227, 0.166, TYMS(3): 0.0796, 0.164, 0.00956, 0.0501. Statistical analysis of densitometry results (mean) revealed statistical significance comparing double combination to triple (lane 2 to 4) using two-tailed t-test at 95% confidence interval.

Treatment	Route	Schedule	Total Dosage (mg/kg)	Body Weight Loss (%)	T/C (%)	Time to 1000 mg in days (range)	Tumor Growth Delay (days)
No Treatment	————	————	————	3.39 (S.D=2.75)	————	42.5 (39-46)	————
Selinexor	Oral Gavage	Q2d Start Day 14	60	-0.333 (S.D= 2.90)	25.53	51 (49-53)	8.5
Oxaliplatin + 5-FU	IV, Peritoneal injection	Q3d, Q2d Start Day 14	60	-0.045 (S.D= 4.34)	23.01	51 (49-53)	8.5
Selinexor + Oxaliplatin + 5-FU	Oral Gavage, IV, Peritoneal injection	Q2d, Q3d, Q2d Start Day 14	60	1.95 (S.D=1.58)	44.93	53 (53-53, 1 mouse)	10.5

**Table 10: *In vivo* efficacies of oxaliplatin, 5-FU and selinexor toward the SNU-16 xenografts. Female ICR-SCID mice (4-6 weeks) were subcutaneously implanted with human SNU-16 tumor fragments on day 0. Beginning on day fourteen the mice were dosed intravenously (IV) as follows: oxaliplatin, Q3dx4 at 5 mg/kg tail vein injection, total dose 60 mg/kg; selinexor Q2dx4 at 7.5 mg/kg oral, total dose 60 mg/kg and 5-fluorouracil Q3dx4 at 5 mg/kg peritoneal injection, total dose 60 mg/kg. Mice were weighted periodically and health conditions were assessed daily; tumors were measured by caliper two-to-three times weekly. Mice were sacrificed when the cumulative tumor burden reached 5-10% of body weight (1-2 g) or were found moribund. Tumor volumes were estimated from two-dimensional caliper measurements, where tumor mass (in mg) = (a x b<sup>2</sup>)/2, and a and b are the tumor length and width in mm, respectively. Quantitative endpoints include: (i) tumor growth delay [T/C, where T is the median time in days required for the treatment group tumors to reach a predetermined size (e.g., 1000 mg), and C is the median time in days for the control group tumors to reach the same size; tumor-free survivors are excluded from these calculations]. Mouse body weight, percent body weight loss were used, along with daily health monitoring, to gauge drug effects and potential toxicity where comparisons occurred between each individual mouse to assess percent body weight loss.**



xenografts with this triple combination (oxaliplatin, 5-FU, and selinexor) showed a significant reduction in tumor burden compared to double combination treatment (oxaliplatin + 5-FU). The ability to achieve an enhanced tumor reduction was coupled with little toxicities, as we have observed no significant changes in body weight. Moving forward we plan to assess these combinations in clinical studies in patients with gastric cancer. The goals are to verify the safety and efficacy of these identified combinations against gastric tumors and the best dosing schedules that will move these studies forward by mitigating potential anticipated toxicities. A schematic of the synergy between XPO1 inhibition and DNA damaging agents can be seen in **Figure 5.12**.

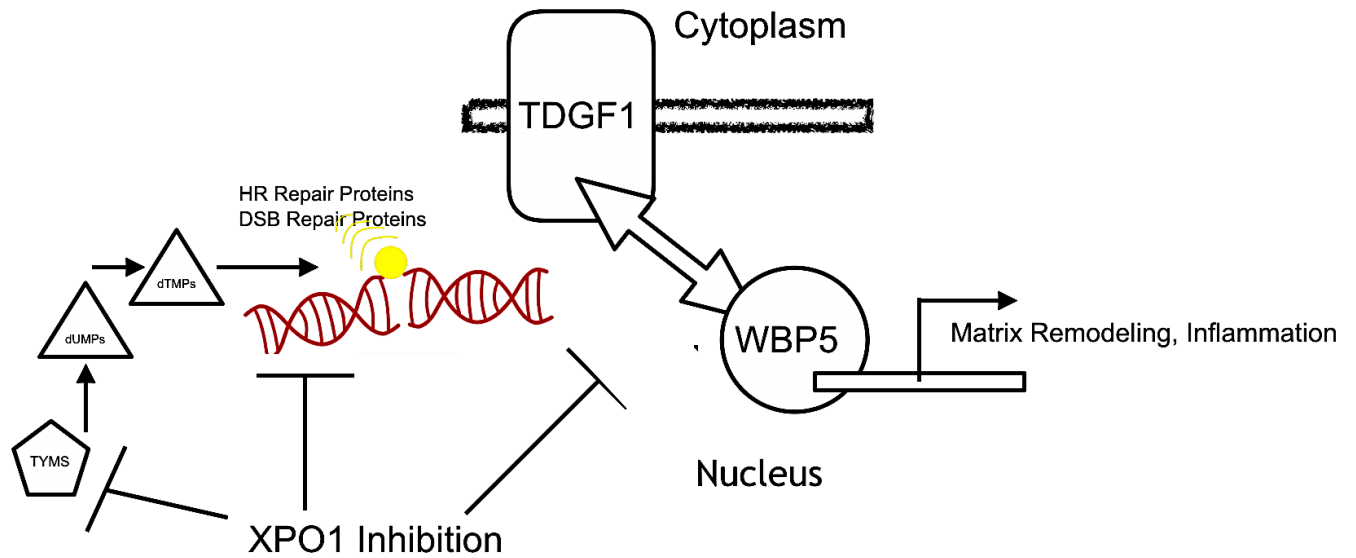


**Figure 5.12: Schematic of Synergy Mechanism for Selinexor plus Oxaliplatin and 5-FU.** XPO1 inhibition alters a variety of cell cycle processes including inhibition of TYMS (one-carbon metabolism) leading to the inability of cellular production of pyrimidines. XPO1 inhibition also induces more DNA damage through double stranded break repairs while simultaneously inhibiting DNA damage repair proteins. XPO1 inhibition also inhibits other cellular oncogenes such as WBP5 which downregulates pro-cancerous cellular behaviors such as matrix remodeling and inflammation.

## **CHAPTER 7- SMALL NONCODING RNAs IN GASTRIC CANCER**

### **7.1 Introduction**

Small noncoding RNAs are a recently discovered cellular component that targets protein-coding genes to alter their normal cellular functions [Choudhuri, 2010]. Some of the alterations that can occur through small noncoding RNA intervention are relevant to gastric cancer progression such as promoting cancer growth, cell viability and cellular dysfunction. Due to the prominence of small-noncoding RNAs within gastric cancer, many groups are interested in studying small noncoding RNAs for their ability to become predictive or prognostic biomarkers. In this chapter, we provide evidence that XPO1 is an alternative transporter for specific microRNAs, circular RNAs and piwiRNAs that are aberrantly expressed during XPO1 overexpression and are differentially expressed after XPO1 knockdown with selinexor. We found, through experimental validation, two microRNAs that are differentially expressed after selinexor treatment: microRNA-7974 and microRNA-129-1-3p. These microRNAs are involved in promoting pro-cancerous properties including the enhancement of cell viability and sustaining cellular growth signals. These results suggest that inhibition of XPO1 goes beyond altering the expression of cellular proteins and is more complex than previously thought.

### **7.2 Background**

#### **7.2.1 Overview of small noncoding RNAs**

Small noncoding RNAs are small-transcribed cellular RNAs not directly involved in coding for proteins [Choudhuri, 2010]. Rather, these RNAs elicit cellular functions by regulating complementary sequence genes either pre-transcriptionally, post-transcriptionally or epigenetically [Yamamura et al., 2018]. Some of the many classes of

small noncoding RNAs include microRNAs (18-29 nucleotides), long noncoding RNAs (> 200 nucleotides), circular RNAs and piwi RNAs (24-31 nucleotides). Small noncoding RNAs are diverse in relation to their structure and function but what remains similar between these is that evidence suggests all these small-noncoding RNAs are found in gastric cancer patients and cell lines. The biogenesis of these small noncoding RNAs is distinctly different and is described below.

### **7.2.2 MicroRNAs**

MicroRNAs normally originate from the alternative splicing of mRNAs within the nucleus [Treiber et al., 2019]. During normal transcription, microRNA genes are transcribed by RNA polymerase II along with the proximal mRNA genes. After splicing and processing by the nuclear enzyme complex DROSHA/DGCR8, the miRNA transcripts are exported from the nucleus by a member of the nuclear export protein family: exportin 5 (XPO5) [Treiber et al., 2019]. Once in the cytoplasm, the miRNA transcripts are spliced by the Dicer/TRBP protein complex and configured by Argonaute protein into a duplex shape which is the mature microRNA-silencing complex [Treiber et al., 2019]. This silencing complex then binds to mRNA transcripts within the cytoplasm and causes translational repression of complementary genes through direct interactions with either their 5' UTR or 3' UTR sequences. MicroRNAs can also bind to enhancer regions to signal for enhanced translation of proteins. MicroRNAs can also be generated as a by-product of long-noncoding RNA biogenesis (**Section 7.2.4**).

### **7.2.3 Circular RNAs**

Circular RNA biogenesis is the simplest cellular process for the generation of small-noncoding RNAs. These products form after normal transcription during RNA

splicing within the nucleus. RNA splicing can take alternative forms than the canonical splicing of introns only. Alternative splicing patterns, or back splicing, produces these species [Kristensen et al., 2019]. Due to alternative splicing, circular RNAs can consist of only introns, only exons or a mixture of both. These small noncoding RNAs are ligated together to form a circular structure through their complementary 5' (splice donor) and 3' (splice acceptor) ends, by DNA ligase enzymes. Circular RNAs have the ability to encode for proteins or sponge other small-noncoding RNAs, such as microRNAs, to alter gene expression.

#### **7.2.4 Long-noncoding RNAs**

Long-coding RNAs form within the nucleus through transcription of a long-noncoding RNA genes by RNA polymerase II/III. These long-noncoding RNA genes are transcribed, depending on the direction of their enhancer/promoter region, either through sense (3' to 5' direction of RNA Polymerase II), antisense (5' to 3' direction of RNA polymerase II), bidirectional transcription, intronic (where only the intronic regions are transcribed), or intergenic transcriptional patterns [Dahariya et al., 2019]. Once transcription is complete, the transcripts are processed into either long-noncoding RNAs which are exported from the nucleus to the cytoplasm where they interact with proteins or microRNA transcripts. Long-noncoding RNAs modulate gene expression at multiple levels including pre and post-transcription and epigenetic mechanisms.

#### **7.2.5 Piwi RNAs**

Piwi RNAs are the latest group within the small-noncoding RNA family and the most complex and unknown in terms of its two-part biogenesis. The process begins by the synthesis of a primary piwiRNA transcript within the nucleus by RNA polymerase II.

The immature transcript is exported to the cytoplasm where it is cleaved and modified by the enzyme complex Zucchini/Mino located on the mitochondrial surface. After unwinding of the transcript by Armi protein, the PIWI transcript is either complete in terms of its processing and goes to perform cellular functions such as germline insertion or it is loaded to a PIWI protein for the second part of this mechanism [Adapted from Iwasaki et al., 2015]. The PIWI protein then binds to a specific region within the transcript and cytoplasmic and/or mitochondrial enzymes such as PAPI/HEN1 and the Zucchini/Mino complex to cleave the overhang product that does not directly associate with PIWI to form a mature product that is methylated on the 3' end [Adapted from Iwasaki et al., 2015]. The overall outcome of this process is to generate piwi-RNAs for either transposon functions or insertion into the germline.

#### **7.2.6 Small noncoding RNAs in gastric cancer**

Small noncoding RNAs have perturbations have been studied for their ability to promote gastric cancer. For example Yu et al. have found six circulating microRNAs and three circulating long-noncoding RNAs in patient tissues that are abnormally expressed and are related to the clinical pathology of gastric cancer patients [Yu et al., 2021]. MicroRNAs have been found to alter gastric cancer and perpetuate disease including miR-155 and miR-223 which correlate to gastric cancer disease in both the antrum and corpus mucosa in patients with *H. Pylori* infection [Wang et al., 2016; Wang et al., 2016]. Over 100 studies have been performed to identify the roles of specific small noncoding RNAs in gastric cancer. From the above review of the literature, it can be concluded that small noncoding RNA perturbations are not only involved in the biogenesis and initiation of gastric cancer but can also contribute to pro-cancerous phenotypes including the

enhancement of various hallmarks of cancer including increased metastasis signaling, increased cellular signaling, immune system evasion, apoptotic evasion and drug resistance [Wei et al., 2020]. Furthermore, these cellular species can be found within the tumor tissue as well as circulating within the serum. For these reasons, small-noncoding RNAs are being investigated as prognostic biomarkers, for gastric cancer detection/clinical outcomes, and predictive biomarkers to clinically relevant chemotherapeutics.

Small non-coding RNAs are vital cellular components that requires further investigation within gastric cancer as to their functions and contribution toward this deadly disease. In the context of our study, we wanted to focus mainly on the roles of microRNA function as they are the most prominent and well-categorized small noncoding RNA species. We utilized three different sources to filter down two microRNAs. (1) publicly available databases; (2) independent small RNA sequencing data from selinexor exposed MiaPaca-2 pancreatic cancer cell lines and 3[Azmi et al., 2017] and (3) data from RNA sequencing of plasma cells from Non-Hodgkin lymphoma patients treated with selinexor-RCHOP and (NCT03147885, unpublished). These results have cumulatively identified two microRNAs (miR-7974 and miR-129-1-3p) of interest that we focused on for further studies. In this chapter, we will describe our results of how these two microRNAs are altered in gastric cancer and will show how their expression may contribute to differences in sensitivity to selinexor. These in *vitro* results suggest that microRNAs can be utilized as a predictive clinical biomarker for selinexor.

## **7.3 Materials and Methods**

### **7.3.1 Cell lines, culture conditions and reagents**

The SNU-1 and NCI-N87 cell lines were used for these studies purchased from American Type Culture Collection (ATCC, Manassas, VA, USA) in 2017 and were maintained in RPMI-1640 (Invitrogen, Carlsbad, CA, USA) supplemented with 10% fetal bovine serum (FBS) and 1% penicillin/streptomycin (P/S) in a 5% CO<sub>2</sub> atmosphere at 37 °C. RASGEF1A siRNA was purchased from Thermo Fisher (Waltham, MA, USA) and siControl was purchased from Santa Cruz Biotechnology. MicroRNA mimics and inhibitors were purchased from Dharmacon Inc (Lafayette, CO, USA). Lipofectamine 3000 (1 mg/mL) was purchased from Thermo Fisher (Waltham, MA, USA).

### **7.3.2 RNA extraction**

NCI-N87 and SNU-1 cells were grown in 100 mm dishes and exposed to media and SINE compound: selinexor at 500 nM or 25 nM, respectively, for 48 h. Total RNAs were extracted using Trizol reagent (Invitrogen, Waltham, MA, USA) following the manufacturer's procedure and isolated with the small RNA isolation kit (Qiagen, Hilden, Germany). The total RNA quality and quantity were first verified using our plate reader measuring at 260 nm (TECAN, Durham, NC, USA). Then, analysis of the total RNA was performed on Bio analyzer 2100 (Agilent, CA, USA) with RIN number >7.0. Approximately 1 µg of total RNA was used to prepare a small RNA library according to protocol of TruSeq Small RNA Sample Prep Kits (Illumina, San Diego, CA, USA). Single-end sequencing was performed 50 bp on an Illumina Hiseq 2500 at LC Sciences (Houston, TX, USA) following the vendor's recommended protocol. Raw reads were subjected to an in-house program, ACGT101-miR (LC Sciences, Houston, Texas, USA) to remove adapter dimers,



low complexity, common RNA families (rRNA, tRNA, snRNA, snoRNA) and repeats. For piRNA the unique sequences with lengths of 25-37 nucleotides were mapped to specific-species precursors in the piRNA database (Available online: <http://pirnabank.ibab.ac.in/request.html>, accessed on 5 July 2018) by BLAST search to identify known piRNAs. One mismatch inside of the sequences was allowed in the alignment. The unique sequences mapping to both the piRNA database and species genome were identified as known piRNAs. The unique sequences only mapping to the genome were considered to be piRNA candidates.

### **7.3.3 Non-coding RNA data analysis (miRNA)**

Subsequently, unique sequences with lengths of 18-26 nucleotides were mapped to specific species precursors in miRBase 22.0 by BLAST search to identify known miRNAs and novel 3p- and 5p-derived miRNAs. Length variation at both the 3' and 5' ends and one mismatch inside of the sequence were allowed in the alignment. Unique sequences mapping to specific-species mature miRNAs in hairpin arms were identified as known miRNAs. The unique sequences mapping to the other arm of known specific-species precursor hairpin opposite to the annotated mature miRNA-containing arm were considered to be novel 5p- or 3p-derived miRNA candidates. The remaining sequences were mapped to other selected species precursors (with the exclusion of specific species) in miRBase 22.0 by BLAST search. The mapped pre-miRNAs were further BLASTed against the specific species genomes to determine their genomic locations. The above two we defined as known miRNAs. The unmapped sequences were BLASTed against the specific genomes, and the hairpin RNA structures containing sequences were predicated from the flank 80 nt sequences using RNAfold software (Available online:

<http://rna.tbi.univie.ac.at/cgi-bin/RNAWebSuite/RNAfold.cgi>, accessed on 5 July 2018.

The criteria for secondary structure prediction were: (1) number of nucleotides in one bulge in stem ( $\leq 12$ ); (2) number of base pairs in the stem region of the predicted hairpin ( $\geq 16$ ); (3) cutoff of free energy (kCal/mol  $\leq -15$ ); (4) length of hairpin (up and down stems + terminal loop  $\geq 50$ ); (5) length of hairpin loop ( $\leq 20$ ); (6) number of nucleotides in one bulge in mature region ( $\leq 8$ ); (7) number of biased errors in one bulge in mature region ( $\leq 4$ ); (8) number of biased bulges in mature region ( $\leq 2$ ); (9) number of errors in mature region ( $\leq 7$ ); (10) number of base pairs in the mature region of the predicted hairpin ( $\geq 12$ ); and (11) percent of mature region in stem ( $\geq 80$ ).

#### **7.3.4 Non-coding RNA data analysis (piRNA)**

piRNA differential expression based on normalized deep-sequencing counts was analyzed by selectively using the Fisher exact test, Chi-squared  $2 \times 2$  test, Chi-squared  $n \times n$  test, Student's t-test and ANOVA based on the experiment design. The significance threshold was set to be 0.01 and 0.05 in each test. To predict the genes targeted by differentially expressed piRNAs, two computational target prediction algorithms (Target Scan 5.0 and miRanda 3.3a) were used to identify piRNA binding sites. Finally, the data predicted by both algorithms were combined and the overlaps were calculated, the Gene Ontology (GO) terms and Kyoto Encyclopedia of Genes and Genomes (KEGG) pathway of these differentially expressed piRNA targets were also annotated.

#### **7.3.5 Circular RNA data analysis (circRNA)**

Total RNA was extracted using Trizol reagent (Invitrogen, CA, USA) following the manufacturer's procedure. The total RNA quantity and purity were analyzed with a Bioanalyzer 2100 and RNA 6000 Nano LabChip Kit (Agilent, CA, USA) with RIN

number>7.0. Approximately 10 µg of total RNA were used to remove ribosomal RNA according to the protocol of the Epicentre Ribo-Zero Gold Kit (Illumina, San Diego, USA). The linear RNA was digested according to the protocol of the Epicentre Ribonuclease R (Illumina, San Diego, USA). Following purification, the linear RNA fractions were fragmented into small pieces using divalent cations at elevated temperature. Then the cleaved RNA fragments were reverse-transcribed to create the final cDNA library in accordance with a strand-specific library preparation by the dUTP method. The average insert size for the paired-end libraries was 300±50 bp. We performed the paired-end 2x150bp sequencing on an Illumina HiSeq 4000 platform housed through LC Sciences following the vendor's recommended protocol. Firstly, Cutadapt and perl scripts in house were used to remove the reads that contained adaptor contamination, low quality bases and undetermined bases. Then sequence quality was verified using FastQC. We used Bowtie2 and Tophat2 to map reads to the genome of species. Remaining reads (unmapped reads) were still mapped to the genome using tophat-fusion. CIRCEXplorer was used to *de novo* assemble the mapped reads to circular RNAs at first; Then, back splicing reads were identified in unmapped reads by tophat-fusion and CIRCEXplorer. All samples generated unique circular RNAs. Circular RNA expressions from different samples or groups were calculated by scripts in house. Only the comparisons with p values <0.05 were regarded as showing differential expression by R package edgeR (Provided by LC Sciences).

### **7.3.6 Trypan blue cell viability assay**

For microRNA transfected growth experiments: Suspension SNU-1 cells were seeded at a density of  $2.5 \times 10^4$  cells/well in a 24-well plate in complete medium. After

subsequent acclimation (24 h), cells were transfected with lipofectamine 3000 (1 mg/ml, Thermo Fisher (Waltham, MA, USA)) and 50 nM of either miRNA mimic control (Dharmacon), miRNA 7974 mimic (Dharmacon), miR-inhibitor control (Dharmacon) or miR-129-1-3p inhibitor (Dharmacon) for 72 hours. After incubation, the cells were mixed well with a pipette, collected, and diluted 1:1 with 20- $\mu$ L Trypan blue. The cells were counted using a hemocytometer.

For microRNA transfected growth experiments plus selinexor: Suspension SNU-1 cells were seeded at a density of  $2.5 \times 10^4$  cells/well in a 24-well plate in complete medium. After subsequent acclimation (24 h), cells were transfected with lipofectamine 3000 (1 mg/ml, Thermo Fisher (Waltham, MA, USA)) and 50 nM of either miRNA mimic control (Dharmacon), miRNA 7974 mimic (Dharmacon), miR-inhibitor control (Dharmacon) or miR-129-1-3p inhibitor (Dharmacon) for 24 hours. After a 24-hour incubation, the cells were treated with increasing concentrations of selinexor for 72 hours (0-300 nM). After incubation, cells were mixed well with a pipette, collected, and diluted 1:1 with 20- $\mu$ L Trypan blue. The cells were counted using a hemocytometer.

### **7.3.7 MTT assay**

Adherent NCI-N87 cells were seeded at a density of  $1 \times 10^4$  cells per well in 96-well micro-titer plate in complete media. After subsequent acclimation (24 h) cells were transfected with lipofectamine 3000 (1 mg/ml, Thermo Fisher (Waltham, MA, USA)), miRNA mimic control (Dharmacon) and 50 nM of either miRNA 7974 mimic (Dharmacon), miR-inhibitor control (Dharmacon) or miR-129-1-3p inhibitor (Dharmacon). These cells were either incubated for 72 h or after 24 h incubation with the microRNA constructs, the cells were treated with increasing concentrations of selinexor for 72 h (0-5  $\mu$ M). After

incubation, the MTT assay was performed by adding 20  $\mu$ L of 3-(4,5-dimethylthiazol-2-yl)-2,5-diphenyltetrazolium bromide (MTT) (Sigma, St. Louis, MO, USA) solution (0.5 mg/mL in PBS) to each well and incubated for 2 h. After incubation, the media was aspirated and the cells were lysed with 100% isopropanol to dissolve the formazan crystals that were taken up by viable cells. The plates were then read at 570 nm on plate reader.

### **7.3.8 RASGEF1A knockdown**

A total of  $5 \times 10^5$  SNU-1 or NCI-N87 cells were plated in 24-well plates with RPMI only and incubated for 24 h. The following day siRASGEF1A or siControl (10  $\mu$ M) were mixed with Lipofectamine (1 mg/mL) according to the manufacturer's protocol for a final concentration of 2.5  $\mu$ g per well and added individually to the cells in medium containing RPMI + 10% FBS. Cells were incubated for 72 h with siRNA/Lipofectamine complexes and then trypsinized. The cells were either re plated for MTT assays, cell viability assay or underwent protein/RNA collection.

### **7.3.9 Colony formation**

Adherent NCI-N87 cells were seeded at a density of  $5 \times 10^5$  cells per dish in 100 mm dishes in complete media. After subsequent acclimation (24 h) cells were transfected with Lipofectamine 3000 (1 mg/ml, Thermo Fisher) and 50 nM of either miRNA mimic control (Dharmacon), miRNA 7974 mimic (Dharmacon), miR-inhibitor control (Dharmacon) or miR-129-1-3p inhibitor (Dharmacon). After 72 h of incubation the cells were re-transfected with Lipofectamine 3000 (1 mg/ml, Thermo Fisher) and 50 nM of either miRNA mimic control (Dharmacon), miRNA 7974 mimic (Dharmacon), miR-inhibitor control (Dharmacon) or miR-129-1-3p inhibitor (Dharmacon) for another 72 hours. After

transfection cells were trypsinized, collected and replaced at a density of 500 cells/dish in 10 mm dishes and incubated ~2-weeks or sufficient colonies were visible (~50 cells/colony).

### **7.3.10 RNA extraction and RT-qPCR**

The SNU-1 and NCI-N87 gastric cancer cell lines were plated at a density of  $2.5 \times 10^5$  cells/ml in 24-well plates in complete media for 24 hours. Cells were silenced with 50 nM of miR-7974 mimic, 50 nM miRNA mimic control, 50 nM miR-129-1-3p inhibitor or miRNA inhibitor control for 24 hours, collected and RNA was extracted using the Trizol RNA isolation protocol. cDNAs were synthesized at 1  $\mu$ g for each sample using a cDNA Reverse Transcription kit (Thermo Fisher, Waltham, MA, USA). Diluted cDNA samples were added to 96-well plate with RASGEF1A or ribosomal 18s subunit primers along with SyBR Green for RT-qPCR (Thermo Fisher, Waltham, MA, USA) and analysis according to standard protocol.

RASGEF1A Forward: 5' CCAGAATGTTCTCCTGGAGCCC 3'

RASGEF1A Reverse: 5' TCCAGGGACCCAGAGATGAG 3'

18s Forward: 5' GCAATTATTCCCCATGAACG 3'

18s Reverse: 5' GGCCTCACTAAACCATCCAA 3'

### **7.3.11 miRNA extraction and RT-qPCR**

For microRNA validation: NCI-N87 cells and SNU-1 cells were plated at a density of  $2.5 \times 10^5$  cells/well in 24-well plate. They were transfected with 50 nM of either miRNA mimic control, miR-7974 mimic, miRNA inhibitor control or miR-129-1-3p inhibitor with Lipofectamine 3000 (Thermo Fisher, Waltham, MA, USA) for 72 hours. After incubation, cells were collected and microRNAs were extracted using Trizol. cDNA was synthesized

using the TaqMan Advanced miRNA cDNA synthesis kit (Thermo Fisher, Waltham, MA, USA). RT-qPCR was run using TaqMan as a fluorescence detector with miR-7974 primer, miR-129-1-3p primer and RNU46B as controls.

For microRNA expression after selinexor treatment: NCI-N87 cells and SNU-1 cells were plated at a density of  $5 \times 10^5$  cells/well in 24-well plates. The cells were treated with 500 nM selinexor (NCI-N87 cells) or 25 nM selinexor (SNU-1 cells) for 24 hours. After incubation, cells were collected and microRNAs were extracted using Trizol. cDNAs were synthesized using the TaqMan Advanced miRNA cDNA synthesis kit (Thermo Fisher, Waltham, MA, USA). RT-qPCR was run using TaqMan as a fluorescence detector with miR-7974 primer, miR-129-1-3p primer, U47 and RNU46B as controls. All primers were obtained from Thermo Fisher (Waltham, MA, USA)

MiR-7974 (miRBase Accession Number MIMAT0031177):

GCUCGGCCCCACAGCGAAACGGCCGCCUAAACCACCCAGGCCUUAUGGCUUC  
AUAGGCUGUGAUGCUCUCCUGAGCCC

MiR-129-1-3p (miRBase Accession Number MIMAT0004548):

GGAUCUUUUUGCGGUCUGGGCUUGCUGUCCUCUCAACAGUAGUCAGGAAGCC  
CUUACCCCAAAAAGUAUCU

U47 (NCBI Accession Number AF141346):

TAATGATTCTGCCAAATGAAATATAATGATATCACTGTAAAACCGTTCCATTTTGATT  
CTGAGGT

RNU58B (NCBI Accession Number AB061824):

CTGCGATGATGGCATTCTTAGGACACCTTTGGATTAATAATGAAAACAACACTACTCT  
CTGAGCAGC

### 7.3.12 Database search

miRWalk 3.0 Database was used to look at the genes of interest that were targeted by miR-129-1-3p or miR-7974.

### 7.3.13 Statistics

Statistical analysis was performed using GraphPad PRISM software using two-tailed t-test at 95% confidence interval. Specific statistics is provided for each figures in the legends.

## 7.4 Results

### 7.4.1 XPO1 transports a variety of small noncoding RNAs to the cytoplasm

As discussed above, nuclear export protein 5 (XPO5) is mainly involved with the transport of small noncoding RNAs: microRNAs, long noncoding RNAs and circular RNAs, from the nucleus to the cytoplasm. There has been a small number of publications that have shown the alternative nuclear transport of small-noncoding RNAs by XPO1 [Muqbil et al., 2013, Azizian et al., 2013]. Our group has previously shown miR-145 is transported by XPO1 and its perturbed expression is related to the pathogenesis of pancreatic cancer [Azmi et al., 2017].

We wanted to identify whether in gastric cancer, XPO1 transports a subset of small noncoding RNAs. To do this we utilized two gastric cancer cell lines: SNU-1 and NCI-N87. The gastric cancer cells were treated with either PBS (control) or selinexor (50 nM or 500 nM, respectively) for 48 hours. Following this, small-noncoding RNAs were isolated and sequenced (LC Sciences). Sequencing revealed a variety of microRNAs, circular RNAs and piwiRNAs which were significantly and differentially expressed after selinexor treatment (**Table 11**). Since XPO1 inhibitors are specific to XPO1, and not



XPO5, the expression changes of a subset of small noncoding RNAs suggests XPO1 transport is an alternative mechanism to the canonical export by XPO5. Although these are the top differentially expressed small noncoding RNAs, there are still many small RNA species with expression changes that differ between the cell lines. These differences can be explained by the fact that gastric cancer is a highly heterogeneous disease and likely, the XPO1 transported noncoding RNAs are subtype specific. The NCI-N87 cell line is similar in histology and differentiation status to the inflammatory subset of gastric cancers, which are induced by *H. pylori* infection [Sato et al., 2020]. These gastric cancers are known to have large perturbations in small noncoding RNA expression [Vasapolli et al., 2021]. For these reasons, we chose to move forward focusing on the NCI-N87 as our model for these studies.

#### **7.4.2 Modulation of microRNAs leads to gastric cancer growth**

The small noncoding RNA sequencing results (**Table 11**) showed after 48 hour selinexor treatment there was a significant downregulation of miR-7974 and significant upregulation of miR-129-1-3p in the NCI-N87 cell line. Based on this, we hypothesized that miR-7974 is naturally upregulated (oncogenic) and miR-129-1-3p is naturally downregulated (tumor-suppressive) in gastric cancer, or at least in intestinal type gastric cancer. miR-7974 is a >24 nucleotide long microRNA located on chromosome 19: 11495544-11495622 (-). In the literature, there is little known about miR-7974 except for its probable role in promoting lung adenocarcinoma, lung squamous cell carcinoma and breast cancer [Dong et al., 2020; Lai et al., 2019]. miR-7974 was also found to be associated with the microbiome present in intestinal carcinomas and was found to be highly expressed in tumor tissues [Lai et al., 2019; Dong et al., 2020; Yuan et al., 2018].

MicroRNA	Piwi RNA	Log2Fold Change
Hsa-miR-130a-3p		-2.16
Hsa-miR-7974		-1.97
Hsa-let-7c-3p		-1.95
Hsa-miR-33b-3p_R-1		-1.89
Hsa-miR-129-1-3p		2.09
Hsa-miR-548az-5p_L-1R+1		2.18
Hsa-miR-147b-5p		2.24
Hsa-miR-376c-3p		2.96
	piRNA-88	-2.78
	piRNA-57	-2.70
	piRNA-76	-2.45
	piRNA-78	-2.00
	piRNA-109	1.34
	piRNA-20	1.96
	piRNA-111	2.55
	piRNA-112	4.13
Circular RNA		
circRNA18683 (NFKB1)		-3.11
circ0004803 (RNF4)		-2.47
Circ0003323 (APP)		-1.56
Circ0001654 (SCAF8)		2.08
Circ0001346 (RNF13)		2.33
Circ003624 (UBE2R2)		2.56
Circ0048005 (ATP9B)		3.10
circRNA13481 (TUT7)		3.83
circ0054853 (XPO1)		4.22

**Table 11: Top differentially expressed small noncoding RNAs after selinexor treatment.** NCI-N87 cells were treated with 500 nM selinexor for 48 hours and assessed for microRNA and piwiRNA. SNU-1 cells were treated with 25 nM selinexor for 48-hours. Statistics were determined based on circular RNA expression, expression profiling, back splicing junctions and TopHat fusion mapping software to determine significance. The p-values < 0.05 were used as the cutoff to denote significant differential expression changes of circular, micro and piwiRNAs.

MicroRNA-129-1-3p is a >24 nucleotide long microRNA located on chromosome 7. In the literature, miR-129-1-3p is found to be downregulated in prostate and breast cancer [Zhang et al., 2015; Jia et al., 2019]. Further, in gastric cancer miR-129-1-3p was found to be lower in expression compared to normal tissues suggestive of being a tumor-suppressor microRNA [Yu et al., 2013]. We tested the expression of baseline miR-7974 and miR-129-1-3p in normal and gastric cancer cells and found significant upregulation of miR-7974 in the NCI-N87 cell line and significant downregulation of miR-129-1-3p in both the NCI-N87 and SNU-1 cell lines. This suggests that these microRNAs are perturbed in gastric cancer compared to normal tissue (**Figure 6.1**).

Using the NCI-N87 cell line as a model we wanted to endogenously express miR-7974 to understand the phenotypic impacts. First, validation of miR-7974 was visualized using Taqman RT-qPCR (**Figure 6.2**). After a 72-hour transfection, we found significant increases in cellular growth in both cell lines as well as enhanced colony formation (**Figure 6.2**). We further used the NCI-N87 cell line as a model to endogenously repress miR-129-1-3p to understand the phenotypic impacts. First, validation of miR-129-1-3p knockdown was confirmed using Taqman RT-qPCR (**Figure 6.3**). After a 72-hour transfection, we found significant increases in cellular growth and colony formation of the (**Figure 6.3**). Further validation was observed in the SNU-1 cell line with either miR-7974 overexpression or miR-129-1-3p downregulation (**Figure 6.2-6.3**). These results suggest that (1) microRNA perturbation can be separated into pathogenic events that enhance gastric cancer, (2) their cellular expression is controlled by XPO1 activity and (3) these microRNAs are relevant to influencing gastric cancer.

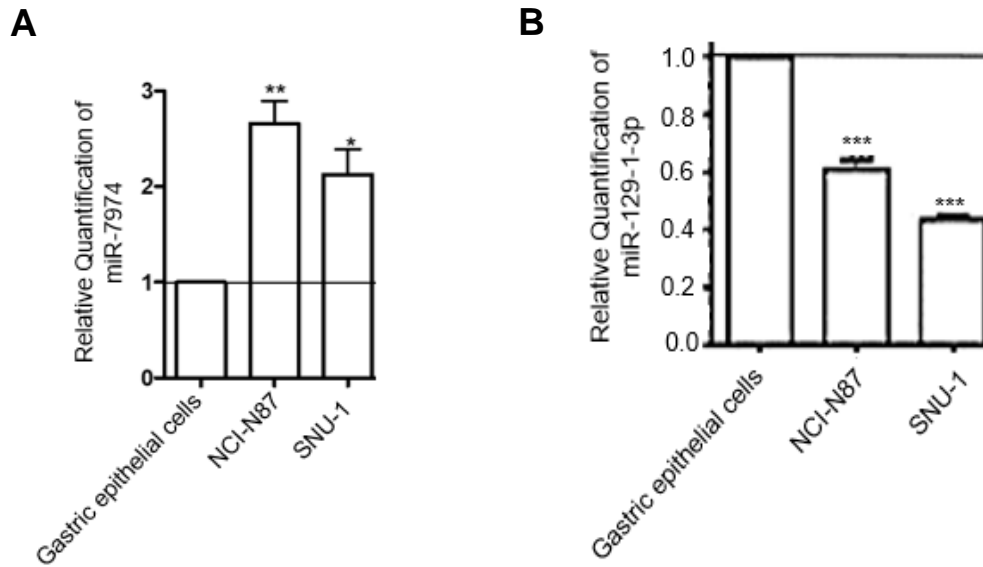


**Figure 6.1: Baseline expression of miR-7974 and miR-129-1-3p in normal and gastric cancer cell lines. [A-B]** RT-qPCR with Taqman primers directed towards miR-7974 and miR-129-1-3p and U7 used as a normalizing control. Experiments are representative of three independent replicates and quantification is an average of the three replicates where \* p-value < 0.05, \*\* p-value < 0.01 and \*\*\* p < 0.001. Graphs (mean) and statistics were obtained using GraphPad Prism software and error bars represent standard deviation.

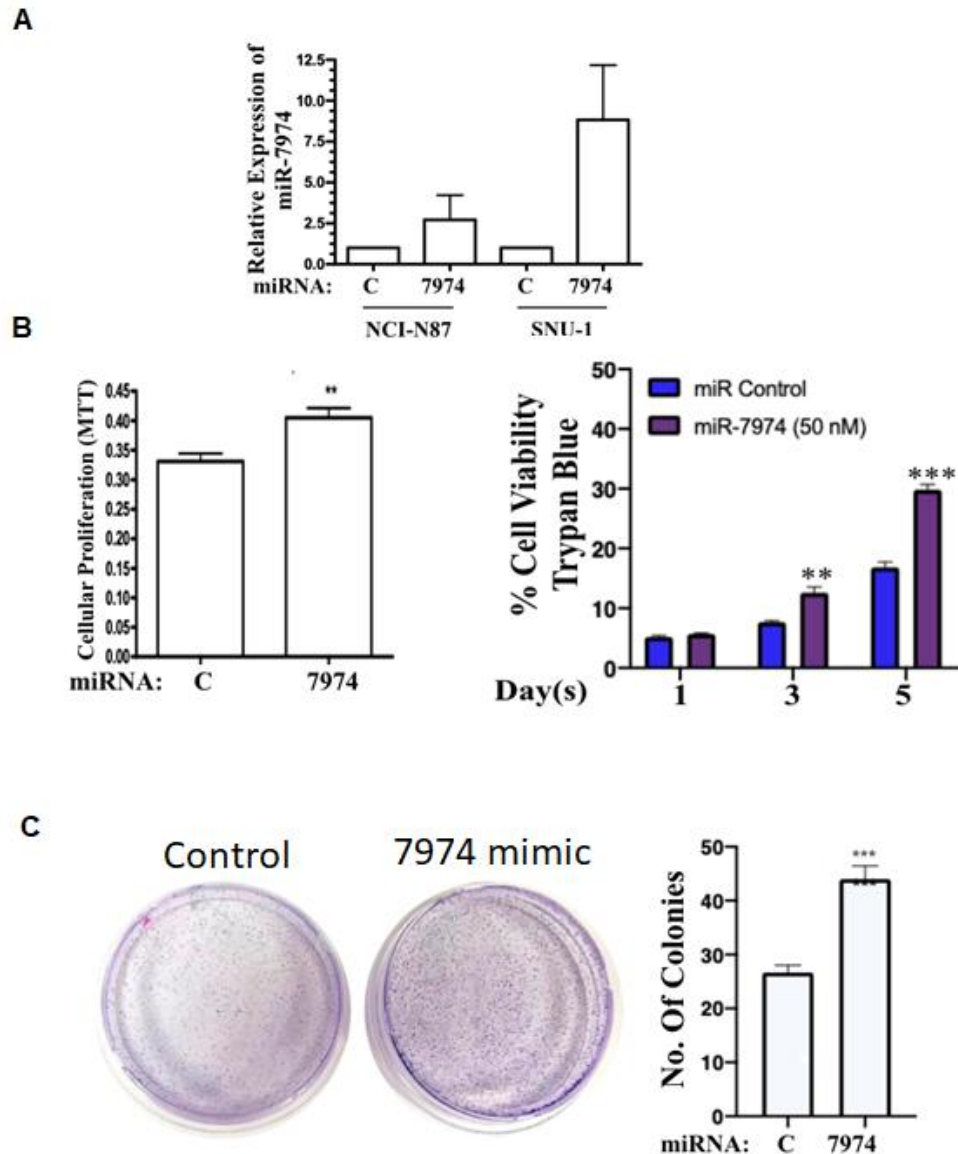


**Figure 6.2: Upregulation of miR-7974 enhances cell viability.** [A] TaqMan RT-qPCR validation of miR-7974 overexpression in NCI-N87 and SNU-1 cell lines. [B] Cell viability assay in the NCI-N87 and SNU-1 cells showed increased proliferation with miR-7974 upregulation after 72 hours (NCI-N87) or 128 hours (SNU-1). Experiments are representative of three independent replicates and quantification is an average of the three replicates where \*\*  $p < 0.01$  and \*\*\*  $p < 0.001$ . Graphs (mean) and statistics were obtained using GraphPad Prism software where error bars represent standard deviation. [C] Colony formation of NCI-N87 cell line. Experiments are representative of three independent replicates and quantification is an average of the three replicates where \*\*\*  $p < 0.001$ . Graphs (means) and statistics were obtained using GraphPad Prism software where error bars denote standard deviation between three experiments.

### 7.4.3 Ras signaling is targeted by miR-7974 and miR-129-1-3p

Since our results highlight that miR-7974 overexpression or miR-129-1-3p downregulation alters gastric cancer growth patterns, we wanted to explore the mechanisms behind this. MicroRNAs target a variety of genes, normally over 3000 genes per microRNA [Fridrich et al., 2019], and to study each microRNA-gene interaction individually would not be possible. In order to circumvent this problem, we decided to utilize the miRWalk 3.0 database, which predicts microRNA-gene interactions, to streamline potential genes of interest. To prioritize the relevance of which microRNAs to study we utilized the other lab generated sequencing results mentioned above. In this comparison, we found RASGEFs were predicted to be modulated by both miR-7974 and miR-129-1-3p (**Table 12**).

*RASGEF1A* expression was predicted to be altered by miR-129-1-3p where miR-7974 was predicted to alter *RASGEF1B* expression (**Table 12**). Publicly available databases routinely use algorithms and prediction models to identify miRNA-gene target interactions. Although this is a useful tool, there has been little effort studying the off-target effects that miRNAs induce on genes with similar structures or isoforms. As with the case of RASGEFs, *RASGEF1A*, *RASGEF1B* and *RASGEF1C* all have significantly similar sequence homology on the RASGEF and RASGEFN domains [Mitin et al., 2005]. We were more interested in studying *RASGEF1A* activity in gastric cancer as it has global cellular functions to stimulate G-protein coupled receptors (GPCRs) and the RET pathway rather than *RASGEF1B* which is involved with only endosome formation and specificity towards Rap2A activation [Yaman et al., 2009; Quilliam et al., 2002]. Compared to normal tissues, *RASGEF1A* was more significantly expressed in the gastric cancer cell lines than

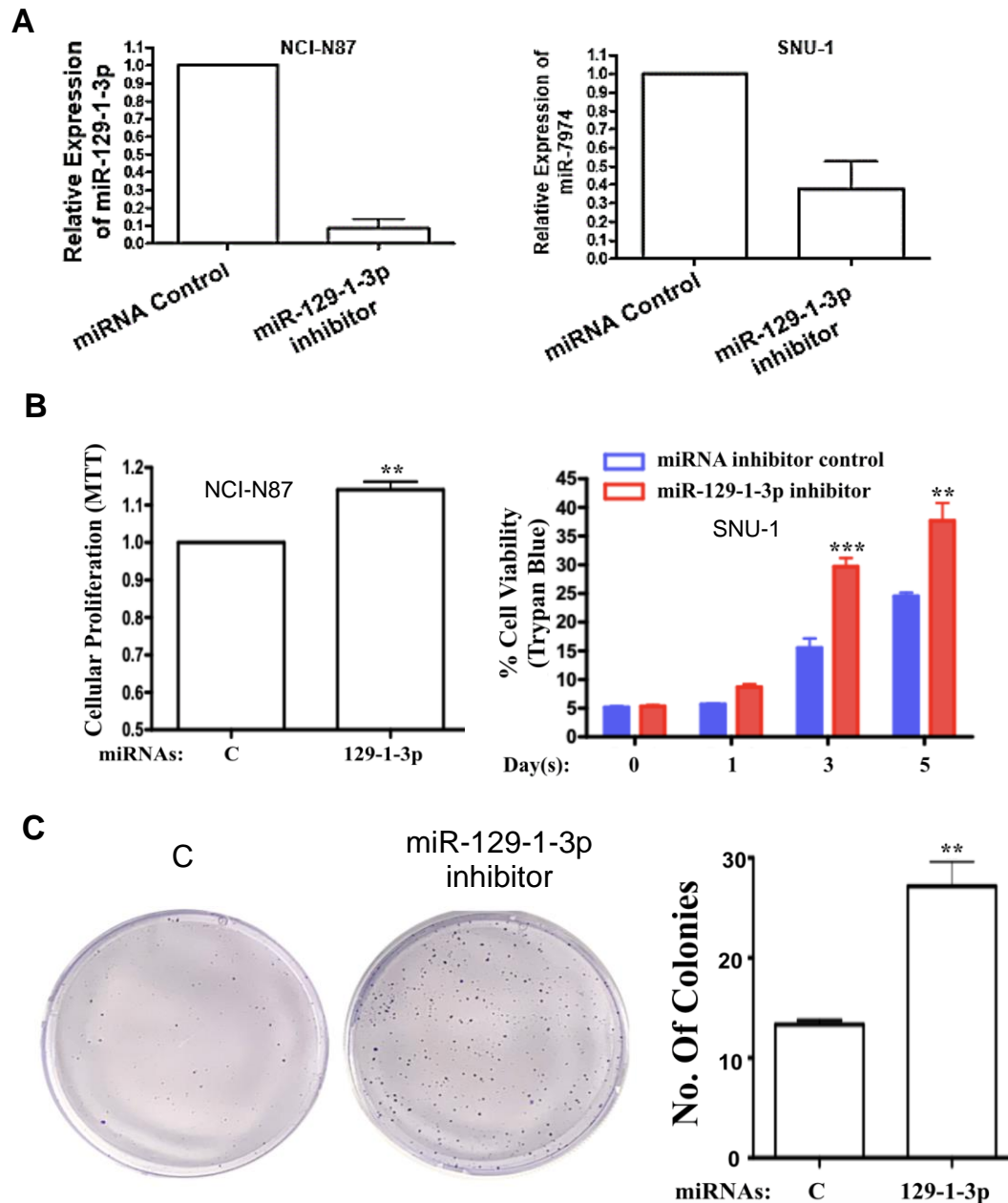


**Figure 6.3: Downregulation of miR-129-1-3p enhances cell viability. [A]** TaqMan RT-qPCR validation of miR-129-1-3p downregulation in NCI-N87 and SNU-1 cell lines. **[B]** Cell viability assay in the NCI-N87 and SNU-1 cells showed increased formation with miR-129-1-3p downregulation after 72 hours (NCI-N87) or 128 hours (SNU-1). Experiments are representative of three independent replicates and quantification is an average of the three replicates where \*\*  $p < 0.01$  and \*\*\*  $p < 0.001$ . Statistical analysis was performed using GraphPad Software. **[C]** Colony formation of NCI-N87 cell line. Experiments are representative of three independent replicates and quantification is an average of the three replicates where \*\*\*  $p < 0.001$ . Graphs and statistics were obtained by GraphPad Prism software.

<b>microRNA</b>	<b>Gene Name</b>	<b>miRNA-Protein Predicted Interaction</b>	<b>Location</b>
miR-7974	RASGEF1B	62:108	5' UTR
miR-129-1-3p	RASGEF1A	1762:1788	3'UTR
miR-129-1-3p	RASGEF1B	2071:2093	3'UTR

**Table 12: RASGEFs are targeted by miR-7974 and miR-129-1-3p.** Using the miRWalk 3.0 database, we found that RASGEFs are predicted to be targeted by miR-7974 and miR-129-1-3p at specific interactions within either the 5' or 3' UTR.

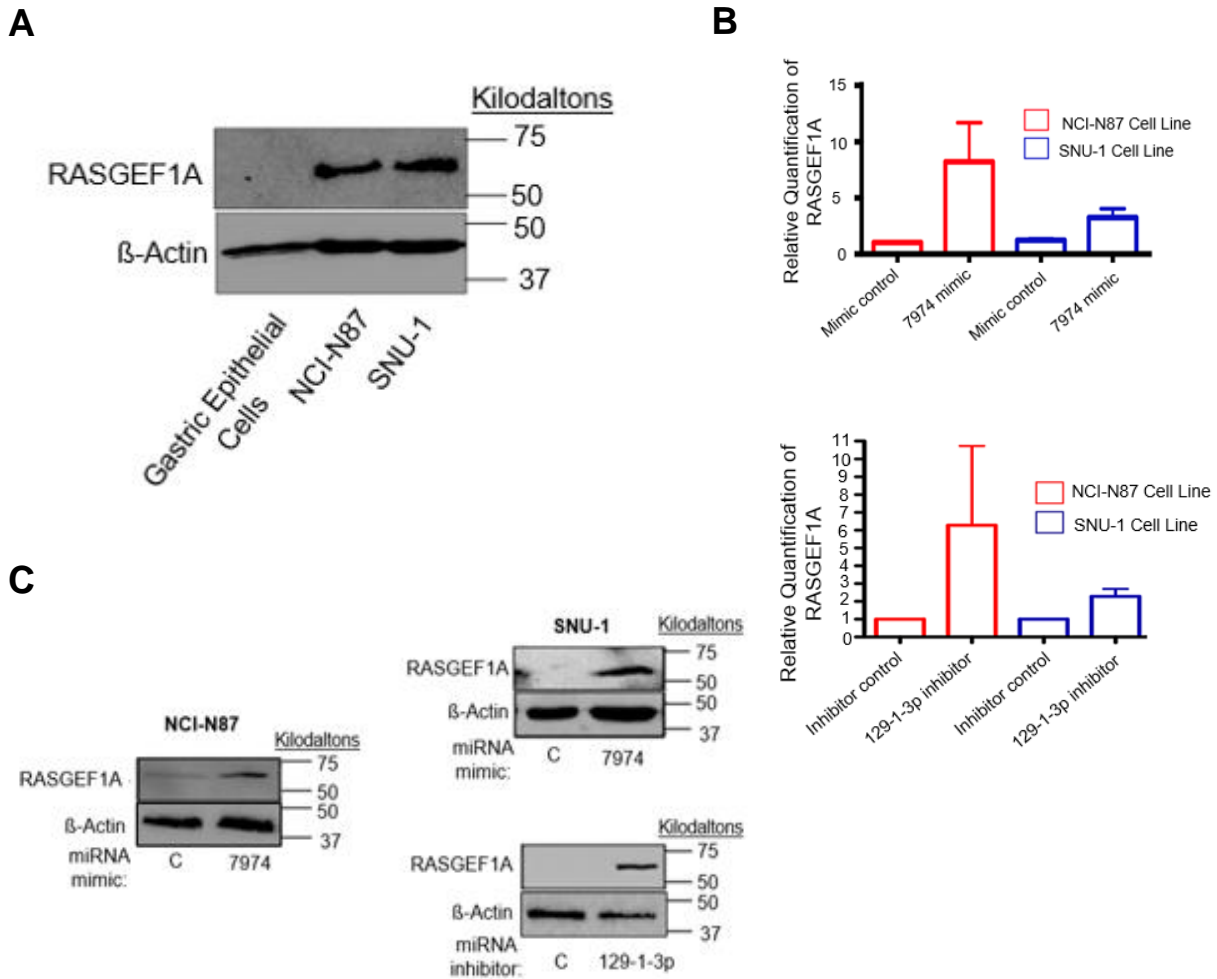


normal epithelial cells suggesting that this is a driving event for gastric cancer growth (**Figure 6.4A**).

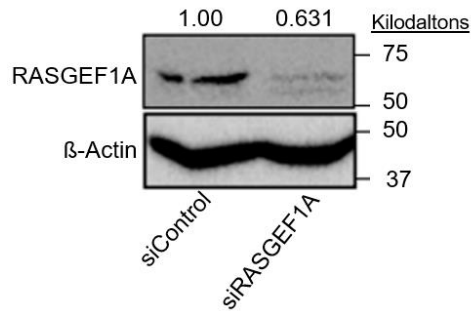
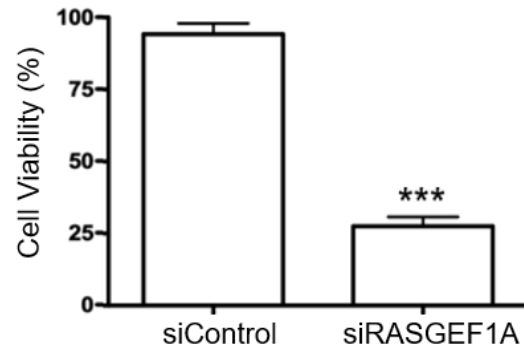
We found with either upregulation of miR-7974 or downregulation of miR-129-1-3p there were inductions in *RASGEF1A* expression and RASGEF1A activity (**Figure 6.4 B-C**). Little is known about RASGEF1A in relation to cancer and there are no studies looking at the role of this protein in gastric cancer. We found downregulation of RASGEF1A was one of the mechanisms that led to reduction in gastric cancer proliferation suggesting the relevance of RASGEFs to this disease (**Figure 6.5A-B**). These results suggest that RASGEF1A plays a potentially prominent role in gastric cancer signaling and can be targeted by small noncoding microRNAs whose expression is controlled by the activity of XPO1. Further investigation is needed to identify the therapeutic potential of directly targeting this protein.

#### **7.4.4 miR-7974 and miR-129-1-3p alter gastric cancer sensitivity to selinexor**

As miR-7974 and miR-129-1-3p were predicted to be differentially expressed in gastric cancer after treatment with selinexor, according to small noncoding RNA sequencing, we wanted to experimentally determine whether we could capture this in our gastric cell lines *in vitro*. To do this, we utilized both the SNU-1 and NCI-N87 cell lines and transfected these cells with either miR-7974, miR-129-1-3p or their respective controls to identify whether there were changes to selinexor sensitivities. A 72-hour transfection of miR-7974 mimic in the NCI-N87 cell line resulted in a resistant phenotype to selinexor compared to mimic control (**Figure 6.6A**). Further, there were no significant changes observed in sensitivity to the negative control (KPT-301) (**Figure 6.6A**). After 72-hour transfection of either miR-7974 mimic or miR-129-1-3p inhibitor in the SNU-1



**Figure 6.4 RASGEF1A is activated by miR-7974 and miR-129-1-3p.** [A] Baseline RASGEF1A activity was measured in normal epithelial gastric tissue, NCI-N87 and SNU-1 cell lines and Beta actin was used as loading control. Densitometry is representative of one independent experiment. [B] RASGEF1A expression was measured using RT-qPCR (24 hours) in the SNU-1 and NCI-N87 cell lines. Graphs were made by GraphPad PRISM software (average) and error bars denote standard deviation. [C] RASGEF1A expression was measured using western blotting (72 hours) after upregulation of miR-7974 or downregulation of miR-129-1-3p in the NCI-N87 and SNU-1 gastric cancer cell lines.

**A****B**

**Figure 6.5: RASGEF1A controls gastric cancer proliferation.** [A] RASGEF1A was knocked down in the SNU-1 cell line and assessed via western blot. Densitometry (mean) is representative of three independent experiments. Standard error is as follows for siControl 0.144, siRASGEF1A 0.0623. [B] RASGEF1A downregulation reduced gastric cancer cell viability. Graph was made by GraphPad PRISM software and is an average of three independent experiments with error bars denoting standard deviation. Statistics were done using GraphPad with two-tailed t-test at 95% confidence interval with \*\*\* denoting p-value < 0.001.

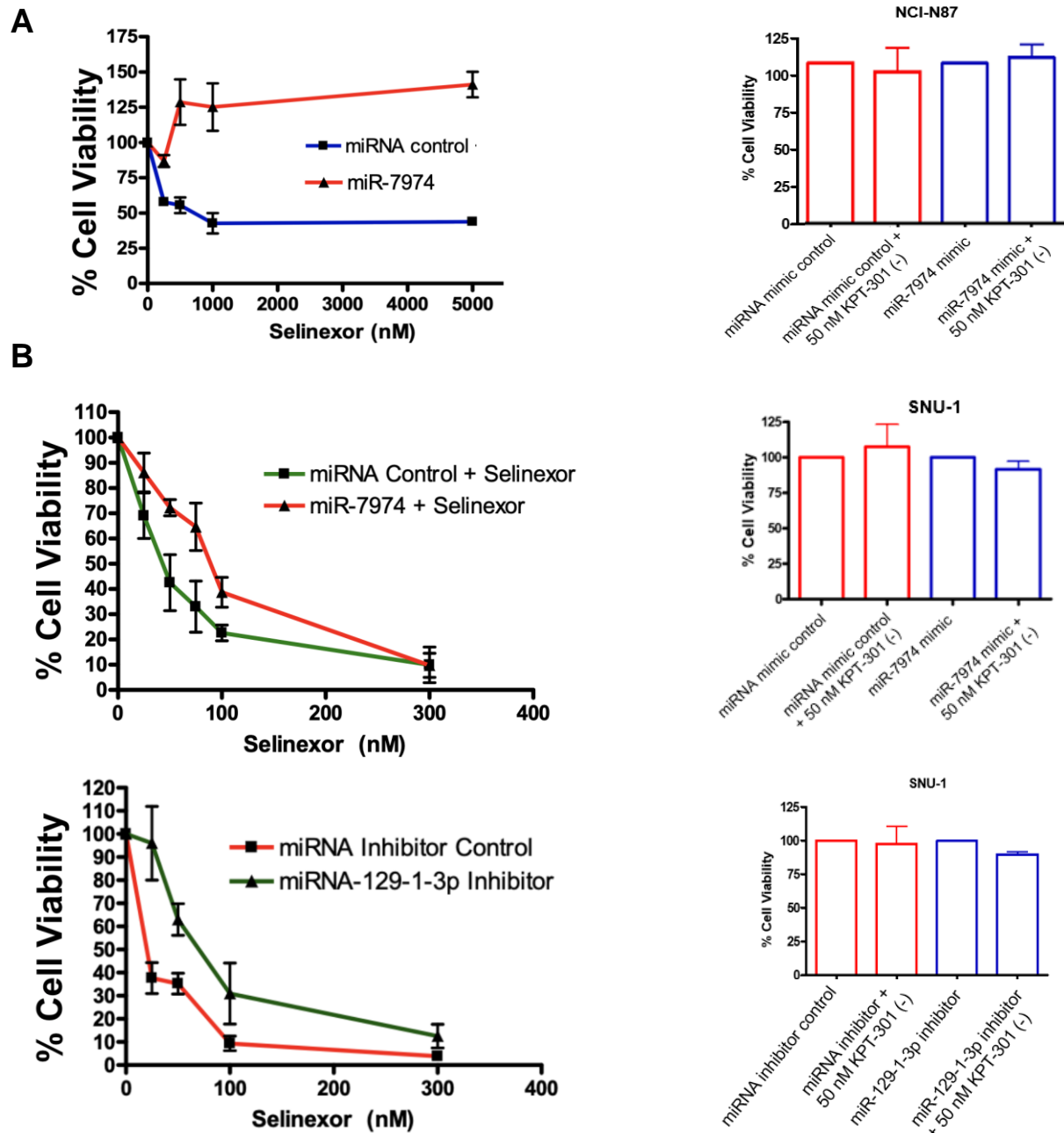


**Figure 6.6 miRNAs alter selinexor sensitivity in gastric cancer.** [A] NCI-N87 cells transfected with the miR-7974 mimic exhibited increased resistance to selinexor at all treatment doses and negative control (KPT-301) showed no significant differences between the two conditions. Graphs were plotted using GraphPad Prism Software and the figures are representative of three independent experiments (mean) where error bars depict standard deviation. [B] SNU-1 cells transfected with either the miR-7974 mimic or miR-129-1-3p inhibitor exhibited increased resistance to selinexor at treatment doses up to 150 nM of selinexor and negative control (KPT-301) showed no significant differences between the two conditions. Graphs were plotted using GraphPad Prism Software and the figures are representative of three independent experiments (mean) where error bars depict standard deviation.

cell line, we observed resistant phenotypes to selinexor compared to their respective controls (**Figure 6.6B**). MicroRNA RT-qPCR revealed a significant reduction of miR-7974 after 24-hour treatment with selinexor (**Figure 6.7**) in the NCI-N87 and SNU-1 cell lines and only a trending change in miR-129-1-3p expression after selinexor in the SNU-1 cell line (**Figure 6.7**). These results suggest that selinexor treatment has the ability to overcome resistance that can be acquired due to perturbations in these specific microRNAs.

#### **7.4.5 Differential changes in small noncoding RNAs are related to chemotherapeutic resistance**

In the literature, some of the noncoding RNAs that have been identified that contribute to chemotherapeutic or small molecule inhibitor resistance such as miR-33b-3p and miR-147a [Xu et al., 2016; Lee et al., 2014] and are altered by treatment with selinexor. For example, microRNA-33b-3p has been identified as upregulated in lung cancer cell lines and contributes to cisplatin resistance through upregulation of DNA damage repair proteins [Xu et al., 2016]. Our data suggests that treatment with selinexor significantly reduces the expression of this oncogenic microRNA (-1.89 log<sub>2</sub> fold change) (**Table 11**). Loss of miR-147a was found to significantly correlate with enhanced EMT expression and resistance to the EGFR inhibitor gefinitinb [Lee et al., 2014]. Our data suggests that treatment with selinexor enhances the expression of this tumor suppressive microRNA (2.24 log<sub>2</sub> fold change) (**Table 11**). Not only does selinexor alter the expression of pathogenic small noncoding RNAs in gastric cancer but also these expression changes can be extrapolated to other disease models such as breast and lung cancer. Further these expression changes of small noncoding RNAs are vast and can

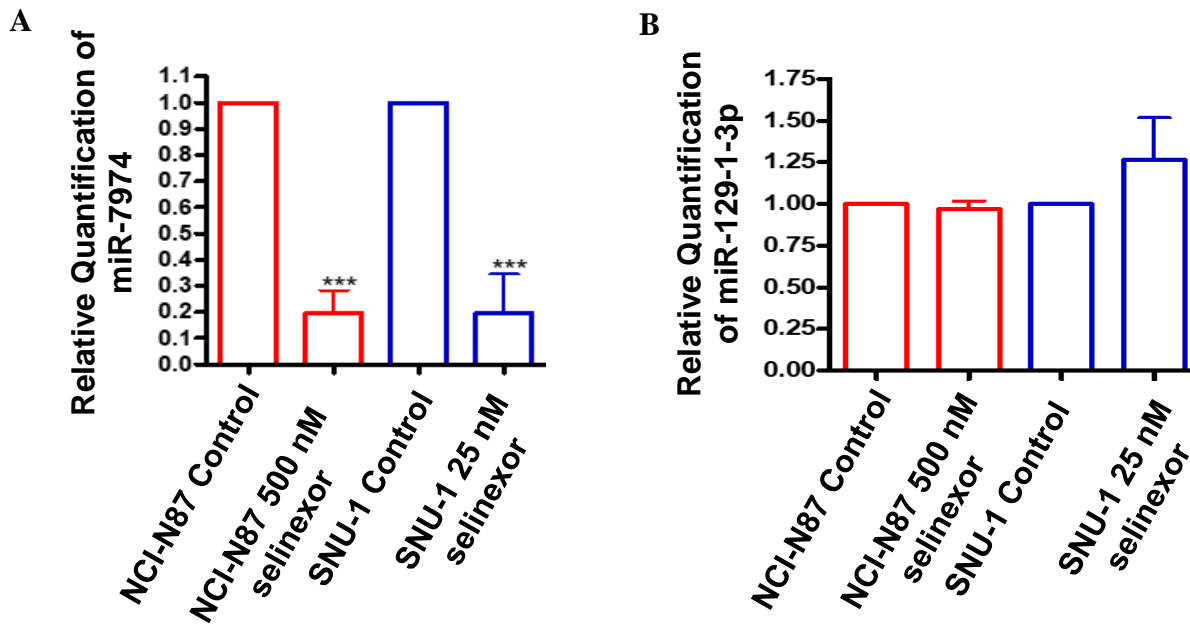


**Figure 6.7 Selinexor can overcome aberrantly expressed microRNAs.** [A-B] TaqMan RT-qPCR analysis of the NCI-N87 and SNU-1 cell lines treated with either 500 nM or 25 nM of selinexor, respectively, for 24-hours. Cells were collected and isolated for miRNA. cDNA was synthesized according to manufacturer protocol and primers specific for miR-7974 and miR-129-1-3p were ran with U47 as the miRNA housekeeping gene. Results were normalized to their respective control and statistical analysis was obtained using GraphPad Prism software. Graphs (mean) are representative of three independent experiments and error bars indicate standard deviation. Results are representative of three independent experiments where \*\*\*  $p < 0.001$ .

contribute to enhanced rates of therapeutic sensitivity in both non-specific and specific compounds used to treat these diseases. Further investigatory work is needed to determine the relevance of these microRNAs in gastric cancer disease specifically

## **7.5 Conclusions**

MicroRNAs are a vital cellular component that can alter normal processes by influencing or changing normal gene expression. Using gastric cancer models, we have identified two critical microRNAs (miR-7974 and miR-129-1-3p) that when differentially expressed can perpetuate disease when compared to normal gastric cells. Some of the phenotypic alterations that can occur when these microRNAs are perturbed include enhanced gastric cancer growth and colony formation. We have found evidence, *in vitro* and in small RNA sequencing screen, that treatment with selinexor can reverse these cancer-promoting phenotypes in gastric cancer cells by altering the expression of these small noncoding RNAs in two gastric cancer cell lines. We have found endogenous up-regulation of miR-7974 or downregulation of miR-129-1-3p enhances resistance to selinexor in gastric cancer cells, dependent on subtype of disease. Moving forward, further investigatory work is needed to fully elucidate whether we can capture these microRNAs in the serum and utilize them as a predictive biomarker for selinexor treatment.

## CHAPTER 8- OVERALL CONCLUSIONS

The overall scope of this work was to identify whether the inhibition of XPO1 protein can be used as a therapeutic target to treat gastric cancer. XPO1 inhibition with selective inhibitors of nuclear export are a novel targeted therapy that has produced survival benefit in different cancer models, such as multiple myeloma (Theodoropoulos et al., 2020). Throughout the course of these studies we have uncovered key observations, with the most important being over-expression of XPO1 in gastric cancer patient tissue. We have found XPO1 overexpression to be prominent within dysplastic tissue and primary gastric cancer. Furthermore, differential expression of XPO1 in African American and Caucasian gastric cancer patients at differing stages of disease. We have validated that XPO1 overexpression is a cancer promoting process using several gastric cancer cell models. We have shown XPO1 overexpression induces gastric cancer growth and colony formation through the alterations in cancer growth pathways, such as upregulation of RAS/MEK/ERK signaling.

Using both siRNA and XPO1 targeted inhibitors; we have found that XPO1 silencing reverses gastric cancer growth and colony formation suggestive that XPO1 inhibition could become a therapeutic strategy to treat gastric cancer. Recently the XPO1 inhibitor selinexor was FDA approved for use in multiple myeloma (Kasamon et al., 2021). Selinexor is tolerated and has produced enhanced survival benefits when compared to standard of care in this disease. Using both selinexor and the second-generation compound eltanexor in gastric cancer models, we found XPO1 inhibition is a viable strategy to treat gastric cancer. XPO1 inhibition causes retention of tumor suppressor proteins, such as P53, inhibits cell cycle progression and induces apoptosis.



Not only is XPO1 inhibition effective as a single agent, but it also has the ability to synergize with different chemotherapeutics that are commonly used to treat gastric cancer. We have found inhibition of XPO1 with selinexor synergizes with paclitaxel *in vitro* and *in vivo* in gastric cancer models through perturbations with normal cell cycle processes. Using gastric cancer xenografts, we found statistically significant reduction in tumor burden along with no discernable differences in body weight indicative of the tolerability of this combination. We have also found inhibition of XPO1 with selinexor synergizes with oxaliplatin and 5-FU both *in vitro* and *in vivo* in gastric cancer models. We have found XPO1 inhibition, in combination with oxaliplatin and 5-FU induces more DNA damage and suppresses normal cellular repair mechanisms leading to gastric cancer cell death. We have also identified a novel resistance marker to 5-FU as WW domain box protein 5 (WBP5). We have found selinexor downregulates the expression of this protein significantly in combination with oxaliplatin and 5-FU compared to oxaliplatin and 5-FU treatment only. Furthermore, treatment with selinexor, oxaliplatin and 5-FU, at lower doses, was effective *in vivo* producing significant decrease in tumor burden compared to oxaliplatin and 5-FU alone. We observed no significant reduction in body weight suggestive of the tolerability of this treatment combination.

Finally, we also demonstrated that XPO1 inhibition not only alters the localization of various tumor suppressors and oncogenes but also can alter the expression of oncogenic and tumor suppressive small noncoding RNAs such as piwiRNAs, circular RNAs and microRNAs. We have identified two key microRNAs that are perturbed in gastric cancer, miR-7974 and miR-129-1-3p. We observed miR-7974 acts as an oncogenic microRNA in gastric cancer and is normally upregulated compared to normal

gastric cells where as miR-129-1-3p acts as a tumor suppressor and is normally downregulated in gastric cancer compared to normal gastric cells. Upregulation of miR-7974 and/or downregulation of miR-129-1-3p results in enhanced gastric cancer growth through alterations in growth signaling pathways by stimulating RASGEFs, proteins which trigger RAS signaling to proceed. Finally, we found the perturbed expression of these microRNAs leads to selinexor resistance differently based on gastric cancer subtype.

Overall, these results highlight the therapeutic benefit of treating gastric cancer with XPO1 inhibitors either as a single agent or in combination with other chemotherapeutics. It is clear that these observations warrant further clinical investigation.

## CHAPTER 9- FUTURE DIRECTIONS

The main future direction of this work is to utilize these observations and results to bring forth selinexor to the bedside for patients with gastric cancer. We will be studying the effect of selinexor in addition to paclitaxel or DNA damaging agents in a multi-institutional study that will be initiated by GI physicians at Karmanos Cancer Institute in collaboration with other institutions. For the clinical trial design, there will be an initial screening of gastric cancer patients to identify the location of the tumor (either esophageal, GEJ or in the stomach) and whether the patient has progressed with a first-line therapy. The patients will be treated with 60 mg of selinexor on Day 1, 3, 8, 10, 15 and 17 whereas 80 mg/m<sup>2</sup> of paclitaxel will be administered on days 1, 8, 15. During this time, the patients will be scanned every 3 cycles (12-weeks) and restaged if necessary according to the Response Evaluation Criteria in Solid Tumors (RECIST). . Moving forward there is more work to be done to identify whether there is an ideal patient population that may benefit from this treatment and whether the combination is effective in patients that have been previously treated with either a platinum or anti-metabolite.

Another future direction we are aiming to pursue is to identify the significance of XPO1 differential expression between African American and Caucasian gastric cancer patients. We have found that there is a trend suggesting the African American cohort has higher expression of XPO1 in tumor tissues and that this varies by stage. We will be pursuing a study in collaboration with epidemiologist at Karmanos Cancer Institute to assess overall survival in relation to XPO1 expression in these patient cohorts. The scope of this work will allow further insight into the survival disparities seen within gastric cancer.

Finally, we also are planning to perform an *in vivo* animal study to investigate whether we can capture our small-noncoding RNAs of interest in the serum after treatment with selinexor. ICR-SCID mice will be implanted with gastric cancer xenograft and mice will be sacrificed before treatment (baseline) and throughout the course of treatment for collection of whole blood and tumor analysis. Serum will be isolated for microRNAs and submitted to LC sciences for sequencing. We hypothesize that (1) we can identify a patient population (African American gastric cancer patients) that would have a greater benefit to selinexor treatment due to their increased upregulation of XPO1 and (2) an identification of these small noncoding RNAs will be useful in guiding clinical decisions in regards to selinexor treatment and can assist in the design of future clinical trials.

## REFERENCES

- Rawla, P., & Barsouk, A. (2019). Epidemiology of gastric cancer: global trends, risk factors and prevention. *Przegląd gastroenterologiczny*, **14**(1): 26–38.
- Wang, X. Q., Terry, P. D., & Yan, H. (2009). Review of salt consumption and stomach cancer risk: epidemiological and biological evidence. *World journal of gastroenterology*, **15**(18): 2204–2213.
- Ma, J., Shen, H., Kapesa, L., & Zeng, S. (2016). Lauren classification and individualized chemotherapy in gastric cancer. *Oncology letters*, **11**(5): 2959–2964.
- Berlth, F., Bollschweiler, E., Drebber, U., Hoelscher, A. H., & Moenig, S. (2014). Pathohistological classification systems in gastric cancer: diagnostic relevance and prognostic value. *World journal of gastroenterology*, **20**(19): 5679–5684.
- Zhang W. (2014). TCGA divides gastric cancer into four molecular subtypes: implications for individualized therapeutics. *Chinese journal of cancer*, **33**(10): 469–470.
- Wang, R, Dang, M, Harada, K, Han, G, Wang, F, Pizzi, M.P., et al (2014). Single-cell dissection of intratumoral heterogeneity and lineage diversity in metastatic gastric adenocarcinoma. *Nature Medicine*. **27**:141-151.
- Odze RD (2005). Unraveling the mystery of the gastroesophageal junction: a pathologist's perspective. *American Journal of Gastroenterol.***100**(8):1853-67.
- Ishaq, S., & Nunn, L. (2015). Helicobacter pylori and gastric cancer: a state of the art review. *Gastroenterology and hepatology from bed to bench*, **8**(Suppl 1), S6–S14.
- Lee, YY, Derakhshan, MH (2013). Environmental and lifestyle risk factors of gastric cancer. *Archives of Iranian Medicine*. **16**(6):358-65
- Zhang, H, Wang, Y, Wang, Y, Wu, D, Lin, E, Xia, Q (2020). Intratumoral and intertumoral

- heterogeneity of HER2 immunohistochemical expression in gastric cancer. *Pathology Research and Practice*. **216**(11): 153229.
- Fu, Y., Du, P., Zhao, J., Hu, C., Qin, Y., & Huang, G. (2018). Gastric Cancer Stem Cells: Mechanisms and Therapeutic Approaches. *Yonsei medical journal*, **59**(10): 1150–1158. Lobo S, Benusiglio PR, Coulet F, Boussemart L, Golmard L, Spier I, Hüneburg, R., Aretz, S., Colas, C., Oliveira, C (2021). Cancer predisposition and germline CTNNA1 variants. *European Journal of Medical Genetics*. **64**(10):104316.
- Gullo, I., Devezas, V., Baptista., M, Garrido., L, Castedo., S, Morais., R, Wen., X, Rios, E., Pinheiro, J., Pinto-Ribeiro, I., et al (2018). Phenotypic heterogeneity of hereditary diffuse gastric cancer: report of a family with early-onset disease. *Gastrointestinal Endoscopy*, **87**(6): 1566-1575.
- Mitani, S., & Kawakami, H. (2020). Emerging Targeted Therapies for HER2 Positive Gastric Cancer That Can Overcome Trastuzumab Resistance. *Cancers*, **12**(2)400.
- Hui, R., Garon, E.B., Goldman, J.W., Leighl, N.B., Hellmann, M.D., Patnaik, A., Gandhi, L., Eder, J.P., Ahn, M.J., Horn, L., et al (2017). Pembrolizumab as a first-line therapy for patients with PDL1 positive advanced non-small cell lung cancer: a phase 1 trial. *Annals of oncology*. **28**(4): 874-881.
- Chau, I., Penel, N., Soriano, A. O., Arkenau, H. T., Cultrera, J., Santana-Davila, R., Calvo, E., Le Tourneau, C., Zender, L., Bendell, J. C., Mi, G., Gao, L., McNeely, S. C., Oliveira, J. M., Ferry, D., Herbst, R. S., & Fuchs, C. S. (2020). Ramucirumab in Combination with Pembrolizumab in Treatment-Naïve Advanced Gastric or GEJ Adenocarcinoma: Safety and Antitumor Activity from the Phase 1a/b JVDF Trial. *Cancers*, **12**(10): 2985.

- Högner, A., & Thuss-Patience, P. (2021). Immune Checkpoint Inhibition in Oesophago-Gastric Carcinoma. *Pharmaceuticals (Basel, Switzerland)*, **14**(2): 151.
- Brar, G., & Shah, M. A. (2019). The role of pembrolizumab in the treatment of PD-L1 expressing gastric and gastroesophageal junction adenocarcinoma. *Therapeutic advances in gastroenterology*, **12**:1756284819869767.
- Arai, H., & Nakajima, T. E. (2020). Recent Developments of Systemic Chemotherapy for Gastric Cancer. *Cancers*, **12**(5): 1100.
- Weledji E. P. (2017). The principles of the surgical management of gastric cancer. *International journal of surgery. Oncology*, **2**(7): e11.
- Fujiwara Y., Fukuda S., Tsujie M., et al (2017). Effects of age on survival and morbidity in gastric cancer patients undergoing gastrectomy. *World Journal of Gastrointestinal oncology*, **9**:257-62
- Kim, H. S., Kim, J. H., Kim, J. W., & Kim, B. C. (2016). Chemotherapy in Elderly Patients with Gastric Cancer. *Journal of Cancer*, **7**(1): 88–94.
- Ahn, S., Kim, KM (2021). PD-L1 expression in gastric cancer: interchangeability of 22C3 and 28-8 pharmDx assays for responses to immunotherapy. *Modern Pathology*, **34**: 1719–1727.
- Kotani, D., & Shitara, K. (2021). Trastuzumab deruxtecan for the treatment of patients with HER2-positive gastric cancer. *Therapeutic advances in medical oncology*, **13**: 1758835920986518.
- Tintelnot, J., Goekkurt, E., Binder, M., Thuss-Patience, P., Lorenzen, S., Knorrenschild, JR., Kretzschmar, A., Ettrich, T., Lindig, U., Jacobasch, L., et al (2020). Ipilimumab or FOLFOX with Nivolumab and Trastuzumab in previously untreated HER2-

- positive locally advanced or metastatic EsophagoGastric Adenocarcinoma - the randomized phase 2 INTEGA trial (AIO STO 0217). *BMC Cancer*. **20**(1): 503
- Schena, M., Battaglia, A. F., & Trogu, A. (2019). Immuno-checkpoint inhibitors in metastatic esophago-gastric cancer. *Journal of thoracic disease*, **11**(Suppl 3): S376–S380.
- Pemberton, L.F., Paschal, B.M (2005). Mechanisms of Receptor-Mediated Nuclear Import and Nuclear Export. *Traffic*. **6**: 187-198.
- Evgeneva, TP., Osobennosti, MS. (1964). RABDOMIOBLASTOMY TSRM-1 [PECULIARITIES OF METASTASIZATION OF CRM-1 RHABDOMYOBLASTOMA STRAIN]. *Biull Eksp Biol Med*, **57**:76-9.
- Adachi, Y., Yanagida, M. (1989). Higher order chromosome structure is affected by cold-sensitive mutations in a *Schizosaccharomyces pombe* gene *crm1+* which encodes a 115-kD protein preferentially localized in the nucleus and its periphery. *Journal of Cellular biology*, **108**(4):1195-207.
- Funabiki, H., Hagan, I., Uzawa, S., Yanagida, M. (1993). Cell cycle-dependent specific positioning and clustering of centromeres and telomeres in fission yeast. *Journal of Cellular biology*, **121**(5): 961-76.
- Toda, T., Shimanuki, M., Saka, Y., Yamano, H., Adachi, Y., Shirakawa, M., Kyogoku, Y., Yanagida, M. (1992). Fission yeast *pap1*-dependent transcription is negatively regulated by an essential nuclear protein, *crm1*. *Molecular Cell Biology* **12**(12): 5474-84.
- Hamamoto, T., Gunji, S., Tsuji, H., Beppu, T. (1983). Leptomycin A and B, new antifungal antibiotics. I. Taxonomy of the producing strain and their fermentation, purification



- and characterization. *Journal of Antibiotics (Tokyo)* **36**(6): 639-45.
- Komiyama, K., Okada, K., Tomisaka, S., Umezawa, I., Hamamoto, T., Beppu, T. (1983). Antitumor activity of Leptomycin B. *Journal of Antibiotics (Tokyo)*, **38**(3): 427-9
- Yoshida, M., Nishikawa, M., Nishi, K., Abe, K., Horinouchi, S., Beppu, T. (1990). Effects of Leptomycin B on the cell cycle of fibroblasts and fission yeast cells. *Experimental Cell Research*. **187**(1): 150-6.
- Abe, K., Yoshida, M., Usui, T., Horinouchi, S., Beppu, T. (1991). Highly synchronous culture of fibroblasts from G2 block caused by staurosporine, a potent inhibitor of protein kinases. *Experimental Cell Research*, **192**(1): 122-7
- Yoshida, M., Beppu, T. [Cell cycle checkpoint control and its inhibitors] (1993). *Tanpakushitsu Kakusan Koso*. **38**(8):1436-41.
- Nishi, K., Yoshida, M., Fujiwara, D., Nishikawa, M., Horinouchi, S., Beppu, T. (1994). Leptomycin B targets a regulatory cascade of crm1, a fission yeast nuclear protein, involved in control of higher order chromosome structure and gene expression. *Journal of Biological Chemistry*. **269**(9): 6320-4.
- Newlands, ES., Rustin, GJ., Brampton, MH. (1996). Phase I trial of elactocin. *British Journal of Cancer*. **74**(4):648-9.
- Wolff, B., Sanglier, JJ., Wang, Y. (1997). Leptomycin B is an inhibitor of nuclear export: inhibition of nucleo-cytoplasmic translocation of the human immunodeficiency virus type 1 (HIV-1) Rev protein and Rev-dependent mRNA. *Chemistry & Biology*. **4**(2):139-47.
- Fornerod, M., Ohno, M., Yoshida, M., Mattaj, IW. (1997). CRM1 is an export receptor for leucine-rich nuclear export signals. *Cell*. **19**;90(6): 1051-60.

- Askjaer, P., Bachi, A., Wilm, M., Bischoff, F. R., Weeks, D. L., Ogniewski, V., Ohno, M., Niehrs, C., Kjems, J., Mattaj, I. W., & Fornerod, M. (1999). RanGTP-regulated interactions of CRM1 with nucleoporins and a shuttling DEAD-box helicase. *Molecular and cellular biology*, **19**(9): 6276–6285.
- Fornerod, M., van Deursen J., van Baal S., Reynolds, A., Davis, D., Murti, KG., Franssen, J., Grosveld, G. (1997). The human homologue of yeast CRM1 is in a dynamic subcomplex with CAN/Nup214 and a novel nuclear pore component Nup88. *The EMBO Journal*. **16**(4):807-16.
- Stade, K., Ford, CS., Guthrie, C., Weis, K. (1997). Exportin 1 (Crm1p) is an essential nuclear export factor. *Cell*. **90**(6):1041-50.
- Yano, R., Oakes, ML., Tabb, MM., Nomura, M. (1994). Yeast Srp1p has homology to armadillo/plakoglobin/beta-catenin and participates in apparently multiple nuclear functions including the maintenance of the nucleolar structure. *Proceedings of the National Academy of Sciences of the United States of America*. **91**(15): 6880-4.
- Van der Watt, PJ., Maske, CP., Hendricks, DT., Parker, MI., Denny, L., Govender, D., Birrer, MJ., Leaner, VD. (2009). The Karyopherin proteins, Crm1 and Karyopherin beta1, are overexpressed in cervical cancer and are critical for cancer cell survival and proliferation. *International Journal of Cancer*. **124**(8):1829-40.
- Azizian, NG., Li, Y. XPO1-dependent nuclear export as a target for cancer therapy (2020). *Journal of Hematology & Oncology*. **13**:61.
- Cheng, Y., Holloway, MP., Nguyen, K., McCauley, D., Landesman, Y., Kauffman, MG., Shacham, S., Altura, RA. (2014). XPO1 (CRM1) inhibition represses STAT3

- activation to drive a survivin-dependent oncogenic switch in triple-negative breast cancer. *Molecular Cancer Therapeutics* **13**(3):675-86.
- Noske, A., Weichert, W., Niesporek, S., Röske, A., Buckendahl, AC., Koch, I., Sehouli, J., Dietel, M., Denkert, C. (2008). Expression of the nuclear export protein chromosomal region maintenance/exportin 1/Xpo1 is a prognostic factor in human ovarian cancer. *Cancer*. **112**(8):1733-43.
- Sexton, R., Mahdi, Z., Chaudhury, R., Beydoun, R., Aboukameel, A., Khan, H. Y., Baloglu, E., Senapedis, W., Landesman, Y., Tesfaye, A., Kim, S., Philip, P. A., & Azmi, A. S. (2019). Targeting Nuclear Exporter Protein XPO1/CRM1 in Gastric Cancer. *International journal of molecular sciences*, **20**(19): 4826.
- Azmi A. S., Li Y., Muqbil I., Aboukameel A., Senapedis W., Baloglu E., Landesman Y., Shacham S., Kauffman M. G., Philip P. A., Mohammad R. M (2017). Exportin 1 (XPO1) inhibition leads to restoration of tumor suppressor miR-145 and consequent suppression of pancreatic cancer cell proliferation and migration. *Oncotarget*. **8**: 82144-82155.
- Boons, E., Nogueira, T.C., Dierckx, T. *et al* (2021). XPO1 inhibitors represent a novel therapeutic option in Adult T-cell Leukemia, triggering p53-mediated caspase-dependent apoptosis. *Blood Cancer J*. **11**: 27 (2021).
- Kashyap, T., Argueta, C., Aboukameel, A., Unger, T. J., Klebanov, B., Mohammad, R. M., Muqbil, I., Azmi, A. S., Drolen, C., Senapedis, W., Lee, M., Kauffman, M., Shacham, S., & Landesman, Y. (2016). Selinexor, a Selective Inhibitor of Nuclear Export (SINE) compound, acts through NF- $\kappa$ B deactivation and combines with

- proteasome inhibitors to synergistically induce tumor cell death. *Oncotarget*, **7**(48): 78883–78895.
- Brownawell, AM., Macara, IG. (2002). Exportin-5, a novel karyopherin, mediates nuclear export of double-stranded RNA binding proteins. *Journal of Cell Biology*. **156**(1): 53-64.
- Bohnsack, MT., Regener, K., Schwappach, B., Saffrich, R., Paraskeva, E., Hartmann, E., Görlich, D. (2002). Exp5 exports eEF1A via tRNA from nuclei and synergizes with other transport pathways to confine translation to the cytoplasm. *The EMBO Journal*. **21**(22): 6205-15
- Calado, A., Treichel, N., Müller, EC., Otto, A., Kutay, U. (2002). Exportin-5-mediated nuclear export of eukaryotic elongation factor 1A and tRNA. *The EMBO Journal*. **21**(22): 6216-24.
- Koch, P., Bohlmann, I., Schäfer, M., Hansen-Hagge, TE., Kiyoi, H., Wilda, M., Hameister, H., Bartram, CR., Janssen, JW. (2000). Identification of a novel putative Ran-binding protein and its close homologue. *Biochemical and Biophysical Research Communications*. **278**(1): 241-9.
- Meissner, T., Krause, E., Vinkemeier, U. (2004). Ratjadone and leptomycin B block CRM1-dependent nuclear export by identical mechanisms. *FEBS Letters*. **576**(1-2):27-30
- Kudo, N., Wolff, B., Sekimoto, T., Schreiner, EP., Yoneda, Y., Yanagida, M., Horinouchi, S., Yoshida, M. (1998). Leptomycin B inhibition of signal-mediated nuclear export by direct binding to CRM1. *Experimental Cell Research*. **242**(2): 540-7.
- Theodopoulos, N., Lancman, G., & Chari, A. (2020). Targeting Nuclear Export Proteins

- in Multiple Myeloma Therapy. *Targeted oncology*, **15**(6): 697–708.
- Jin T. R. (2018). Curcumin and dietary polyphenol research: beyond drug discovery. *Acta pharmacologica Sinica*, **39**(5): 779–786.
- Niu, M., Wu, S., Mao, L., Yang, Y. (2013). CRM1 is a cellular target of curcumin: new insights for the myriad of biological effects of an ancient spice. *Traffic*. **14**(10):1042-52.
- Lopresti A. L (2018). The Problem of Curcumin and Its Bioavailability: Could Its Gastrointestinal Influence Contribute to Its Overall Health-Enhancing Effects?, *Advances in Nutrition*, **9**(1): 41-50.
- Liu, Y., Cai, Y., He, C., Chen, M., Li, H. (2017). Anticancer Properties and Pharmaceutical Applications of Plumbagin: A Review. *American Journal of Chinese Medicine*. **45**(3):423-441.
- Sun, Q., Chen, X., Zhou, Q., Burstein, E., Yang, S., & Jia, D. (2016). Inhibiting cancer cell hallmark features through nuclear export inhibition. *Signal transduction and targeted therapy*, **1**: 16010.
- Muqbil, I., Azmi, A. S., & Mohammad, R. M. (2018). Nuclear Export Inhibition for Pancreatic Cancer Therapy. *Cancers*, **10**(5): 138.
- Daelemans, D., Afonina, E., Nilsson, J., Werner, G., Kjemis, J., De Clercq, E., Pavlakis, GN., Vandamme, AM. (2002). A synthetic HIV-1 Rev inhibitor interfering with the CRM1-mediated nuclear export. *Proceedings of the National Academy of Sciences of the United States of America*. **99**(22):14440-5.
- Sakakibara, K., Saito, N., Sato, T., Suzuki, A., Hasegawa, Y., Friedman, JM., Dufe, DW., Vonhoff, DD., Iwami, T., Kawabe, T. (2011) CBS9106 is a novel reversible oral

- CRM1 inhibitor with CRM1 degrading activity. *Blood*. **118**(14):3922-31.
- Sun, Q., Carrasco, Y.P., Hu, Y., Guo, X., Mirzaei, H., MacMillan, J., Chook, Y.M. (2013). Nuclear export inhibition through covalent conjugation and hydrolysis of Leptomycin B by CRM1. *PNAS*. **110**(4): 1303-1308.
- Lapalombella, R., Sun, Q., Williams, K., Tangeman, L., Jha, S., Zhong, Y., Goettl, V., Mahoney, E., Berglund, C., Gupta, S, et al (2012). Selective inhibitors of nuclear export show that CRM1/XPO1 is a target in chronic lymphocytic leukemia. *Blood*, **120**(23): 4621–4634.
- Rosen, JC., Weiss, J., Pham, NA., Li, Q., Martins-Filho, SN., Wang, Y., Tsao, MS., Moghal, N. (2021). Antitumor efficacy of XPO1 inhibitor Selinexor in KRAS-mutant lung adenocarcinoma patient-derived xenografts. *Translational Oncology*. **14**(10):101179.
- Kasamon, YL., Price, LSL., Okusanya, OO., Richardson, NC., Li, RJ., Ma, L., Wu, YT., Theoret, M., Pazdur, R., Gormley, NJ. (2021). FDA Approval Summary: Selinexor for Relapsed or Refractory Diffuse Large B-Cell Lymphoma. *The Oncologist*. **26**(10): 879-886.
- Gavriatopoulou, M., Chari, A., Chen, C., Bahlis, N., Vogl, D.T., Jakubowiak, A., et al (2020). Integrated safety profile of selinexor in multiple myeloma: experience from 437 patients enrolled in clinical trials. *Leukemia*. **34**: 2430-2440.
- clinicaltrials.gov. Identifier: NCT02649790. Study of the Safety, Tolerability and Efficacy of KPT-8602 in Participants with Relapsed/Refractory Cancer Indications Karyopharm Therapeutics Inc. Selinexor for the Treatment of Triple Class

- Refractory Multiple Myeloma (2019). *FDA Advisory Committee Meeting Briefing Document*.
- Bader, J.C., Abdul Razak, A.R., Shacham, S., Xu, H. Pharmacokinetics of Selinexor: The First-in-Class Selective Inhibitor of Nuclear Export (2021). *Clin Pharmacokinet.* **60(8):957-969**
- Garzon, R., Savona, M., Baz, R., et al. A phase 1 clinical trial of single-agent selinexor in acute myeloid leukemia (2017). *Blood.* **129(24):3165-3174.**
- Tremblay, G., Daniele, P., Breeze, J., Li, L., Shah, J., Shacham, S., Kauffman, M., Engelhardt, M., Chari, A., Nooka, A., et al (2021). Quality of life analyses in patients with multiple myeloma: results from the Selinexor (KPT-330) Treatment of Refractory Myeloma (STORM) phase 2b study. *BMC Cancer.* **21(1):993.**
- Ku, J. L., & Park, J. G. (2005). Biology of SNU cell lines. *Cancer research and treatment*, **37(1)**, 1–19.
- Park, J.G., Frucht, H., LaRocca, R.V., Bliss, D.P. Jr., Kurita, Y., Chen, T.R., Henslee, J.G., Trepel, J.B., Jensen, R.T., Johnson, B.E., et al (1990). Characteristics of cell lines established from human gastric carcinoma. *Cancer Research.* **50(9): 2773-80.**
- Ashktorab, H., Kupfer, S. S., Brim, H., & Carethers, J. M. (2017). Racial Disparity in Gastrointestinal Cancer Risk. *Gastroenterology*, **153(4): 910–923.**
- Merchant, S. J., Li, L., & Kim, J. (2014). Racial and ethnic disparities in gastric cancer outcomes: more important than surgical technique?. *World journal of gastroenterology*, **20(33): 11546–11551**
- Bliton, J.N., Parides, M., Muscarella, P., Papalezova, K.T., In, H. (2021). Understanding Racial Disparities in Gastrointestinal Cancer Outcomes: Lack of Surgery

- Contributes to Lower Survival in African American Patients. *Cancer Epidemiology Biomarkers & Prevention*. **30**(3):529-538
- van Beek, E.J.A.H., Hernandez, J.M., Goldman, D.A., Davis, J.L., McLaughlin, K., Ripley, R.T., Kim, T.S., Tang, L.H., Hechtman, J.F., Zheng, J., et al (2018). Rates of TP53 Mutation are Significantly Elevated in African American Patients with Gastric Cancer. *Annals of Surgical Oncology*. **25**(7): 2027-2033.
- Rashid, N.S., Hairr, N.S., Murray, G., Olex, A.L., Leftwich, T.J., Grible, J.M., Reed, J., Dozmorov, M.G., Harrell, J.C. (2021). Identification of nuclear export inhibitor-based combination therapies in preclinical models of triple-negative breast cancer. *Translational Oncology*. **14**(12):101235.
- Galinski, B., Luxemburg, M., Landesman, Y., Pawel, B., Johnson, K.J., Master, S.R., Freeman, K.W., Loeb, D.M., Hébert, J.M., Weiser, D.A. (2021). XPO1 inhibition with selinexor synergizes with proteasome inhibition in neuroblastoma by targeting nuclear export of I $\kappa$ B. *Translational Oncology*. **14**(8):101114.
- Lee, J.W., Sung, J.S., Park, Y.S., Chung, S., Kim, Y.H (2018). Isolation of Spheroid-forming single cells from gastric cancer cell lines: enrichment of cancer stem-like cells. *Biotechniques*. **65**:197–203
- Muqbil, I., Aboukameel, A., Elloul, S., Carlson, R., Senapedis, W., Baloglu, E., Kauffman, M., Shacham, S., Bhutani, D., Zonder, J., Azmi, A. S., & Mohammad, R. M. (2016). Anti-tumor activity of selective inhibitor of nuclear export (SINE) compounds, is enhanced in non-Hodgkin lymphoma through combination with mTOR inhibitor and dexamethasone. *Cancer letters*, **383**(2): 309–317.



- Crochiere, M.L., Baloglu, E., Klebanov, B., Donovan, S., del Alamo, D., Lee, M., Kauffman, M., Shacham, S., Landesman, Y. (2016). A method for qualification of exportin-1 (XPO1) occupancy by Selective Inhibitor of Nuclear Export (SINE) compounds. *Oncotarget*. **7**(2):1863-78.
- Zheng, Y., Gery, S., Sun, H., Shacham, S., Kauffman, M., Koeffler, H.P. (2014). KPT-330 inhibitor of XPO1-mediated nuclear export has anti-proliferative activity in hepatocellular carcinoma. *Cancer Chemotherapeutic Pharmacology*. **74**(3):487-95.
- Kim, J., McMillan, E., Kim, H. S., Venkateswaran, N., Makkar, G., Rodriguez-Canales, J., Villalobos, P., Neggers, J. E., Mendiratta, S., Wei, S, et al (2016). XPO1-dependent nuclear export is a druggable vulnerability in KRAS-mutant lung cancer. *Nature*, **538**(7623): 114–117.
- Stommel, J.M., Marchenko, N.D., Jimenez, G.S., Moll, U.M., Hope, T.J., Wahl, G.M. (1999). A leucine-rich nuclear export signal in the p53 tetramerization domain: regulation of subcellular localization and p53 activity by NES masking. *The EMBO Journal*. 1999, **18**(6):1660-72.
- Koopman, G., Reutelingsperger, C.P., Kuijten, G.A., Keehnen, R.M., Pals, S.T., van Oers, M.H. (1994). Annexin V for flow cytometric detection of phosphatidylserine expression on B cells undergoing apoptosis. *Blood*. **84**(5):1415-20.
- Zembruski, N.C., Stache, V., Haefeli, W.E., Weiss, J. (2012). 7-Aminoactinomycin D for apoptosis staining in flow cytometry. *Anal Biochem*, **429**(1):79-81.

- Gadgeel, S.M., Shields, A.F., Heilbrun, L.K., Labadidi, S., Zalupski, M., Chaplen, R., Philip, P.A. (2003). Phase II study of paclitaxel and carboplatin in patients with advanced gastric cancer. *American Journal of Clinical Oncology*. **26**(1):37-41
- Wilke, H., Muro, K., Van Cutsem, E., Oh, S.C., Bodoky, G., Shimada, Y., Hironaka, S., Sugimoto, N., Lipatov, O., Kim, T.Y., et al (2014). Ramucirumab plus paclitaxel versus placebo plus paclitaxel in patients with previously treated advanced gastric or gastro-oesophageal junction adenocarcinoma (RAINBOW): a double-blind, randomized phase 3 trial. *Lancet Oncology*. **15**(11):1224-35
- Vishnu, P., Roy, V. (2011). Safety and Efficacy of *nab*-Paclitaxel in the Treatment of Patients with Breast Cancer. *Cancer: Basic and Clinical Research*.
- Staff, N. P., Fehrenbacher, J. C., Caillaud, M., Damaj, M. I., Segal, R. A., & Rieger, S. (2020). Pathogenesis of paclitaxel-induced peripheral neuropathy: A current review of in vitro and in vivo findings using rodent and human model systems. *Experimental neurology*, **324**: 113121.
- Sakamoto, J., Matsui, T., Kodera, Y. (2009). Paclitaxel chemotherapy for the treatment of gastric cancer. *Gastric Cancer*. **12**, 69–78
- Zhu, L., Chen, L. (2019). Progress in research on paclitaxel and tumor immunotherapy. *Cell & Molecular biology letters* **24**: 40
- Chou, T.C. (2010). Drug combination studies and their synergy quantification using the Chou-Talalay method. *Cancer Research*. **70**(2):440-6.
- Lim, S., & Ganem, N. J. (2014). Tetraploidy and tumor development. *Oncotarget*, **5**(22), 10959–10960.
- Wang, T.H., Wang, H.S., Soong, Y.K. (2000) Paclitaxel-induced cell death: where the cell

- cycle and apoptosis come together. *Cancer*. **88**(11):2619-28.
- Bozkurt, M., Amlashi, F.G., Blum Murphy, M. (2017). The role of chemotherapy in unresectable or metastatic adenocarcinoma of the stomach and gastroesophageal junction. *Minerva Chirurgica*. 2017 **72**(4):317-333
- Nakayama, R., Zhang, Y.X., Czaplinski, J.T., Anatone, A.J., Sicinska, E.T., Fletcher, J.A., Demetri, G.D., Wagner, A.J. (2016). Preclinical activity of selinexor, an inhibitor of XPO1, in sarcoma. *Oncotarget*. **7**(13):16581-92.
- Miura, K., Kinouchi, M., Ishida, K., Fujibuchi, W., Naitoh, T., Ogawa, H., Ando, T., Yazaki, N., Watanabe, K., Haneda, S., Shibata, C., & Sasaki, I (2010). 5-fu metabolism in cancer and orally-administrable 5-fu drugs. *Cancers*, **2**(3): 1717–1730.
- Joyce, K., Saxena, S., Williams, A. *et al* (2010). Antimicrobial spectrum of the antitumor agent, cisplatin. *Journal of Antibiotics* **63**: 530–532
- Lippard, S.J. (1982) New chemistry of an old molecule: cis-[Pt(NH<sub>3</sub>)<sub>2</sub>Cl<sub>2</sub>]. *Science*. **218**(4577):1075-82.
- Newell, D., Searle, K., Westwood, N. *et al* (2003). Professor Tom Connors and the development of novel cancer therapies by the Phase I/II Clinical Trials Committee of Cancer Research UK. *British Journal of Cancer* **89**: 437–454
- Graham, J., Muhsin, M. & Kirkpatrick, P (2004). Oxaliplatin. *Nature Reviews Drug Discovery* **3**:11–12
- Hosoda, K., Azuma, M., Katada, C., Moriya, H., Mieno, H., Ishido, K., et al. (2019). A phase II study of neoadjuvant chemotherapy with docetaxel, cisplatin, and S-1, followed by gastrectomy with D2 lymph node dissection for high-risk advanced gastric cancer: results of the KDOG1001 trial. *Gastric Cancer*, **22**:598–606

- Masuishi, T., Kadowaki, S., Kondo, M., Komori, A., Sugiyama, K., Mitani, S., Honda, K., Narita, Y., Taniguchi, H., Ura, T., et al (2017). FOLFOX as First-line Therapy for Gastric Cancer with Severe Peritoneal Metastasis. *Anticancer Research*. **37**(12): 7037-42.
- Schoch, S., Gajewski, S., Rothfuß, J., Hartwig, A., & Köberle, B. (2020). Comparative Study of the Mode of Action of Clinically Approved Platinum-Based Chemotherapeutics. *International journal of molecular sciences*, **21**(18), 6928.
- Shirasaka, T. (2009). Development history and concept of an oral anticancer agent S-1 (TS-1): its clinical usefulness and future vistas. *Japanese journal of clinical oncology*, **39**(1): 2–15.
- Tagoug, I., Neri, P., Slaby, J., Babich, J., Simms, J., Gratton, K., Ren, L., Bahlis, N.J. (2013). XPO1 Inhibition Disrupts Ribosomal Subunits Assembly and Induces Multiple Myeloma (MM) Cell Death. *Blood* **122** (21): 3165
- Kashyap T., Argueta C., Unger T., Klebanov B., Debler S., Senapedis W., Crochiere M. L., Lee M. S., Kauffman M., Shacham S., Landesman Y (2018). Selinexor reduces the expression of DNA damage repair proteins and sensitizes cancer cells to DNA damaging agents. *Oncotarget*. **9**: 30773-30786
- Weber, AM., Ryan, A.J. (2015). ATM and ATR as therapeutic targets in cancer. *Pharmacology Therapeutics*. **149**:124-38.
- Bradbury, J.M., Jackson, S.P. (2003). ATM and ATR. *Current Biology* **13**(12):R468.
- Peters GJ, van der Wilt CL, van Triest B, Codacci-Pisanelli G, Johnston PG, van Groeningen CJ, Pinedo HM (1995). Thymidylate synthase and drug resistance. *European Journal of Cancer*. **1**(7-8):1299-305.

- Rose, M.G., Farrell, M.P., Schmitz, J.C. (2002). Thymidylate synthase: a critical target for cancer chemotherapy. *Clinical Colorectal Cancer*. **4**:220–229
- Bissoon-Haqqani, S., Moyana, T., Jonker, D., Maroun, J.A., Birnboim, H.C. (2006). Nuclear expression of thymidylate synthase in colorectal cancer cell lines and clinical samples. *Journal of Histochemistry and Cytochemistry*. **54**(1):19-29.
- Qian, Y., Pan, Z., Guo, Z., Ge, X., Zheng, G., Cao, J., Huang, P., Zhu, X., Zhu, X., Wen, Q., & Ge, M. (2019). Clinicopathological and Prognostic Significance of WW Domain Binding Protein 5 Expression in Papillary Thyroid Carcinoma. *BioMed research international*.
- Nilsson, S., Stein, A., Rolfo, C., Kranich, A.L., Mann, J., Papadimitriou, K., Theile, S., Amberg, S., Bokemeyer, C. (2020). Selinexor (KPT-330), an Oral Selective Inhibitor of Nuclear Export (SINE) Compound, in Combination with FOLFOX in Patients with Metastatic Colorectal Cancer (mCRC) - Final Results of the Phase I Trial SENTINEL. *Current cancer drug targets* **20**(10):811-817.
- Aziz, F., Yang, X., Wen, Q., Yan, Q. (2015). A method for establishing human primary gastric epithelial cell culture from fresh surgical gastric tissues. *Molecular Medicine Reports*. **12**(2):2939-44.
- Choudhuri, S. (2010). Small noncoding RNAs: biogenesis, function, and emerging significance in toxicology. *Journal of Biochemical and Molecular Toxicology* **24**(3):195-216.
- Yamamura, S., Imai-Sumida, M., Tanaka, Y., Dahiya, R. (2018). Interaction and cross-talk between non-coding RNAs. *Cell & molecular life sciences* **75**(3):467-484.
- Treiber, T., Treiber, N. Meister, G. (2019). Regulation of microRNA biogenesis and its

- crosstalk with other cellular pathways. *Nature Reviews of Molecular and Cellular biology* **20**: 5–20
- Kristensen, L.S., Andersen, M.S., Stagsted, L.V.W. *et al* (2019). The biogenesis, biology and characterization of circular RNAs. *Nature Reviews Genetics* **20**, 675–691
- Dahariya, S., Paddibhatla, I., Kumar, S., Raghuwanshi, S., Palapati, A., Gutti, R.K. (2019). Long non-coding RNA: Classification, biogenesis and functions in blood cells. *Molecular Immunology* **112**:82-92.
- Iwasaki, Y.W., Siomi, M.C., Siomi, H. (2015). PIWI-Interacting RNA: Its Biogenesis and Functions. *Annual Review of Biochemistry* **84**:405-33
- Yu, Z., Rong, A., Sheng, J., Luo, Z., Zhang, J., Li, T., Zhu, Z., Fu, Z., Qin, Z., Huang, C. (2021). Aberrant Non-Coding RNA Expressed in Gastric Cancer and Its Diagnostic Value. *Frontiers of Oncology*.
- Wang, J., Wu, J., Cheng, Y., Jiang, Y., & Li, G. (2016). Over-expression of microRNA-223 inhibited the proinflammatory responses in Helicobacter pylori-infection macrophages by down-regulating IRAK-1. *American journal of translational research*, **8**(2): 615–622.
- Wang, J., Deng, Z., Wang, Z., Wu, J., Gu, T., Jiang, Y., & Li, G. (2016). MicroRNA-155 in exosomes secreted from helicobacter pylori infection macrophages immunomodulates inflammatory response. *American journal of translational research*, **8**(9): 3700–3709.
- Wei, L., Sun, J., Zhang, N. *et al* (2020). Noncoding RNAs in gastric cancer: implications for drug resistance. *Molecular cancer* **19**: 62

- Azmi, A. S., Li, Y., Muqbil, I., Aboukameel, A., Senapedis, W., Baloglu, E., Landesman, Y., Shacham, S., Kauffman, M. G., Philip, P. A., & Mohammad, R. M. (2017). Exportin 1 (XPO1) inhibition leads to restoration of tumor suppressor miR-145 and consequent suppression of pancreatic cancer cell proliferation and migration. *Oncotarget*, **8**(47): 82144–82155.
- Muqbil, I., Bao, B., Abou-Samra, A. B., Mohammad, R. M., & Azmi, A. S. (2013). Nuclear export mediated regulation of microRNAs: potential target for drug intervention. *Current drug targets*, **14**(10): 1094–1100.
- Azizian A., Kramer F., Jo P., Wolff H.A., Beißbarth T., Skarupke R., Bernhardt M., Grade M., Ghadimi B.M., Gaedcke J (2015). Preoperative Prediction of Lymph Node Status by Circulating Mir-18b and Mir-20a during Chemoradiotherapy in Patients with Rectal Cancer. *World Journal of Surgery*. **39**:2329–2335.
- Sato, C., Hirasawa, K., Tateishi, Y., Ozeki, Y., Sawada, A., Ikeda, R., Fukuchi, T., Nishio, M., Kobayashi, R., Makazu, M., Kaneko, H., Inayama, Y., Maeda, S. (2020). Clinicopathological features of early gastric cancers arising in *Helicobacter pylori* uninfected patients. *World Journal of Gastroenterology*. **26**(20):2618-2631.
- Vaspolli, R., Venerito, M., Schirrmeister, W., Thon, C., Weigt, J., Wex, T., Malfertheiner, P., Link, A. (2021). Inflammatory microRNAs in gastric mucosa are modulated by *Helicobacter pylori* infection and proton-pump inhibitors but not by aspirin or NSAIDs. *PLOS One*.
- Dong, R., Liu, J., Sun, W., Ping, W. (2020). Comprehensive Analysis of Aberrantly Expressed Profiles of lncRNAs and miRNAs with Associated ceRNA Network in

- Lung Adenocarcinoma and Lung Squamous Cell Carcinoma. *Pathology Oncology Research*. **26**(3): 1935-1945.
- Lai, J., Wang, H., Pan, Z., Su, F. (2019). A novel six-microRNA-based model to improve prognosis prediction of breast cancer. *Aging (Albany NY)*. 11(2): 649-662.
- Yuan, C., Burns, M.B., Subramanian, S., Blekhman, R, (2018). Interaction between Host MicroRNAs and the Gut Microbiota in Colorectal Cancer. *mSystems*. **3**(13): e00205-17.
- Zhang, Y., Wang, Y., Wei, Y. *et al* (2015). MiR-129-3p promotes docetaxel resistance of breast cancer cells via CP110 inhibition. *Scientific Reports* **5**: 15424
- Jia, Y., Gao, Y., & Dou, J. (2020). Effects of miR-129-3p on biological functions of prostate cancer cells through targeted regulation of Smad3. *Oncology letters*, **19**(2), 1195–1202
- Yu, X., Luo, L., Wu, Y., Yu, X., Liu, Y., Yu, X., Zhao, X., Zhang, X., Cui, L., Ye, G., Le, Y., Guo, J. (2013). Gastric juice miR-129 as a potential biomarker for screening gastric cancer. *Medical Oncology*. **30**(1):365.
- Fridrich, A., Hazan, Y., Moran, Y. (2019). Too Many False Targets for MicroRNAs: Challenges and Pitfalls in Prediction of miRNA Targets and Their Gene Ontology in Model and Non-model Organisms. *Bioessays*. **41**(4):e180016
- Jun, J.E., Rubio, I., Roose, J.P. (2013). Regulation of ras exchange factors and cellular localization of ras activation by lipid messengers in T cells. *Frontiers in Immunology*. 2013 **4**:239.
- Mitin N., Rossman K. L., Der C. J (2005). Signaling interplay in Ras superfamily function *Current Biology*. **15**:R563–574



- Yaman, E., Gasper, R., Koerner, C., Wittinghofer, A., Tazebay, U.H. (2009). RasGEF1A and RasGEF1B are guanine nucleotide exchange factors that discriminate between Rap GTP-binding proteins and mediate Rap2-specific nucleotide exchange. *FEBS Journal*. **276**(16):4607-16.
- Andrade, W., Silva, A., Alves, V. *et al* (2010). Early endosome localization and activity of RasGEF1b, a toll-like receptor-inducible Ras guanine-nucleotide exchange factor. *Genes & Immunity* **11**: 447–457
- Xu, S., Huang, H., Chen, Y.N., Deng, Y.T., Zhang, B., Xiong, X.D., Yuan, Y., Zhu, Y., Huang, H., Xie, L., Liu, X. (2016). DNA damage responsive miR-33b-3p promoted lung cancer cells survival and cisplatin resistance by targeting p21<sup>WAF1/CIP1</sup>. *Cell Cycle*. **15**(21): 2920-2930
- Lee, C. G., McCarthy, S., Gruidl, M., Timme, C., & Yeatman, T. J. (2014). MicroRNA-147 induces a mesenchymal-to-epithelial transition (MET) and reverses EGFR inhibitor resistance. *PloS one*, **9**(1): e84597.

**ABSTRACT****XPO1 AS A THERAPEUTIC TARGET IN GASTRIC CANCER**

by

**Rachel Sexton****May 2022****Advisor:** Dr. Asfar S. Azmi**Major:** Cancer Biology**Degree:** Doctor of Philosophy

Gastric cancer is a leading cause of cancer related deaths worldwide. Throughout the world, there is around one million new diagnosed cases per year and only an approximate 25% survival rate. This disease is highly heterogeneous, chemotherapy resistant and deadly. Currently there is no gold standard of care treatment but rather it is physician's choice. Various chemotherapeutic agents can be used, normally in combination, including microtubule inhibitors, DNA damaging agents and anti-metabolite compounds. We have found that nuclear export protein 1 (XPO1) is overexpressed in gastric cancer patients and cell lines compared to normal gastric tissues. The result of XPO1 overexpression leads to enhanced growth signaling pathways, such as KRAS activation. Further, we have found that within the African American gastric cancer cohort, there is increased expression of XPO1 compared to the Caucasian gastric cancer cohort. The overexpression of XPO1 may provide explanation for cancer related disparities found within this disease.

We have further found that inhibition of XPO1, with siRNA, results in suppression of gastric cancer growth and viability. Using selective inhibitors of nuclear export

(selinexor, eltanexor), that have recently achieved FDA approval; we have found these compounds are effective in reducing gastric cancer growth both *in vitro* and *in vivo*. We have found inhibition of XPO1, with selinexor, is also an effective strategy to overcome resistance to commonly used chemotherapeutics such as microtubule inhibitors (nab-paclitaxel), DNA damaging agents (oxaliplatin) and anti-metabolites (5-fluorouracil) both *in vitro* and *in vivo*. Resistance can be overcome through altering the cell cycle, enhancing the amount of DNA damage and inhibiting DNA damage repair mechanisms. Furthermore, treatment with selinexor, oxaliplatin and 5-FU or selinexor and nab-paclitaxel were found to be effective against gastric cancer xenografts at sub-optimal doses with little toxicities suggesting the tolerability of these treatment combinations.

Last, we have found overexpression of XPO1 leads to the differential expression of cancer driving small noncoding RNAs, relevant to gastric cancer, which is involved with perpetuating cancer growth and viability. XPO1 suppression, with SINE, differentially expresses these microRNAs significantly. The interaction between XPO1 and small noncoding RNAs is an alternative mechanism of transport that is normally carried out by nuclear export protein 5 (XPO1). Within gastric cancer, we focused on two particular microRNAs for further evaluation: miR-7974 and miR-129-1-3p. We have found these microRNAs are differentially expressed in cancer cell lines compared to normal gastric cells. These observations correlate with literature studies in other disease models suggesting differential microRNA expression. We have uncovered that aberrant expression of these microRNAs, either upregulation of miR-7974 or downregulation of miR-129-1-3p, leads to selinexor resistance in two gastric cancer cell lines. Future

biomarker studies are needed to explore the therapeutic potential of these small-noncoding RNAs in gastric cancer.

## AUTOBIOGRAPHICAL STATEMENT

**Rachel Sexton**

### Education

**Wayne State University**, Detroit, MI 2017-2022  
Ph.D. Graduate Program, Cancer Biology

**Michigan State University**, East Lansing, MI 2013-2017  
Bachelor of Science (B.S.) in Molecular Biology/Biochemistry  
with additional major in Molecular Genetics/Genomics

### Awards, Grants, & Scholarships

CA191011, US Department of Defense, Horizon Award 2020-2022  
DeRoy Fellowship/Graduate Research Assistantship (GRA) 2019-2020  
Wayne State University

### Publications

1. Sexton R; Khan, H.Y.; Uddin, Md. H; Bannoura, S; Li, Y; Aboukameel, A; Al-Hallak, M.N.; Tesfaye, A; Azmi, A.S. Connecting the Human Microbiome and Pancreatic Cancer. **2022**. *Cancer Metastasis Reviews*.
2. Sexton R; Danasekaran, K; Khan, H.Y.; Uddin, M.H.; Al-Hallak, M.N.; Landesman, Y; Kashyap, T; Li, Y; Aboukameel, A; Azmi, A.S. Identifying the Mutational Profile of ABCB5 Upregulation in Colorectal Cancer: A Comprehensive Database Analysis. *Journal of Cancer Science and Clinical Therapeutics*. **2021**.
3. Sexton, RE; Al Hallak, M.N.; Diab, M; Azmi, A. Gastric cancer: a comprehensive review of current and future treatment strategies. *Cancer Metastasis Reviews*. **2020**.
4. Khan, H.Y.; Li, Y; Aboukameel, A; Mpilla, G; Sexton, R; Kanbur, T; Cetinkaya, H; Cagir, A; Al-Hallak, M.N; Sukari, A; Azmi, A.S.; Nagasaka, M. A Novel Inhibitor for KRASG12C Mutant Lung Carcinoma. *Journal of Thoracic Oncology*. **2020**; 15(2): S15.
5. Sexton R, Al-Hallak MN, Uddin, M.H.; Diab M, Azmi AS. Gastric Cancer Heterogeneity and Clinical Outcomes. *Technology in Cancer Research & Treatment*. **2020**. DOI: 10.1177/1533033820935477.
6. Nagasaka M, Sexton R, Alhasan R, Azmi AS, Sukari A. Gut microbiome and response to checkpoint inhibitors in non-small cell lung cancer- A review. *Crit Rev Oncol Hematol*. **2019**; 145: 102841.
7. Sexton R, Mahdi Z, Chaudhury R, Beydoun R, Aboukameel A, Khan H.Y. et al. Targeting Nuclear Exporter Protein XPO1/CRM1 in Gastric Cancer. *Int. J. Mol. Sci*. **2019**; 20(19): 4826.
8. Sexton R, Mpilla G, Kim S, Philip P, Azmi AS. Ras and Exosome Signaling. *Seminars in Cancer biology*. 2019.
9. Sexton RE, Metabotropic glutamate receptor-1 regulates inflammation in triple negative breast cancer. *Sci Rep*. **2018**, 8:16008